INVESTIGATION OF SINGLE TRYPTOPHAN PROTEINS ENCAPSULATED IN TEOS-DERIVED SOL-GEL MATRICES BY FLUORESCENCE SPECTROSCOPY

Lili Zheng

A thesis submitted to the Department of Chemistry, Brock University
in partial fulfillment of the requirements for the degree of
Master of Science

Brock University, St. Catharines, ON
December 1997

© Lili Zheng

ABSTRACT

In the work reported here, optically clear, ultrathin TEOS derived sol-gel slides which were suitable for studies of tryptophan (Trp) fluorescence from entrapped proteins were prepared by the sol-gel technique and characterized. The monitoring of intrinsic protein fluorescence provided information about the structure and environment of the entrapped protein, and about the kinetics of the interaction between the entrapped protein and external reagents. Initial studies concentrated on the single Trp protein monellin which was entrapped into the sol-gel matrices. Two types of sol-gel slides, termed "wet aged", in which the gels were aged in buffer and "dry-aged", in which the gels were aged in air , were studied in order to compare the effect of the sol-gel matrix on the structure of the protein at different aging stages. Fluorescence results suggested that the mobility of solvent inside the slides was substantially reduced. The interaction of the entrapped protein with both neutral and charged species was examined and indicated response times on the order of minutes. In the case of the neutral species the kinetics were diffusion limited in solution, but were best described by a sum of first order rate constants when the reactions occurred in the glass matrix. For charged species, interactions between the analytes and the negatively charged glass matrix caused the reaction kinetics to become complex, with the overall reaction rate depending on both the type of aging and the charge on the analyte.

The stability and conformational flexibility of the entrapped monellin were also studied. These studies indicated that the encapsulation of monellin into dry-aged monoliths caused the thermal unfolding transition to broaden and shift upward by 14°C, and caused

the long-term stability to improve by 12-fold (compared to solution). Chemical stability studies also showed a broader transition for the unfolding of the protein in dry-aged monoliths, and suggested that the protein was present in a distribution of environments. Results indicated that the entrapped proteins had a smaller range of conformational motions compared to proteins in solution, and that entrapped proteins were not able to unfold completely. The restriction of conformational motion, along with the increased structural order of the internal environment of the gels, likely resulted in the improvements in thermal and long-term stability that were observed.

A second protein which was also studied in this work is the metal binding protein rat oncomodulin. Initially, the unfolding behavior of this protein in aqueous solution was examined. Several single tryptophan mutants of the metal-binding protein rat oncomodulin (OM) were examined; F102W, Y57W, Y65W and the engineered protein CDOM33 which had all 12 residues of the CD loop replaced with a higher affinity binding loop. Both the thermal and the chemical stability were improved upon binding of metal ions with the order apo < Ca^{2+} < Tb^{3+}. During thermal denaturation, the transition midpoints (T_{un}) of Y65W appeared to be the lowest, followed by Y57W and F102W. The placement of the Trp residue in the F-helix in F102W apparently made the protein slightly more thermostable, although the fluorescence response was readily affected by chemical denaturants, which probably acted through the disruption of hydrogen bonds at the C-terminal end of the F-helix. Under both thermal and chemical denaturation, the engineered protein showed the highest stability. This indicated that increasing the number of metal ligating oxygens in the binding site, either by using a metal ion with a higher coordinate

number (i.e. Tb^{3+}) which binds more carboxylate ligands, or by providing more ligating groups, as in the CDOM33 replacement, produces notable improvements in protein stability.

Y57W and CDOM33 OM were chosen for further studies when encapsulated into sol-gel derived matrices. The kinetics of interaction of terbium with the entrapped proteins, the ability of the entrapped protein to binding terbium, as well as thermal stability of these two entrapped protein were compared with different levels of Ca^{2+} present in the matrix and in solution. Results suggested that for both of the proteins, the response time and the ability to bind terbium could be adjusted by adding excess calcium to the matrix before gelation. However, the less stable protein Y57W only retained at most 45% of its binding ability in solution while the more stable protein CDOM33 was able to retain 100% binding ability. Thermally induced denaturation also suggested that CDOM33 showed similar stability to the protein in solution while Y57W was destabilized. All these results suggested that "hard" proteins (i.e. very stable) can easily survive the sol-gel encapsulation process, but "soft" proteins with lower thermodynamic stability may not be able to withstand the sol-gel process. However, it is possible to control many parameters in order to successfully entrap biological molecules into the sol-gel matrices with maximum retention of activity.

ACKNOWLEDGMENTS

I would like to give thanks to my supervisor, Dr. John D. Brennan, for his trust, encouragement, guidance, patience and wisdom throughout this work. The extensive training I received during my two years of graduate study will be immensely beneficial to my future career.

I would also like to acknowledge my thesis committee members, Dr. Jack Miller and Dr. Jeffrey Atkinson, as well as my external examiner, Dr. Ulrich J. Krull for their helpful advice, invaluable comments and suggestions.

I would like to make special mention of Dr. Arthur G. Szabo of the University of Windsor for donating the rat oncomodulin protein; Dr. Christopher W. V. Hogue for helping me prepare the manuscript for my third paper; and Dr. David Wails for doing the pore size analysis of the sol-gel samples.

I would like to extend my sincere gratitude to my group members, especially Kulwinder K. Flora, William R. Reid and Mike Rakic who made the lab like a home, for their friendship and helpful discussion which gave me the joy of working in the lab.

Finally, I would like to take this specially opportunity to give thanks to my husband and my parents, for their constant encouragement, understanding and support.

Table of Contents

Chapter 1 Introduction and Theory 1

- 1.1 Introduction 1
  - 1.1.1 Biosensors 1
  - 1.1.2 Sol-Gel Encapsulation of Biomolecules 3
- 1.2 Research Motivation 8
  - 1.2.1 Project Objectives 8
  - 1.2.2 Thesis Outline 9
- 1.3 Theory and Techniques 10
  - 1.3.1 Fluorescence Spectroscopy 10
  - 1.3.2 Intrinsic Tryptophan Fluorescence 15
  - 1.3.3 Proteins Studied 15
  - 1.3.4 Protein Unfolding Studies 19
    - 1.3.4.1 Chemical Denaturation Studies 19
    - 1.3.4.2 Thermal Denaturation Studies 21
  - 1.3.5 Kinetics of Reactions 22
- 1.4 References for Chapter 1 23

Chapter 2 Environment and Reaction Kinetics within TEOS Derived Sol-Gel Matrix Containing the Single Trp Protein Monellin 28

- 2.1 Introduction 28
- 2.2 Experimental 33
  - 2.2.1 Chemicals 33
  - 2.2.2 Procedures 33
    - 2.2.2.1 Purification of Proteins 33
    - 2.2.2.2 Preparation of TEOS Derived Matrices 34
    - 2.2.2.3 Pore Size Analysis 35
    - 2.2.2.4 UV-Vis Absorbance 35
    - 2.2.2.5 Fluorescence Measurements in Solution 36
    - 2.2.2.6 Fluorescence Measurements of Proteins in the Sol-Gel Slides 37

2.2.2.7 Fluorophore and Protein Leaching Studies 39

2.2.2.8 Photobleaching Studies 40

2.2.2.9 Response Time and Kinetics Studies 40

2.2.2.10 Acrylamide Quenching Studies 41

2.3. Results and Discussions 42

2.3.1 Preparation of Sol-Gel Slides Containing Proteins 42

2.3.1.1 Hydrolysis and Gelation: 42

2.3.1.2 Aging of the Slides: 43

2.3.2 Physical Characteristics of Sol-Gel Slides Containing Proteins 44

2.3.2.1 Pore Size Analysis 44

2.3.2.2 Elimination of Scattering from TEOS Derived Slides 45

2.3.2.3 Photobleaching in Sol-Gel Slides 48

2.3.2.4 Limit of Detection for Measuring Protein Fluorescence in a Slide 49

2.3.2.5 Fluorophore and Protein Leaching 50

2.3.3 Kinetics of Reactions in Sol-gel Slides 50

2.3.3.1 Interaction of Neutral Analytes with Entrapped Monellin 50

2.3.3.2 Interaction of Charged Analytes with Entrapped Monellin 55

2.3.4 Internal Environment of Protein Doped Gels 59

2.3.4.1 Acrylamide Quenching Studies 59

2.3.4.2 Fluorescence Spectra of Entrapped Species 64

2.3.4.3 Steady-State Anisotropy of Entrapped Species 68

2.4 Conclusions 71

2.5 References for Chapter 2 73

Chapter 3 The Study of the Conformational Flexibility and Stability of Monellin Entrapped in the Sol-Gel Matrix 76

3.1 Introduction 76

3.2 Experimental 78

3.2.1 Chemicals and Equipment 78

3.2.2 Procedures 78
3.2.2.1 Preparation and Fluorescence Measurements of Protein Doped Sol-Gel Slides 78
3.2.2.2 Thermal Denaturation Studies 79
3.2.2.3 Chemical Denaturation Studies 80
3.2.2.4 Acrylamide Quenching Studies 81
3.3 Results and Discussions 81
3.3.1 Thermal Stability Studies 81
3.3.2 Chemical Stability Studies 92
3.3.3 Acrylamide Quenching 100
3.3.4 Long Term Stability 105
3.3.5 Basis of the Stability Enhancement 106
3.4 Conclusions 108
3.5 References for Chapter 3 110

Chapter 4 Study of the Effects of Metal Binding Affinity and Metal Loading on the Stability of Rat Oncomodulin Mutants in Solution 113
4.1. Introduction 113
4.2. Experimental 118
4.2.1 Chemicals 118
4.2.2 Precedures 118
4.2.2.1 Sample Preparation 118
4.2.2.2 Absorbance Spectra 119
4.2.2.3 Fluorescence Spectra 119
4.2.2.4 EGTA Titration 119
4.2.2.5 Terbium Titration 120
4.2.2.6 DPA Titration 120
4.2.2.7 Thermal Denaturation Studies 121
4.2.2.8 Chemical Denaturation Studies 122
4.2.2.9 Acrylamide Quenching Studies 122

4.3. Results and Discussions 123
    4.3.1 Fluorescence Properties of Native Oncomodulin Mutants 123
    4.3.2 Chemical Denaturation of Apo Proteins 127
    4.3.3 Chemical Denaturation of Holo (Ca^{2+}-loaded) Proteins 132
    4.3.4 Chemical Denaturation of Tb^{3+}-loaded Proteins 138
    4.3.5 Thermal Denaturation of Ca^{2+} -free Proteins 142
    4.3.6 Thermal Denaturation of Ca^{2+} -loaded Proteins 147
    4.3.7 Thermal Denaturation of Tb^{3+}-loaded Proteins 150
4.4 Conclusion 153
4.5 References for Chapter 4 154

Chapter 5 Investigation of the Thermal Stability and Terbium Binding Ability of Rat Oncomodulin Entrapped in a sol-gel Matrix 157
5.1 Introduction 157
5.2 Experimental Procedures 161
    5.2.1 Preparation of Protein Doped Sol-Gel Slides 161
    5.2.2 Measurement of Fluorescence Excitation Spectra 161
    5.2.3 Response Time and Kinetics Studies 162
    5.2.4 Thermal Denaturation Studied 162
    5.2.5 Reversibility Studied 163
5.3 Results and Discussions 163
    5.3.1 Spectroscopic Properties of Entrapped Proteins 163
        5.3.1.1 No Extra Calcium Added 163
        5.3.1.2 Extra Calcium Added in gelation buffer 164
    5.3.2 Response Time and Kinetics Studies of Entrapped Proteins 170
    5.3.3 Comparison of the Terbium Binding Ability of CDOM33 and Y57W OM 174
        5.3.3.1 No Extra Calcium Added 174
        5.3.3.2 Extra Calcium Added 175
    5.3.4 Reversibility for Loading of Tb^{3+} with encapsulated CDOM33 178

5.3.5 Thermal Stability Studies for Encapsulated CDOM33 and Y57W 179
5.3.6 Long Term Stability 185
5.4 Conclusions 185
5.5 References for Chapter 5 186

Chapter 6 Conclusions and Future Prospects 188
6.1 Conclusions 188
6.2 Suggestions for Future Work 190
6.2.1 Modification of the sol-gel matrix 191
6.2.2 Encapsulation Proteins with Different Size and Further Stability Studies 191

List of Figures

Figure 1.1 Formation of a protein-doped sol-gel matrix. 4

Figure 1.2 Structure of the tryptophan residue. 15

Figure 1.3 Ribbon diagram of monellin based on the crystal structure. 17

Figure 1.4 The crystal structure of rat oncomodulin. 18

Figure 2.1 Optimal orientation of the sol-gel slide in the light path of the fluorimeter. 38

Figure 2.2 Scattering of light from monoliths containing NATA in the presence and absence of buffer and as a function of different sample orientations. 47

Figure 2.3a Response curves for the addition of various species to free and entrapped monellin. (a). Addition of acrylamide to monellin 53

Figure 2.3b Response curves for the addition of various species to free and entrapped monellin. (b) Addition of GdHCl to monellin 58

Figure 2.4 Stern-Volmer plots for acrylamide quenching of NATA (open symbols) and monellin (closed symbols). 63

Figure 2.5 Fluorescence spectra of 10 mM monellin in 100 mM phosphate buffer solution, pH 7 65

Figure 2.6 Fluorescence spectra of 10 mM NATA. 66

Figure 3.1 Changes in fluorescence intensity for monellin as a function of temperature. 86

Figure 3.2 Changes in fluorescence anisotropy for monellin as a function of temperature. 87

Figure 3.3 Changes in fluorescence intensity for monellin as a function of GdHCl concentration. 94

Figure 3.4 Changes in fluorescence anisotropy for monellin as a function of GdHCl concentration. 95

Figure 3.5 Stern-Volmer plots for acrylamide quenching of monellin at different concentration of GdHCl. 102

Figure 4.1 Fluorescence intensity changes as a function of GdHCl concentration for calcium loaded oncomodulin proteins 130
Figure 4.2 Fluorescence intensity changes as a function of GdHCl concentration for calcium free oncomodulin proteins 135
Figure 4.3 Changes of fluorescence intensity during chemical denaturation of terbium loaded oncomodulin proteins 141
Figure 4.4 Changes of fluorescence intensity as a function of temperature for calcium free oncomodulin proteins 145
Figure 4.5 Changes of fluorescence intensity during thermal denaturation of calcium loaded oncomodulin proteins 149
Figure 4.6 Fluorescence intensity changes during thermal denaturation of terbium loaded oncomodulin proteins 152
Figure 5.1a Fluorescence emission spectra of CDOM33. 166
Figure 5.1b Fluorescence emission spectra of Y57W. 167
Figure 5.2a Fluorescence excitation spectra of CDOM33. 168
Figure 5.2b Fluorescence excitation spectra of Y57W. 169
Figure 5.3 Response curves for interaction of terbium with entrapped CDOM33 with different levels of calcium in the sol-gel matrices. 173
Figure 5.4 Spectra of terbium loaded CDOM33 encapsulated in the sol-gel matrices with different levels of calcium in the matrices. 177
Figure 5.5a Changes in fluorescence intensity for CDOM33 as a function of temperature. 182
Figure 5.5b Changes in fluorescence intensity for Y57W as a function of temperature. 183

List of Tables

Table 1.1 Sol-Gel Entrapment of Biological Molecules. 7

Table 2.1 Response times, time constants and normalized pre-exponential factors for addition of GdHCl, acrylamide or iodide to monellin in solution, wet-aged and dry-aged monoliths. 52

Table 2.2 Stern-Volmer analysis of acrylamide quenching for NATA and monellin in solution, wet-aged and dry-aged TEOS slides. 62

Table 3.1 Fluorescence spectral and steady-state anisotropy data for thermal denaturation of monellin. 83

Table 3.2 Thermodynamic parameters for thermal unfolding of monellin in solution and in wet-aged or dry-aged slides. 90

Table 3.3 Spectral data for chemical denaturation of monellin in solution, wet-aged monoliths and dry-aged monoliths. 93

Table 3.4 Thermodynamic parameters for the GdHCl induced unfolding of monellin. 99

Table 3.5 Stern-Volmer analysis of acrylamide quenching for native and partially denatured monellin in solution. 101

Table 3.6 Stern-Volmer analysis of acrylamide quenching for native and chemically denatured monellin in wet-aged and dry-aged TEOS slides. 101

Table 4.1 Changes in fluorescence properties for apo, Ca^{2+}-loaded and Tb^{3+}-loaded oncomodulin mutants during chemical denaturation. 127

Table 4.2 Free energy changes for chemical unfolding of oncomodulin. 131

Table 4.3a K_{SV} values from acrylamide quenching of holo F102W OM. 133

Table 4.3b Stern-Volmer quenching constants and bimolecular quenching rate constants from acrylamide quenching of oncomodulin mutants. 134

Table 4.4 Changes in fluorescence properties of apo, Ca^{2+}-loaded and Tb^{3+}-loaded oncomodulin mutants during thermal denaturation. 144

Table 4.5 Enthalpy changes for thermal unfolding of oncomodulin mutants. 146

Table 5.1 Kinetics study of the interaction of Tb^{3+} with entrapped CDOM33. 172

Table 5.2 Kinetics study of the interaction of Tb^{3+} with entrapped Y57W. 172

Table 5.3 Percent of Tb^{3+} signal obtained from encapsulated CDOM33 and Y57W. 172

Table 5.4 Comparison of the thermodynamic parameters for thermally induced denaturation of entrapped CDOM33. 181

Chapter 1 Introduction and Theory

1.1 Introduction

1.1.1 Biosensors

Over the past two decades, research on biosensors has increased very rapidly.[1,2,3,4] Numerous reports have reviewed progress and developments on biosensors.[5,6,7,8] Typical biosensors consist of two components: 1) a biologically sensitive molecule which can provide a selective molecular-level recognition reaction and; 2) a transducer which can convert the molecular-level recognition reaction into an analytical signal. Biological materials which are utilized for the development of biosensors include antibodies,[9,10] enzymes,[11,12] DNA/RNA[13,14] and artificial receptors[15] which can interact selectively with a desired analyte. An ideal sensor is required to not only possess high selectivity, but also to have high sensitivity, short response time, long lifetime and good reversibility or regenerability.[1-8] Because of the difficulties associated with interfacing biological materials with inorganic transducers, most biosensors which have been described are still at the development stage, and have not been commercialized.

In order to successfully interface biological materials with inorganic transducers, an efficient immobilization method is required. Traditional immobilization methods include physical adsorption,[16] entrapment inside a semi-permeable membrane,[17] covalent binding[18] and encapsulation into porous organic[19] or inorganic[20] polymer matrices. Although there has been a large amount of work done to improve the efficiency of methods for the

immobilization of biological molecules, there are still a number of problems associated with these methods. For example, desorption and leaching of biomolecules from semi-permeable membranes or polymer matrices results in short lifetimes and difficulty in calibration of the sensor[17]. In addition, denaturation of biomolecules both during and after immoblization or entrapment can dramatically affect the sensitivity and long-term usefulness of biosensors.

In 1990, Avnir and co-workers first demonstrated that active proteins could be encapsulated into an inorganic silica glass matrix derived by the sol-gel process with excellent retention of activity and good long-term stability.[21] This was thought to be because the sol-gel process resulted in a relatively mild environment which was close to physiological conditions. The sol-gel method of encapsulation is unique since the resulting matrices are porous and able to trap large biomolecules with no leaching, but allow small analyte molecules to diffuse in and interact with the entrapped biomolecules. Additionally, the sol-gel derived glass matrices are transparent down to the UV range which make them extremely useful for spectroscopic analysis. Recently, there has been an increasing number of reports concerning the encapsulation of biomolecules within sol-gel derived glasses for biosensor development.[20,22,23,24,25] However, there has been a lack of studies aimed at understanding the internal environment of the silicate matrix and the effect of the internal environment on the structure, stability and activity of the entrapped biomolecules. Furthermore, there have been almost no studies regarding the effect of the sol-gel entrapment on the kinetics of reactions between entrapped proteins and externally added analytes.

1.1.2 Sol-Gel Encapsulation of Biomolecules

While sol-gel based protein encapsulation is relatively new, the sol-gel process itself is not so contemporary in its origins. The first sol-gel synthesis dates back to the mid 1800's when Ebelmen hydrolyzed tetraethylorthosilicate (TEOS) using acid as the catalyst to form glass-like monoliths.[26]

The standard sol-gel process generally begins with an alkoxysilane precursor such as TEOS or tetramethylorthosilicate (TMOS).[27] The formation of sol-gel derived materials has four stages: formation of the sol, gelation, aging and drying. Typically, formation of the gel involves hydrolysis and gelation of TEOS/TMOS in the presence of acid and a large amount of ethanol as a co-solvent. Aging and drying of the sol-gel derived silicate involves heating the gel at high temperatures (between 100 and 180 °C) to efficiently remove the alcohol and water produced during aging. This process has several problems for entrapment of proteins. First, low pH values and large amounts of alcohol during hydrolysis can denature most proteins. Second, high drying temperatures generally prohibit the encapsulation of biomolecules owing to denaturation which occurs at high temperatures and the removal of the internal water which is required for the entrapped biomolecules to be functional. Finally, high drying temperatures can also result in cracking of the silicate and a loss of transparency. For this reason, a modified sol-gel process involving hydrolysis under weak acidic conditions and lower temperature aging and drying is used for encapsulation of biomolecules.[20]

The low temperature sol-gel process consists of a number of modified steps: hydrolysis of alkoxide precursor in aqueous acid or base with subsequent condensation

and polycondensation to form sol, addition of an aqueous buffer solution (containing the proteins) to initiate gelation, preliminary aging either in buffer or in air and finally aging and partial drying of the gel at room temperature or lower over a period of several weeks. The formation of a protein-doped sol-gel material is shown in steps (1) to (4) in Figure 1.1.

Hydrolysis of TEOS is performed under weak acidic conditions at room temperature, usually with the aid of sonication. The hydrolyzed TEOS is a dispersion of colloidal particles in a liquid with diameters from 1-100 nm and is defined as a sol. The pH of the sol can be anywhere from 1-6 depending on the concentration of the acid used. The sol can be used immediately or can be stored at -20°C for several days or weeks to allow condensation and polycondensation to occur at a very slow rate, "ripening" the sol.

(1) $\mathrm{Si(OEt)_4 + nH_2O + H^+ \rightarrow Si(OEt)_{4-n}(OH)_n + n\ EtOH}$ ***Hydrolysis***

(2) $\mathrm{2\ Si(OEt)_{4-n}(OH)_n \rightarrow (OH)_{n-1}(OEt)_{4-n}Si\text{-}O\text{-}Si(OEt)_{4-n}(OH)_n + H_2O}$ ***Condensation***

$\mathrm{n\ \text{-}Si\text{-}O\text{-}Si\text{-} \rightarrow [\text{-}Si\text{-}O\text{-}Si\text{-}O\text{-}Si\text{-}O\text{-}Si\text{-}O\text{-}]_n + H_2O}$ ***Polycondensation***

(3) $\mathrm{n\ [\text{-}Si\text{-}O\text{-}Si\text{-}O\text{-}Si\text{-}O\text{-}Si\text{-}O]_n}$ + buffer + protein → Entrapped Protein ***Gelation***

(4) Condensation and Polycondensation continue for many days, shrinking gel ***Aging***

Figure 1.1 Formation of a protein-doped sol-gel matrix.

Gelation is induced by adding a buffer containing biomolecules to the sol to bring the pH from ~5 up to close to physiological pH. This process causes gelation to occur within several minutes. The resulting gel is an interconnected rigid network with pores of submicrometer dimensions and polymeric chains whose average length is greater than a micrometer.[27] At this point, the material is a solid containing the entrapped protein with a large amount of entrapped water and a relatively high amount of residual alcohol from the hydrolysis of TEOS.

Following gelation, the matrix can be aged under ambient conditions or at a reduced temperature of 4°C. Aging at 4°C is preferred for gels containing biomolecules to prevent denaturation and improve the long term stability of the biomolecules. During aging, both condensation and polycondensation will continue, leading to a higher degree of cross-linking and further entrapping of the internal matrix (i.e., biomolecules) inside the gel. The liquid in the pore is excluded during aging and the gel shrinks and hardens to form a transparent glass. Uniform drying of the gel is required to prevent cracking during aging. Aging and drying can take up to 30 days during which time the gel will shrink by up to 80% in weight and volume.

Since the entrapped protein needs to be hydrated to function, the aged gels must be re-hydrated before use. The average final pore size of gels formed by the previously described method is usually between 6 and 10 nm in diameter.[28] The small pore radii lead to large capillary pressures when the aged gels are exposed to liquid. The gel also contains a very large amount of chemisorbed hydroxyl groups on the surface of the pores which increases the capillary pressure within the gel. For these reasons, rehydration of the

gels has to be performed slowly and carefully to avoid large hydrostatic pressure gradients which can crack the gel. In addition, if rehydration is not done, the pore sizes may decrease too much during aging and either "crush" the protein, irreversibly altering its conformation, or inhibit the passive diffusion of the analytes into the gels. For this reason, after the aging process reaches a certain degree, the gels need to be stored under 100% humidity conditions to stop the condensation and shrinkage of the gel.

There has been a large amount of research which has shown that active biological molecules can be encapsulated into a sol-gel matrix with maintenance of their bioactivity using the above protocols.[20] Various biological molecules have been successfully encapsulated into sol-gel derived matrices, including proteins,[29,30,31,32] enzymes,[19,33,34,35,36,37] antibodies,[38] antigens[39] as well as whole cells.[40] Table 1.1 summarizes the results obtained from sol-gel encapsulated biological molecules to date.

Even though many reports have shown that enzymes and other biological molecules can retain their activity and native structure upon encapsulation into the sol-gel matrices, in many cases only a fraction of the bioactivity of the entrapped molecules was retained.[20] In some cases, the entrapped molecules also lost their native structure and virtually all of their activity.[29] Such results indicated a lack of understanding of how the sol-gel process and the internal environment affect the structure and stability of the entrapped proteins. An understanding of the effects of the sol-gel process on the structure and stability of entrapped biological molecules is essential for the development of biosensor devices since the calibration curve, linear range, detection limit and long

term stability of the sensor will be affected by the encapsulation process. Control of all these parameters is required for the commercialization of the biosensors.

Table1.1 Sol-Gel Entrapment of Biological Molecules.

Biorecognition molecules	**comments**	**references**
Glucose oxidase	80% activity retained, stable for over 2 months.	32
Alkaline phosphatase	10% activity retained, active for over 2 months	19
trypsin	45% activity retained regularly, but close to 100% activity was obtained by adding nonactive BSA to prevent aggregation, retained full activity for several months.	33
CuZn-superoxide dismutase	retained activity, able to bind with metal ions reversibly*	31
urease	retained >95% activity for over 6 weeks	34
cytochrome c	able to perform oxidation-reduction reaction repeatedly*	30, 31
oxalate oxidase	retained activity, the coupled enzyme reactions occurred fully in the gel	35
cholinesterase	retained activity*	36
bovine serum albumin	retained native structure, lost conformational motion	28,29
horse heart myoglobin	lost structure and most of the activity	28
antifluorescein	affinity constant decreased 2-order-of-magnitude, stable for 5 weeks	37
yeast cells	retained activity*	39

* no long-term stability study mentioned.

1.2 Research Motivation

1.2.1 Project Objectives

Our group is interested in the development of efficient protein immobilization methods for the purpose of developing optical biosensors. The sol-gel encapsulation method attracted us because of its potential advantages, including optical transparency, ability to cast the silicate material into different shapes (monoliths or thin films), ability to control the final characteristics of the material by use of organic silane polymer precursors, potential to improve protein stability, low cost and relatively straight forward preparation procedures. Almost all reports on the stability of sol-gel entrapped proteins have concerned only the measurement of enzyme activity. However, there are very few studies which describe the initial structure and stability of entrapped proteins, and how the sol-gel process affects the evolution of protein structure and therefore the long-term stability.

In this project, we have studied single tryptophan proteins encapsulated inside TEOS derived sol-gel thin slides (final dimensions 20 mm x 5 mm x 0.2 mm). The thin sol-gel slides were used since they are the intermediate form between the bulk monolith and the thin film. Thus, this format provides higher signal-to-noise ratios than thin films and shorter kinetics than bulk monoliths.

By examining the protein-doped thin sol-gel slides by fluorescence methods, we are attempting to answer questions such as: 1) What is the internal environment of the sol-gel matrix like? 2) Can the encapsulated protein maintain its native structure? 3) Can the encapsulated protein still be functional and interact with various species? 4) What is the

rate of the protein-analyte reactions? 5) Is it possible for entrapped proteins to undergo conformational changes? 6) Is sol-gel encapsulation able to improve the thermal and chemical stability of proteins, and if so, how? 7) Can the encapsulation protocol be manipulated to maximize stability, reactivity while minimizing response time?

1.2.2 Thesis Outline

This thesis is organized such that it begins with simple systems and issues and then moves toward more complex topics. The structure is as follows: 1) Relevant background and theory. 2) Examination of the environment and reaction kinetics within the TEOS derived sol-gel matrix containing the single Trp protein monellin. In this section, various parameters of the sol-gel encapsulation method are optimized and a model experimental system is established for further experiments. 3) The study of the conformational flexibility and stability of monellin in solution and when entrapped in TEOS derived sol-gel matrices. 4) The study of the effects of metal binding affinity and metal loading on the stability of site-directed rat oncomodulin mutants in solution. In this section, the focus shifts to the protein oncomodulin. This was done since monellin can not bind with any analytes and thus, the bioactivity of monellin could not be monitored. A detailed study of the behaviour of oncomodulin in solution was required prior to encapsulation to obtain a better understanding of the factors which affect the stability of the protein. 5) A study of the terbium binding capability, kinetics and thermal stability of oncomodulin proteins encapsulated in TEOS derived sol-gel matrices. In this section, two oncomodulin mutants were chosen for entrapment in sol-gel derived matrices. The ability of the entrapped

proteins to bind terbium and the thermal stability of these proteins were studied at different levels of calcium. 6) Conclusions and suggestions for future work.

1.3 Theory and Techniques

1.3.1 Fluorescence Spectroscopy

Fluorescence is the most commonly used technique for optical biosensor development. The main reason for this is that fluorescence offers extremely high sensitivity, high information content and has a low detection limit. In addition, the fluorescence signal is extremely sensitive to the local environment of the probe, which makes it very useful for examining the internal environment of protein doped sol-gel derived matrices. A detailed description of fluorescence principles and applications is given by Lakowicz.[41,42,43,44,45]

Fluorescence measurements can be broadly classified as steady-state techniques and time-resolved techniques. In this project, the majority of experiments involved the measurement of steady-state fluorescence . However, we made use of lifetime (τ) values to get bimolecular quenching rate constant (k_q) values from quenching studies.

Information obtained from steady-state fluorescence spectroscopy includes intensity, quantum yield, excitation and emission wavelength, and spectral full width at half maximum (FWHM) values. All of these parameters will change when the local environment of the probe is changed.

The fluorescence emission wavelength is most commonly associated with solvent polarity. The orientation of solvent dipoles around the excited state dipole produces an

electric field which stabilizes the excited state at a lower energy than is observed in the absence of a polar solvent, thus producing a shift of the fluorescence emission to longer wavelengths.[41] An equation which can be used to estimate the magnitude of the wavelength shift has been presented by Lippert:[46]

$$\bar{\nu}_a - \bar{\nu}_f \cong \frac{2}{hc}\left(\frac{\varepsilon - 1}{2\varepsilon + 1} - \frac{n^2 - 1}{2n^2 - 1}\right)\frac{(\mu^* - \mu)}{a^3} + const \qquad (1.1)$$

where $\bar{\nu}_a$ and $\bar{\nu}_f$ represent the absorption and fluorescence transition maxima in wavenumbers (cm^{-1}), respectively, h is the Planck's constant, c is the velocity of light, n is the refractive index of the solvent, ε is the dielectric constant which describes the orientational polarizablility of the fluorophore, μ^* and μ are the dipole moments of the excited state and ground state fluorophores, respectively, a is the radius of the fluorophore cavity in the solvent matrix, and *const* represents the inherent Stoke's shift due to vibrational relaxation of the excited state. This parameter is very important for our studies since it indicates the local environment of the entrapped proteins and provides information on whether the entrapped proteins maintain their native structure or not.

The intensity of fluorescence radiation is dependent on a number of parameters as described in the following equation:

$$F(\lambda_{em}) = 2.303K(\lambda_{em})I_0(\lambda_{ex})\varepsilon(\lambda_{ex})bC\Phi \qquad (1.2)$$

where $F(\lambda_{em})$ is the fluorescence intensity at a given wavelength, K represents a wavelength dependent instrumental response coefficient, $I_0(\lambda_{ex})$ is the excitation intensity, $\varepsilon(\lambda_{ex})$ is the molar extinction coefficient at the excitation wavelength, b is the excitation

pathlength, C is the molar concentration of the fluorophore, and Φ is the quantum yield of the fluorophore.

The quantum yield (Φ) is defined as the ratio of molecules that fluoresce to the total number of molecules excited. This ratio is usually determined from the ratio of the radiative rate constants to the sum of the radiative and all the non-radiative rate constants as shown in the following equation:

$$\Phi = \frac{k_r}{k_r + \sum k_{nr}} = k_r \tau \qquad (1.3)$$

where k_r is the rate constant for radiative emission, Σk_{nr} is the sum of all the non-radiative rate constants, and τ is the average lifetime of the excited fluorophore.

Another parameter which can give information on the environment of fluorophores is defined as the steady-state anisotropy (r). Anisotropy is given as:

$$r = \frac{I_z - I_y}{I_z + 2I_y} \qquad (1.4)$$

where I_z represents the parallel polarized emission of the fluorophore with respect to the polarized excitation source and I_y represents the perpendicular polarized emission. From the anisotropy values, the mobility of a fluorescent moiety in a protein molecule can be obtained. A mobile fluorophore will have a small anisotropy value (lowest limit $r = 0$) and an immobile fluorophore will have a large anisotropy value (highest limit $r_0 = 0.4$).

The fluorescence lifetime (τ) is defined as the average time required for an ensemble of excited fluorophores to decay to $1/e$ of its initial intensity(I_0), and is given by the following equation:

pathlength. F is the total integrated emission of the fluorophore, and Φ is the quantum yield of the fluorophore.

The quantum yield (Φ) is defined as the ratio of the number of photons emitted to the total number of molecules excited. The quantum yield describes the efficiency of the radiative processes relative to the sum of the radiative and all the non-radiative rate constants as shown in the following equation:

$$\Phi = \frac{k_f}{k_f + \sum k_{nr}} = k_f \tau \qquad (1.3)$$

where k_f is the rate constant for radiative emission, $\sum k_{nr}$ is the sum of all the non-radiative rate constants, and τ is the average lifetime of the excited fluorophore.

Another parameter which can give information on the environment of fluorophores is defined as the steady-state anisotropy (r). Anisotropy is given as:

$$r = \frac{I_{\parallel} - I_{\perp}}{I_{\parallel} + 2I_{\perp}} \qquad (1.4)$$

where $I_{\parallel}$ represents the parallel emission intensity of the fluorophore with respect to the polarized excitation source and $I_{\perp}$ represents the perpendicular polarized emission. From the anisotropy values, the mobility of a fluorescent moiety in a polymer system can be measured. A mobile fluorophore will have a small anisotropy value (close to 0) while an immobile fluorophore will have a large anisotropy value (closer to 0.4).

The fluorescence lifetime (τ) is defined as the average time required for a population of excited fluorophores to decay to 1/e of its initial intensity, and is related to the following equation:

$$I(\tau) = I_0 e^{-t/\tau} \tag{1.5}$$

where :

$$\tau = \frac{1}{k_r + k_{nr}} \tag{1.6}$$

Another technique which is often used to examine protein structure is fluorescence quenching. Information on the accessibility of the analyte to the fluorophore can be obtained by examining the quenching of the fluorophore by the external quencher. Fluorescence quenching simply refers to any process in which the interaction of an external reagent (a quencher) with the fluorophore results in a decrease in the fluorescence intensity. Quenching of the fluorophore can occur dynamically when the quencher diffuses through the surrounding media to contact with the fluorophore or statically when the quencher is very close to the fluorophore at the moment of excitation and diffusion of the quencher is no longer a consideration. Usually, both dynamic and static quenching can be observed concurrently. A modified form of Stern-Volmer equation accounting for both dynamic and static quenching can be used to study the accessibility of the quencher to the fluorophore, as given by:

$$\frac{F_0}{Fe^{V[Q]}} = 1 + K_{SV}[Q] = 1 + k_q \tau_0 [Q] \tag{1.7}$$

where F_0 is the initial fluorescence in the absence of quencher, F is the fluorescence intensity at a given concentration of quencher, V represents the active volume of the quencher sphere in M^{-1}, $[Q]$ represents the molar concentration of the quencher, K_{SV} is the Stern-Volmer quenching constant (M^{-1}) and k_q is the bimolecular quenching constant (M^{-}

$^{1}.s^{-1}$). Higher K_{SV} or k_q values indicate more accessiblility of the quencher to the fluorophore.

Another fluorescence parameter used in this thesis was energy transfer. Energy transfer occurs in cases where an excited fluorophore encounters a second species with an available excited state of equal energy. The transfer of energy occurs mainly by two mechanisms, electron exchange (Dexter) and dipole-dipole (Förster) energy transfer. Dexter energy is of direct relevance to this work, and is described in more detail below.

Energy transfer by electron exchange, as described by Dexter,[47] requires spectral overlap of the donor emission spectrum with the acceptor absorption spectrum. It usually happens as a result of a short range (<10 Å) interaction between the donor and the acceptor. Generally, physical contact of the donor and acceptor molecules is required for efficient energy transfer, and the transfer rate decreases rapidly as the donor-acceptor distance increases. Dexter described the rate of electron exchange, k_{EE}, as a function of distance between donor and acceptor species by:[47]

$$k_{EE} = KJ_D \cdot e^{-2R_{DA}/L} \tag{1.8}$$

where K is a constant related to specific orbital interactions, J_D is the spectral overlap integral of donor emission and acceptor absorbance normalized to the molar absorptivity of the acceptor, R_{DA} is the donor-acceptor separation distance and L is the mean contact radius of the two species. In this thesis, Dexter energy transfer is utilized for terbium binding studies with oncomodulin mutants.

1.3.2 Intrinsic Tryptophan Fluorescence

There are three amino acid residues responsible for intrinsic protein fluorescence, phenylalanine (Phe), tyrosine (Tyr) and tryptophan (Trp). All these residues can be excited in the UV region, but only Trp can be exclusively excited (at 295 nm or greater) in the presence of both Phe and Tyr.

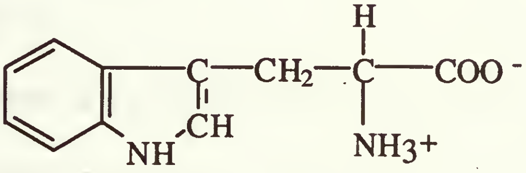

Figure 1.2 Structure of the tryptophan residue with the charges present at pH 7.

Trp exhibits a high quantum yield of 0.20 at 350 nm when excited at 280 nm and is much more sensitive to local environmental polarity than the other two fluorescent residues.[48] These characteristics make it most suitable for protein structural studies. Proteins which contain a single Trp residue are usually used for such studies since they provide a relatively simple system for examining fluorescence lifetimes and a simpler system for probing rotational anisotropy or exposure of Trp to quenchers. An advantage of utilizing the intrinsic fluorescence of Trp residues is that it eliminates the possibility of altering protein structure, which may occur for extrinsic fluorescence labelling protocols.[49]

1.3.3 Proteins Studied

The proteins studied in this project were monellin and rat oncomodulin site-directed mutants each containing a single Trp residue. Both of these proteins are relatively

small in size. Monellin is an incredibly sweet tasting protein which is isolated from the serendipity berry found in Western Africa.[50] The MW of monellin is 11 kDa. It is comprised of 95 residues which are present as two strands; an A strand which has 45 residues and a B strand which has 50 residues.[51] The two strands are held together through strong hydrophobic interactions leaving one free sulfhydryl group at Cys-41.[52] The Trp residue is located at position 3 on the B strand. The structure of monellin is shown in Figure 1.3.

Oncomodulin is comprised of 108 residues with the MW of 12 kDa. Natural (wild-type) oncomodulin does not have a Trp residue.[53] The site-directed mutagenesis technique makes it possible to insert a Trp residue at different locations within the protein.[54] The crystal structure of oncomodulin is shown in Figure 1.4. What is unique for this protein is that it possesses two calcium binding loops in its structure and the stability of this protein can be altered by loading different types and amounts of metal ions. This protein is able to bind with the lanthanide ion terbium, which provides an addition fluorescence signal due to energy transfer. This property makes it possible to monitor both the stability and bioactivity of this protein.

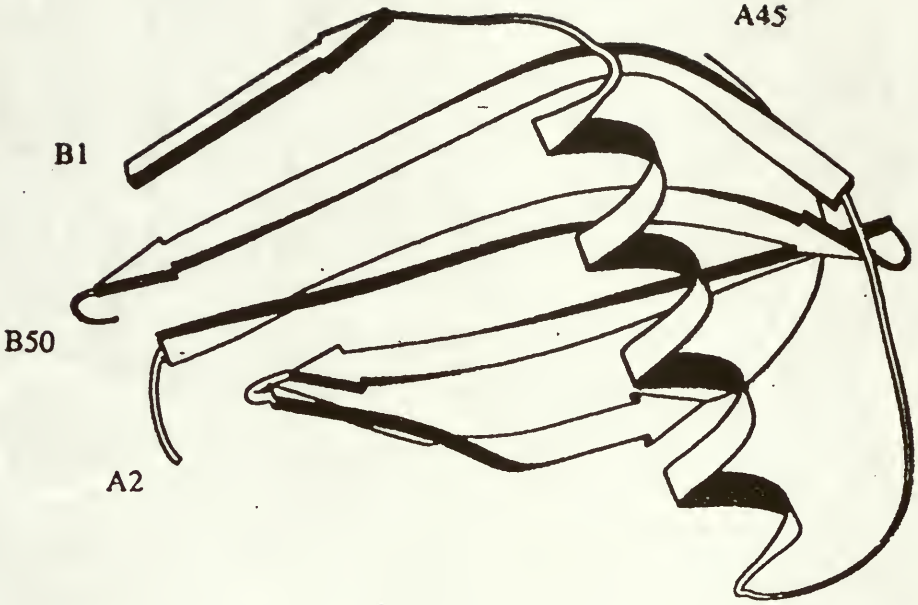

A1 A5 A10 A15 A20
A chain Phe Arg Glu Ile Lys Gly Tyr Glu Tyr Gln Leu Tyr Val Tyr Ala Ser Asp Lys Leu Phe
A25 A30 A35 A40
Arg Ala Asp Ile Ser Glu Asp Tyr Lys Thr Arg Gly Arg Lys Leu Leu Arg Phe Asn Gly
A45
Pro Val Pro Pro Pro

B1 B5 B10 B15 B20
B chain Gly Glu Trp Glu Ile Ile Asp Ile Gly Pro Phe Thr Gln Asn Leu Gly Lys Phe Ala Val
B25 B30 B35 B40
Asp Glu Glu Asn Lys Ile Gly Gln Tyr Gly Arg Leu Thr Phe Asn Lys Val Ile Arg Pro
B45 B50
Cys Met Lys Lys Thr Ile Tyr Glu Asn Glu

Figure 1.3. Ribbon diagram of monellin based on the crystal structure. The primary sequence of monellin is shown below.(from reference 52)

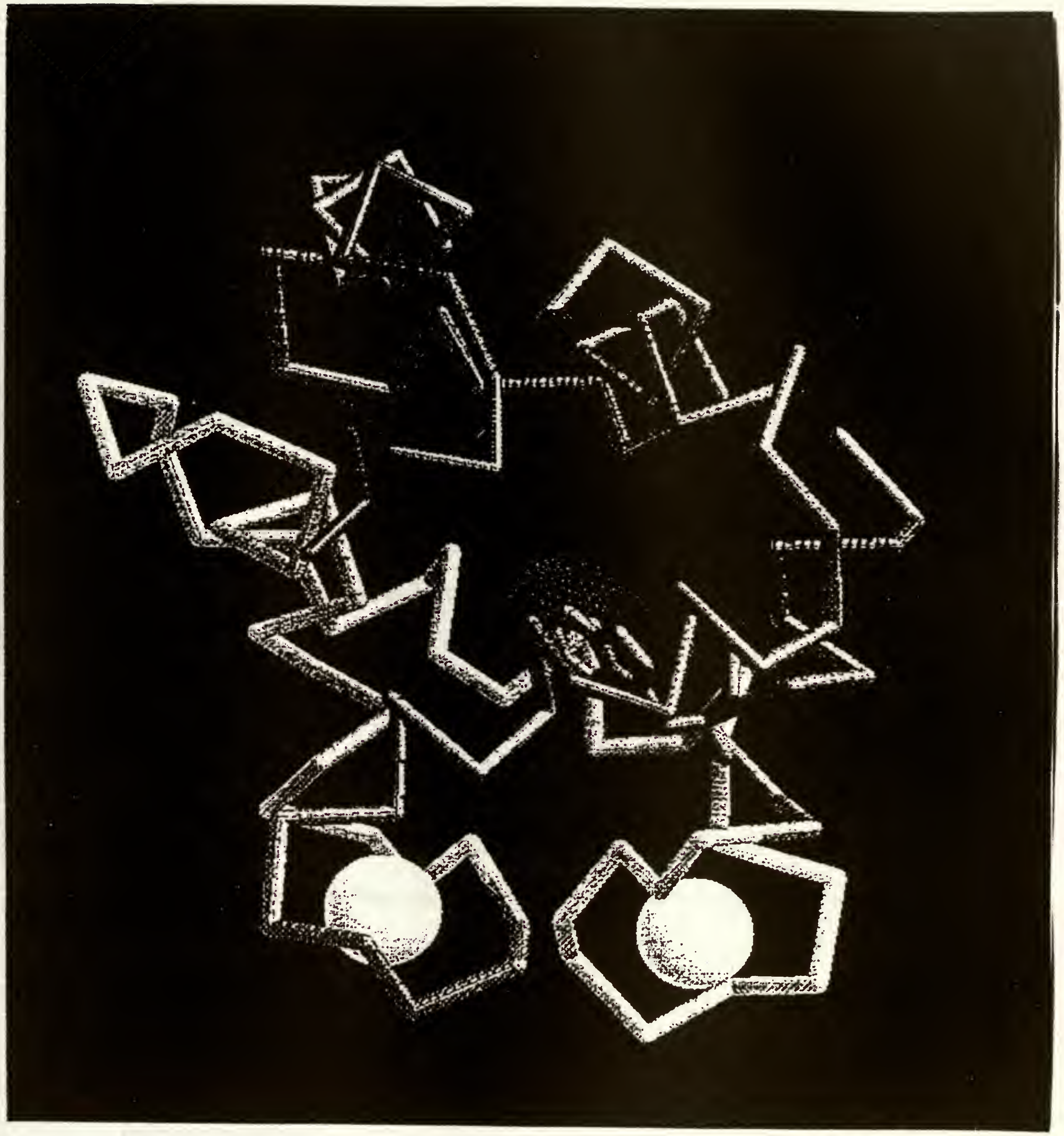

Figure 1.4 Crystal structure of rat oncomodulin.(from Entrez 3D Structure Database)

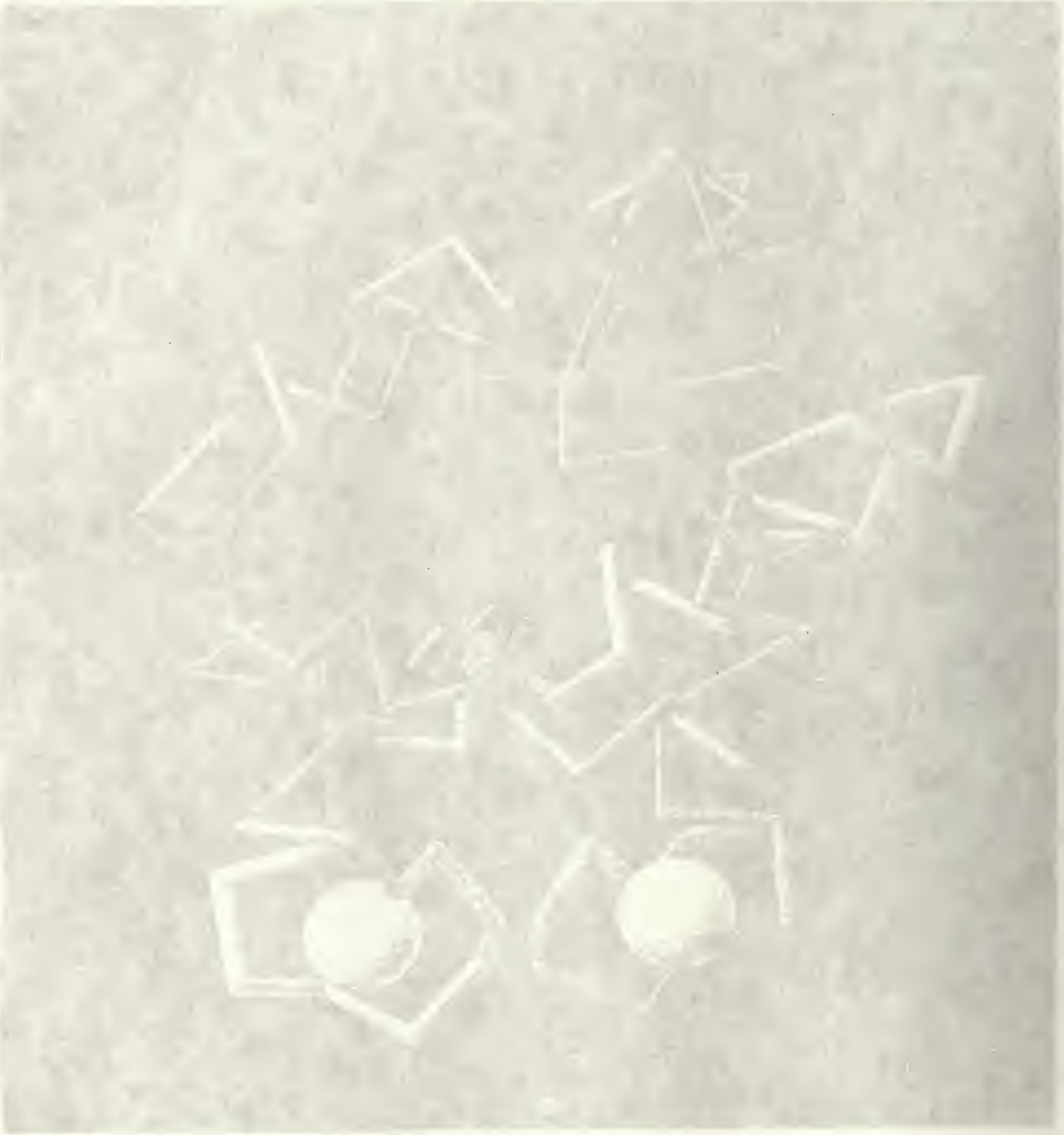

[illegible]

1.3.4 Protein Unfolding Studies

1.3.4.1 Chemical Denaturation Studies

Solvent-induced protein unfolding can be detected as a function of denaturant concentration by using any observable signal giving a detectable difference between the native and denatured states. Since the unfolding process is considered to be a reversible process, the unfolding free energy $\Delta G_{F\rightarrow U}$ can be calculated from the unfolding curve. In our case, the integrated fluorescence intensity (F_D) was plotted versus the concentration of denaturant and the linear extrapolation method[55,56,57] was used evaluate the free energy change for conversion of native to denatured protein in the presence of denaturant. The following linear relationship describes the thermodynamics of denaturant induced unfolding of proteins:[58,59]

$$\Delta G_{F\rightarrow U} = \Delta G^{0}{}_{(F\rightarrow U)} + m_G[D] \tag{1.9}$$

Plotting the observed free energy data ($\Delta G_{F\rightarrow U}$) as a function of denaturant and extrapolating the data to zero denaturant concentration will give the unfolding free energy $\Delta G^{\circ}{}_{F\rightarrow U}$. The observed free energy $\Delta G_{F\rightarrow U}$ is related to the equilibrium constant for unfolding by the following equation:

$$\Delta G_{F\rightarrow U} = -RT\ln K_{obsd} \tag{1.10}$$

The equilibrium constant K_{obsd} can be related to the change of fluorescence intensity by the following equation:

$$K_{obsd} = (F_N - F_D)/(F_D - F_U) \tag{1.11}$$

where F_D is the value of the fluorescence intensity at a given concentration of denaturant, $[D]$, F_N and F_U are the initial and final intensity respectively. Evaluation of equilibrium constants in the transition region requires extensions of the pre- and postunfolding base lines into the transition region. These extensions are represented by the following equations:

$$F_{\mathrm{N}} = F^{\circ}_{\mathrm{N}} + m_{\mathrm{N}}[\mathrm{D}] \quad \text{and} \quad F_{\mathrm{U}} = F^{\circ}_{\mathrm{U}} + m_{\mathrm{U}}[\mathrm{D}] \tag{1.12}$$

Combination of equations 1.9-1.12 results in a single expression as shown below:

$$F_D = \frac{(F_N + m_N[D]) + (F_U + M_U[D]\exp\{\Delta G^0{}_{(F\rightarrow U)} / RT + m_G[D] / RT\}}{1 + \exp[-(\Delta G^0{}_{(F\rightarrow U)} / RT + m_G[D] / RT)]} \tag{1.13}$$

where F_D is the value of the fluorescence intensity at a given concentration of denaturant, $[D]$, R is the gas constant and T is the temperature. The remaining six terms are fitting parameters, where F_N and F_U are the values of the intensity extrapolated to zero concentration of denaturant for the native and unfolded states, respectively, m_N and m_U are the slopes for the dependencies of F_N and F_U on denaturant concentration, $\Delta G_{(F\rightarrow U)}$ is the free energy of unfolding, and m_G is the slope describing the dependence of $\Delta G_{(F\rightarrow U)}$ on denaturant concentration. This equation relates F_{D} and denaturant concentration, [D], with F°_{N}, F°_{U}, m_{N}, m_{U}, m_{G}, and $\Delta G^0{}_{(F\rightarrow U)}$ as fitting parameters. Transition midpoint ($C_{1/2}$) is calculated by dividing $\Delta G^0{}_{(F\rightarrow U)}$ by $-m_{\mathrm{G}}$.

1.3.4.2 Thermal Denaturation Studies

For thermally induced unfolding, analysis of fluorescence data provides information regarding the values of the enthalpy change ΔH^0_{un} and entropy change ΔS^0_{un} for protein unfolding, and also provides the transition temperature, T_{un}, which equals $\Delta H^0_{un} / \Delta S^0_{un}$.[52] The enthalpy change and entropy change can be obtained by fitting the following equation:

$$F_T = \frac{(F_{0N} + s_N T) + (F_{0U} + s_U T)\exp\{-\Delta H^0{}_{un} / RT + \Delta S^0{}_{un} T / RT\}}{1 + \exp[-(\Delta H^0{}_{un} / RT + \Delta S^0{}_{un} T / RT)]} \tag{1.14}$$

where F_T is the fluorescence intensity at a given temperature T, F_{0N} and F_{0N} are the fluorescence intensity of the native state and unfolded state at a given reference temperature (20°C), s_N and s_U are the temperature dependence of the fluorescence of the native and denatured state and R is the gas constant. The free energy change for unfolding (ΔG^0_{un}) can be determined by using equation (1.15), with a reference temperature (T_r) of 293K(20°C)

$$\Delta G^0{}_{un}(T_r) = \Delta H^0_{un} - T_r \Delta S^0_{un} + \Delta C_{p,un}[(T_r - T_{un}) - T \ln(T_r / T_{un})] \tag{1.15}$$

where $\Delta C_{p,un}$ is differential heat capacity for unfolding, and accounts for the temperature sensitivity of the entropy and enthalpy terms on going from T_r to T_{un}. Assuming that $\Delta C_{p,un}$ is not very sensitive to the temperature in the vicinity of T_r to T_{un}, ΔH^0_{un} and ΔS^0_{un} will not depend on temperature. Thus, the above equation can be simplified to the following equation.[60]

$$\Delta G^0{}_{un}(T_r) = \Delta H^0_{un} - T_r \Delta S^0_{un} \tag{1.16}$$

1.3.5 Kinetics of Reactions

The kinetics of protein-analyte interactions can be examined by analyzing the response curves using kinetic rate equations.[61] Both the orders of the reactions and rate constants or mean response times can be determined by fitting the response curves to different kinetic rate equations.

If the reaction is a zero order one, the response curve is a linear equation. If the reaction is a first order one, the response curve can be fit to an exponential equation. For a second order reaction, the response curve can be fit to a reciprocal equation. A general first order rate equation is shown below:[61]

$$I(t) = I_0 + A_1 e^{-t/t_1} \tag{1.17}$$

where $I(t)$is the fluorescence intensity at a given time t, I_0 is the initial fluorescence intensity at time zero, A_1 is the amplitude and t_1 represents the time constant. The mean response time is defined as the time required for the intensity to reach $1/e$ of it's initial intensity. When there are two components in the reaction system and both of the two components proceed by a first order reaction, the response curve can be fit to a sum of two first order rate equations as shown below:

$$I(t) = I_0 + A_1 e^{-t/t_1} + A_2 e^{-t/t_2} \tag{1.18}$$

where t_1 and t_2 represent the time constants of the first and second components respectively, and $A_1$and A_2 are the normalized amplitudes of each component ($\sum_i A_i = 1$).

Here, the mean response time is given by:

$$\langle t \rangle = \sum_i A_i t_i \tag{1.19}$$

1.4 References for Chapter 1

1. Vo-Dinh, T.; Griffin, G. D.; Sepaniak, M. J. *Fiber Optic Chemical Sensors and Biosensors*; Vol. II, Wolfbeis, O. S., Ed., CRC Press, Boca Raton, **1991**.
2. Vadgama, P.; Crump, P.W. *Analyst.* **1992**, 117, 1657.
3. Mathewson, P. R.; Finley, J. W. *Biosensor Design and Application*; American Chemical Society , Washington D. C. **1992**.
4. Taylor, R. F. *Immobilized Antibody- and Receptor-Based Biosensors in Protein Immobilization; Fundamentals and Applications*; Taylor, R. F., Ed., Marcel Dekker, Inc,: New York, **1991**.
5. Thompson, M.; Krull, U. J. *Anal. Chem.* **1991**, 63, 393A.
6. Janata, J.; Josowicz, M.; DeVaney, D. M. *Anal. Chem.* **1994**, 66, 207R.
7. Rogers, K. S.; Gerlach, C. L. *Environmental Science & Technology/ News*, **1996**, 30, 478A.
8. Morgan, C. L.; Newman, D. J.; Price, C. P. *Clin. Chem.* **1996**, 42, 193.
9. Bright, F. V.; Betts, T. A.; Litwiler, K. S. *Anal. Chem.* **1990**, 62, 1065.
10. Shriver-Lake, L. C.; Breslin, K. A.; Charles, P. T.; Conrad, D. W.; Golden, J. P.; Ligler, F. S. *Anal. Chem.* **1995**, 67, 2431.
11. Riklin, A.; Katz, E.; Willner, I.; Stocker, A.; Buckman, A. *Nature* **1995**, 376, 672.
12. Willer, I.; Heleg-Shabati, V.; Blonder, R.; Katz, E.; Tao, G. *J. Am. Chem. Soc.* **1996**, 118, 10321.
13. Vo-Dinh, T.; Houck, k.; Stokes, D. L. *Anal. Chem.* **1996**, 66, 3379.

14. Abel, A. P.; Weller, M. G.; Duveneck, G. L.; Ehrat, M.; Widmer, M. *Anal. Chem.* **1996**, 68, 2905.

15. Lundgren, J. S.; Bright, F. V. *Anal. Chem.* **1996**, 68, 3377.

16. Okahata, Y.; Ebato, H. *Anal. Chem.* **1991**, 63, 203.

17. Blair. T. L.; Yang, S.; Smith-Palmer, T.; Bachas, L. G. *Anal. Chem.* **1994**, 66, 330.

18. Tromberg, B. J.; Sepaniak, M. J.; Vo-Dinh, T.; Griffin, G. D. *Anal. Chem.* **1987**, 59, 1226.

19. Pantano, P.; Walt, D. R. *Anal. Chem.* **1995**, 67, 481A.

20. Avnir, D.; Braun, S.; Lev, O.; Ottolenghi, M. *Chem. Mater.* **1994**, 6, 1605.

21. Braun , S.; Rappoport, S.; Zusman, R.; Avnir, D.; Ottolenghi, M. *Mater. Lett.* **1990**, 10, 1.

22. Lundgren, J.S.; Bright, F.V. *Anal. Chem.* **1996**, 68, 3377.

23. Narang, U.; Jordan, J.D.; Bright, F.V.; Prasad, P.N. *J. Phys. Chem.* **1994**, 98, 8101.

24. Nishida, F.; McKiernan, J.M.; Dunn, B.; Zink, J.I.; Brinker, C.J.; Hurd, A.J. *J. Amer. Ceram. Soc.* **1995**, 78, 1640.

25. Dave, B.C.; Soyez, H.; Miller, J.M.; Dunn, B.; Valentine, J.S.; Zink, J.I. *Chem. Mater.* **1995**, 7, 1431.

26. Ebelmen, M. *Ann. Chimie. Phys.* **1846**, 16, 129.

27. Brinker, C.J.; Scherer, G.W. *Sol-Gel Science*, Academic Press: New York, **1989**.

28. Braun, S.; Shtelzer, S.; Rappoport, S.; Avnir, D.; Ottolenghi, M. *J. Non-Cryst. Solids*, **1992**, 147, 739.

29. Edmiston, P.L.; Wambolt, C.L.; Smith, M.K.; Saavedra, S.S. *J. Coll. Int. Sci.* **1994**, 163, 395.

30. Wambolt, C.L.; Saavedra, S.S. *J. Sol-Gel Sci. Tech.* **1996**, 7, 53.

31. Dave. B. C.; Miller, J.M.; Dunn, B.; Valentine, J.S.; Zink, J. I. *J. Sol-Gel Sci. Tech.* **1997**, 8, 629.

32. Ellerby, L. M.; Nishida, C. R.; Nishida, F.; Yamanaka, S. A.; Dunn, B.; Valentine, J.S.; Zink, J.I. *Science* **1992**, 255, 1113.

33. Narang, U.; Prasad, P.N.; Bright, F.V.; Kumar, A.; Ramanathan, K.; Kumar, N.D.; Malhotra, B.D.; Kamalasanan, M.N.; Chandra, S. *Anal. Chem.* **1994**, 66, 3139.

34. Shtelzer, S.; Rappoport, S.; Avnir, D.; Ottolenghi, M.; Braun, S. *Appl. Biochem.* **1992**, 15, 227.

35. Narang, U.; Prasad, P.N.; Bright, F.V.; Kumar, A.; Kumar, N.D.; Malhotra, B.D.; Kamalasanan, M.N.; Chandra, S. *Chem. Mater.* **1994**, 6, 1596.

36. Yamanaka, S. A.; Nguyen, N.; Dunn, B.; Valentine, J.S.; Zink, J. I. *J. Sol-Gel Sci. Tech.* **1996**, 7, 117.

37. Akbarian, F.; Lin, A.; Dunn, B.; Valentine, J.S.; Zink, J. I. *J. Sol-Gel Sci. Tech.* **1997**, 8, 1067.

38. Wang, R.; Narang, U.; Prasad, P.N.; Bright, F.V. *Anal. Chem.* **1993**, 65, 2671.

39. Roux; C.; Livage, J.; Farhati, K.; Monjour, L. *J. Sol-Gel Sci. Tech.* **1997**, 8, 663.

40. Inama, L.; Dire, S.; Carturan, G.; Carazza, A. J. *Biotechnol.* **1993**, 30, 1997.

41. Lakowicz, J. R. *Principles of Fluorescence Spectroscopy*, Plenum Press, New York, **1983**.

42. Lakowicz, J. R. (Ed.) *Topics in Fluorescence Spectroscopy, Vol. 1.: Techniques*, Plenum Press, New York, **1991**.

43. Lakowicz, J. R. (Ed.) *Topics in Fluorescence Spectroscopy, Vol. 2.: Principles*, Plenum Press, New York, **1991**.

44. Lakowicz, J. R. (Ed.) *Topics in Fluorescence Spectroscopy, Vol. 3.: Biochemical Applications*, Plenum Press, New York, **1991**.

45. Lakowicz, J. R. (Ed.) *Topics in Fluorescence Spectroscopy, Vol. 4.: Probe Design and Chemical Sensing*, Plenum Press, New York, **1994**.

46. Lippert, V. E., Z. *Electrochem.* **1957**, 61, 962.

47. Dexter, D. L.J. *Chem. Phys.* **1953**, 21, 836.

48. Privalov, P. L., *Protein Folding*, Creighton, T. E. Ed., W. H. Freeman and Co. , New York, **1992**, p.84.

49. Frieden, C.; Jiang, N.; Cistola, D.P. *Biochem.* **1995**, *34*, 2724.

50. Penarrubia,L.; Kim, R.; Giovannoni, J.; Kim, S. H.; Fischer, R. L. *Biotechnology*, **1992**, 10, 561.

51. a) Morris, J.; Cagan, R.H. *Biochim. Biophys. Acta* **1972**, 261, 114.

b) Van der Wel, H. *FEBS Lett.*, **1972**, 21, 88.

52. Ogata, C.; Hatada, M.; Tomlinson, G.; Shin, W.C.; Kim, S. H. *Nature*, **1987**, 328, 739

53. MacManus, J. P. *Cancer Res.* **1979**, 39, 3000.

54. Clark, I. D.; Bruckman, A. J.; Hogue, C. W. V.; MacManus, J. P.; Szabo, A. G., *J. Fluorescence*, **1994**, 4, 235.

55. Eftink, M.R. *Biophys. J.* **1994**, 66, 482.

56. Santoro, M.M.; Bolen, D.W. *Biochem*. **1988**, 27, 8063.

57. Steer, B. A. & Merrill, A. R. *Biochem*. **1995**, Vol. 34, No. 21, 7225.

58. Schellman, J. A. *Biopolymers*. **1978**, 17, 1305.

59. Pace, C. N. *Methods Enzymol*. **1986**, 131, 266.

60. Privalo, P. L., *Annual Review of Biophysics and Biophysical Chemistry* **1989**, Vol. 18. p.47.

61. Atkins, P. W. *Physical Chemistry, Fourth Edition*, W.H. Freeman and Company, New York, **1990**, p.788.

Chapter 2 Environment and Reaction Kinetics within TEOS Derived Sol-Gel Matrix Containing the Single Trp Protein Monellin

2.1 Introduction

The development of chemical sensors and biosensors have been extensively studied over the past few decades. A large number of sophisticated sensing schemes have been developed over the years, most involving the interfacing of a biological recognition element (usually an antibody or enzyme) to an inorganic transducer which converts the interaction of the recognition element with an analyte into a measurable signal. As mentioned in Chapter 1, a key difficulty with such schemes has always been the poor stability of the biological species when interfaced to the physical device. A relatively new technique for interfacing of active proteins to devices in a format that is suitable for sensing applications is encapsulation in an inorganic silicate matrix which is formed by the sol-gel process.[1-9] The hydrated glass (sometimes referred to as a hydrogel or biogel) contains a substantial amount of entrapped water that is able to solvate the entrapped protein. In addition, the glass is porous and allows relatively small molecules to enter and interact with the much larger proteins which remain trapped inside.

There are two key issues must be addressed when developing sol-gel based sensors; the characteristics and the local environment of the entrapped protein (since this will affect both stability and accessibility to analyte), and the ability of the analyte to enter the glass and diffuse to the entrapped protein so that a measurable signal is produced.

A large number of studies have been reported regarding the first issue. These studies including the polarity[2] and microviscosity[3,4] of the environment within sol-gel derived matrices, as well as the structure,[5] dynamics[2,5b] and activity[6] of the entrapped proteins, and long-term stability of the entrapped proteins.[7,8] Most of these studies used either intrinsic absorbance (in cases where heme proteins were studied)[5a] or fluorescence techniques[5b,6] to monitor the entrapped proteins. Most of the fluorescence studies concentrated on extrinsically labelled proteins such as acrylodan labelled bovine serum albumin (BSA-Ac),[5b] or used enzymes such as glucose-6-phosphate dehydrogenase which produced species that emit in the visible range.[6e] There have also been a few studies reported which have used intrinsic tryptophan (Trp) fluorescence to examine the effects of encapsulation on the structure and environment of proteins such as BSA and horse heart myoglobin (Mb).[9,10] The results demonstrated that the fluorescence from Trp potentially can be used to monitor the structure and accessibility of entrapped proteins. However, only a small amount of the total information available from the fluorescence of Trp was utilized in this study. Additionally, since the proteins that were studied contained multiple Trp residues, the interpretation of the data is more complex.

The second issue has been much less widely studied. The interaction of an entrapped recognition element (i.e. an enzyme or antibody) with an analyte requires that the analyte first diffuse to the glass, then overcome an Arrhenius energy barrier to enter the glass,[11] and finally diffuse through the pores of the glass to reach the protein.[9,10] It is known that solvents which are entrapped in sol-gel derived matrices do not behave in a manner similar to bulk solvents,[12] and this can result in complicated reaction kinetics. Furthermore,

alkoxysilane derived matrices are negatively charged at physiological pH, causing further kinetic complications when charged analytes are involved.[13] Finally, the relative similarity in the size of the pores and the entrapped proteins has been shown to result in the potential for the presence of an inaccessible fraction of protein.[7,8] These factors play a critical role in the performance of sensors which utilize entrapped proteins since the signal measured is affected by the kinetics of protein-analyte interactions.

The measurement of the intrinsic fluorescence of Trp residues within proteins can be utilized to monitor both the structure and environment of entrapped proteins and the ability of entrapped proteins to interact with analytes. The biochemical community has a long history of using fluorescence from Trp to monitor protein structure,[14] dynamics,[15] stability,[16] and folding and unfolding phenomena,[17] and several useful methods have been developed for relating fluorescence from Trp to protein structure.[13,18] In most cases proteins which contain a single Trp residue are used since they provide a relatively simple system for examining fluorescence lifetimes and a simpler system for probing rotational anisotropy or exposure of Trp to quenchers. An advantage of utilizing the intrinsic fluorescence of Trp residues is that it eliminates the possibility of altering protein structure, which may occur for extrinsic fluorescence labelling protocols.[19] In addition, Trp has also been used to examine the kinetics of reactions involving proteins in solution,[20] and thus, should be suitable for kinetics studies of entrapped proteins.

Even though there are many advantages associated with using intrinsic fluorescence, the application of this method on sol-gel encapsulated proteins has not been prevalent for several reasons. Firstly, excitation of proteins with UV light (usually at 295 nm) can result

in a high degree of photobleaching.[21] The photobleaching can be even more extensive in cases where proteins are encapsulated or immobilized since proteins are unable to diffuse. This problem limits the reliability of quantitative measurements based on intensity data. Secondly, the sensitivity for detection of fluorescence from Trp is much lower than for commonly used extrinsic labels such as fluorescein or acrylodan. Thirdly, monoliths which are derived from alkoxysilane precursors tend to scatter light efficiently at UV wavelengths, which may obscure the fluorescence signal.[9] Lastly, many of the standard experiments for investigating protein stability or exposure of Trp require titrations with species such as guanidine hydrochloride (GdHCl) or acrylamide. Thus, rapid diffusion of species into the silane matrix was required to obtain rapid equilibrium and accomplish the experiment in a relatively short amount of time. Unfortunately, monoliths which are thicker than about 1 mm show response times on the order of hours for addition of analytes or other species,[6d] so that titrations require several days to complete.[9]

In this part of the thesis, we have developed methods for preparing extremely thin slides for subsequently collecting high-quality spectra from Trp residues within encapsulated proteins which effectively eliminate many of the above problems. Two types of sol-gel slides, termed "wet-aged" and "dry-aged", were prepared from TEOS and characterized. The wet-aged sides were aged in buffer, and thus did not shrink substantially. This type of slide was studied since it allows for an investigation of the entrapped proteins at early stages of sol-gel formation. The dry-aged slides were aged in air, and underwent a substantial amount of shrinkage as the silane structure became more highly crosslinked and the solvent was excluded. This type of aging is similar to that used

by most groups,[1-5] and permits comparisons of our results to those reported from other groups. The gels are thin enough to allow titrations to be done in a matter of a few hours, but are thick enough to provide an acceptable signal-to-noise level for detection of intrinsic fluorescence from entrapped proteins.

Experimental conditions for collecting fluorescence spectra and steady-state fluorescence anisotropy from entrapped proteins have been optimized. These parameters were measured for the probe N-acetyltryptophanamide (NATA) and the single Trp protein monellin to investigate the internal environment of both the wet-aged and dry-aged gels. We show that the combination of fluorescence spectra and steady-state anisotropy with acrylamide quenching experiments provides information on the structure, dynamics, distribution and average environment of the entrapped protein. Parameters such as leaching of proteins from monoliths and diffusion of species into monoliths have also been investigated, and the response time and kinetics for interaction of entrapped species with neutral, positively charged and negatively charged species have been determined for both wet-aged and dry-aged monoliths under conditions of continuous stirring. These studies suggest that both the environment of proteins and the kinetics describing the interaction of analytes with proteins are different in glasses than in solution, indicating that such factors must be taken into account when designing sensors.

2.2 Experimental

2.2.1 Chemicals

Monellin, *N*-acetyltryptophanamide (NATA) and polymethacrylate fluorimeter cuvettes (transmittance curve C) were obtained from Sigma (St. Louis, MS). Tetraethylorthosilicate (TEOS, 99.999+%), acrylamide (99+%) and sodium azide (99%) were supplied by Aldrich (Milwaukee, WS). The guanidine hydrochloride (GdHCl, Sequanol grade) was from Pierce (Rockford, IL). The Sephadex G-25 fine powder was supplied by Pharmacia Biotech (Uppsala, Sweden). All water was twice distilled and deionized to a specific resistance of at least 18 MΩ.cm using a Milli-Q 5 stage water purification system. All other chemicals were of analytical grade and were used without further purification.

2.2.2 Procedures

2.2.2.1 Purification of Proteins

A small amount of protein (1 mg) was dissolved into 1 mL of 100 mM phosphate buffer containing 100 mM KCl at pH 7.2. This was then passed through a Sephadex G-50 column (height 10-20 cm, diameter 1 cm) using the 100 mM phosphate buffer to elute the protein. The columns were calibrated with blue dextran and the fractions were collected in 1.5 mL eppendorf tubes. The purified protein eluted out into a volume of 3 to 4 mL. Each tube was tested by UV-Vis absorbance to confirm the presence of protein and to determine protein concentration.

2.2.2.2 Preparation of TEOS Derived Matrices

Sols were prepared by sonicating a mixture of 4.5 mL of TEOS, 1.4 mL of water and 100 μL of 0.1 N HCl for one hour at ambient temperature until the mixture became clear, colourless and monophasic. The solution was then cooled and kept in a freezer at -20°C for 7 to 10 days before the addition of protein. A volume of 300 μl of the prehydrolyzed TEOS solution was rapidly mixed with an equal volume of cold phosphate buffer (100 mM, pH 7.2, with 100 mM KCl, with or without 0-30 μM protein or with 10 μM NATA) and immediately placed into a disposable acrylate cuvette (1 cm pathlength) which was then sealed with Parafilm and placed on its side until gelation occurred (normally about 1-2 minutes). Following gelation the cuvettes were immediately filled with 100 mM phosphate buffer and allowed to stand overnight at 4°C. The slide was then rinsed for 5 minutes two more times and was allowed to age by two different methods. In the first method (wet-aging), the slide was aged in buffer at 4°C for a period of 10 days, until 20% shrinkage occurred. In the second method (dry-aging), the slide was rinsed as described above and was then aged at 4°C for 30 days until 80% shrinkage(by weigth) occurred. At this point, the slides were removed from the acrylate cuvettes and were carefully rehydrated by incubating the slides in a 100% humidity environment at 4°C overnight followed by slow immersion into 2 mL of buffer. The 100% humidity environment was created by adding a small amount of distilled water (about 0.5 cm in height) in a 50 mL beaker, sealed the beaker with Parafilm and kept the beaker at 4°C. This method prevented cracking, which occurred for less than 5% of slides.

2.2.2.3 Pore Size Analysis

Pore size analysis was performed on a Coulter SA3100 surface area/pore size analyzer. Before analysis, the monoliths (either with or without encapsulated protein) were crushed to a fine powder and outgassed at either 100°C or 200°C for 12 hours to remove air and bound water from the surface of the powder. The pressure was measured as nitrogen was adsorbed and desorbed at a constant temperature of -196°C. From the resulting isotherm, the average pore size and distribution of sizes was determined using the BJH (Barrett, Joyner and Halenda) calculation.[22]

2.2.2.4 UV-Vis Absorbance

UV-Vis absorbance spectra were obtained on an ATI Unicam UV-4 spectrophotometer. Absorbance spectra of NATA or monellin in solution were collected in 0.2 nm increments from 240 nm to 350 nm using a scan speed of 30 nm per minute and a bandpass of 1.5 nm. In all cases, a blank scan of buffer vs. buffer was collected and this was subtracted from the sample vs. buffer scan. The concentrations of the solutions were then determined using $\varepsilon_{280} = 5,600\ M^{-1}.cm^{-1}$ for NATA[9] or $\varepsilon_{277} = 14,600\ M^{-1}.cm^{-1}$ for monellin.[23] The transmittance of TEOS derived monoliths was examined by placing the monolith in the light path with the broad face of the monolith oriented toward the beam. The reference light path contained no sample. Transmittance curves were collected from 240 nm to 350 nm using the conditions described above.

2.2.2.5 Fluorescence Measurements in Solution

Fluorescence spectra were collected on a SLM-Aminco 8100 spectrofluorimeter. Light from a 450 W ozone generating Xe arc lamp was passed through a double grating excitation monochromator and then through a 1 cm^2 quartz cuvette containing the sample. Emission was collected at a right angle to the exciting radiation and was passed through a single grating emission monochromator and detected using a R928 PMT in a Peltier cooled housing operated in photon counting mode. A 4 nm bandpass was used in both the excitation and emission paths and no polarizers were used in cases where fluorescence spectra were collected. The sample intensity was divided by the signal from a reference channel containing a quantum counter solution of 3 $g.L^{-1}$ of rhodamine B in ethanol to account for signal fluctuations resulting from deviations in the lamp power output.

For fluorescence spectra, samples containing 10 μM of monellin or NATA were excited at 295 nm and emission was collected from 305 nm to 450 nm in 1 nm increments at a rate of 180 $nm.min^{-1}$ and with an integration time of 0.30 seconds. Solution samples were continuously stirred throughout the experiments and were maintained at a temperature of 20 ± 0.2°C (except where otherwise stated) using a Neslab R110 recirculating water bath. Appropriate blanks were subtracted from each sample and the spectra were corrected for deviations in emission monochromator throughput and PMT response.

Fluorescence anisotropy measurements were performed in the L-format using Glan-Taylor prism polarizers in both the excitation and emission paths. A macro program provided by SLM-Aminco was used to first generate a G-factor and then to measure

anisotropy values from the samples in quartz cuvettes. The sample anisotropy was automatically corrected for the G-factor. Single point anisotropy measurements were generally made at 295 nm excitation and 340 nm emission with 4 nm slits and a 3.0 second integration time. All other settings were identical to those described above. These experiments were done with 30 µM of protein to provide sufficient signal with the polarizers in place. The intensity and anisotropy values of the blank at this excitation/emission setting were less than 0.5% of the sample intensity and anisotropy and thus the blank value was not subtracted from the sample anisotropy. All anisotropy values reported are the average of 5 measurements each on 2 different samples.

2.2.2.6 Fluorescence Measurements of Proteins in the Sol-Gel Slides

Initial fluorescence studies were primarily concerned with minimizing the scattering from aged gels, both with and without protein present. Upon determining the orientation with the least scattering (see Results and Discussion), a holder was built which could suspend the gels in the proper orientation approximately 5 mm above the bottom surface of the cuvette so that a stirring bar could be placed in the cuvette for titration experiments. The holder, showing the optimal orientation of the monolith with respect to the excitation and emission paths, is shown in Figure 2.1.

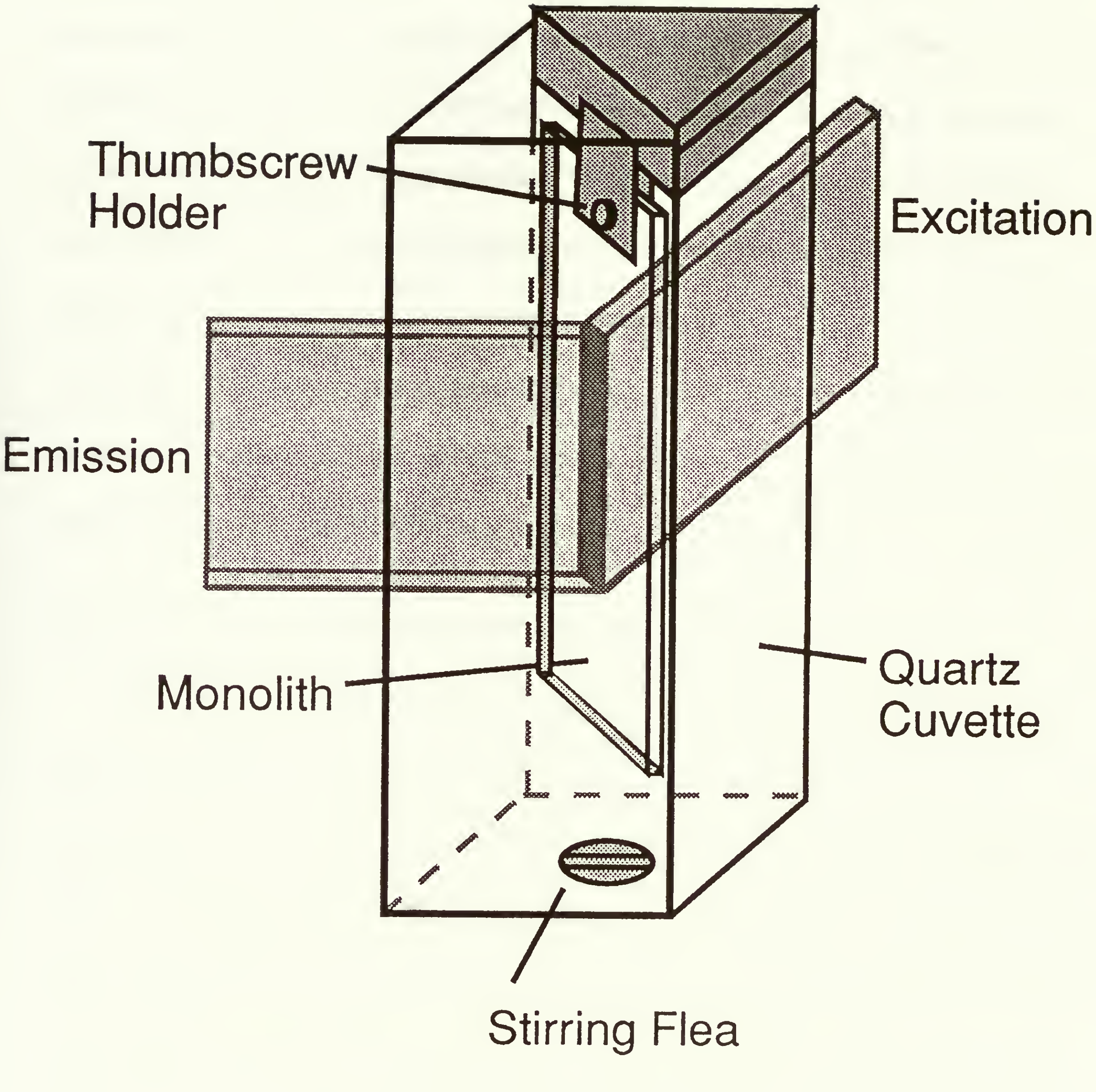
Thumbscrew Holder
Excitation
Emission
Monolith
Quartz Cuvette
Stirring Flea

Figure 2.1 Optimal orientation of the sol-gel slide in the light path of the fluorimeter.

Aged gels, both with and without protein, were carefully removed from acrylate cuvettes (used for aging), rehydrated and mounted in a quartz cuvette for all fluorescence studies. Fluorescence spectra were collected from a monolith containing 10 μM of monellin or NATA, and from a monolith containing no protein using the same instrumental configuration as described above for the solution based studies. All protein spectra had appropriate blanks subtracted and were corrected for instrument response factors. Anisotropy values were generated by first collecting a number of anisotropy values from wet-aged or dry-aged monoliths which contained no protein. Anisotropy values were then collected from monoliths containing 30 μM of monellin or NATA. The variability in the blank anisotropy was very small, and the intensity and anisotropy values of the blanks were usually less than 1% of those obtained from the protein loaded monoliths, thus no blank subtraction was performed.

2.2.2.7 Fluorophore and Protein Leaching Studies

Gels with 10 μM monellin or NATA were studied. The fluorescence spectra of several protein or NATA loaded wet-aged or dry-aged monoliths were recorded at different points during aging and the integrated intensities from the emission maximum to 450 nm were determined. These intensity values were divided by the integrated intensity derived from the spectrum of a reference solution containing 10 μM of NATA in buffer to account for any variations in lamp output and PMT sensitivity with time. The protein loaded monoliths were then placed into a 100 mM phosphate buffer solution at 4°C and were left to incubate for varying lengths of time. The fluorescence spectra of the monoliths, the buffer solutions and the reference solution were then recorded and the ratio

of intensities of the monolith or the buffer solution against the NATA standard solution were calculated to determine the extent of leaching as a function of time. All leaching values were normalized to the intensity recorded from freshly prepared monoliths.

2.2.2.8 Photobleaching Studies

Dry-aged monoliths containing 10 μM monellin were mounted in the sample compartment as described above and were irradiated continuously at 295 nm for a period of 15 minutes. The emission intensity at 340 nm was recorded each second over the 15 minute period. The intensities were normalized to the maximum intensity obtained at time zero. The effects of excitation slit widths and neutral density screens on photobleaching efficiency and signal-to-noise ratio were examined.

2.2.2.9 Response Time and Kinetics Studies

The fluorescence intensity of solutions (1.5 mL volume), wet-aged monoliths and dry-aged monoliths containing 10 μM of monellin was recorded at 1 second intervals using 295 nm excitation and 340 nm emission after the addition of either 2.0 mL of 8.0 M GdHCl, 0.2 mL of 6.0 M potassium iodide or 0.2 mL of 8.0 M acrylamide. In all cases, two neutral density screens were placed in the excitation beampath to minimize photobleaching. All experiments were done with continuous stirring. For solution-based studies the initial drop in intensity observed due to dilution was corrected by multiplying the intensity values by an appropriate dilution factor. No corrections for dilution were

required for the monolith-based studies. The change in the intensity was recorded over a 10-15 minute period, and was normalized to the initial intensity recorded before the addition of reagent. The response curves were analyzed using non-linear curve fitting algorithms available in the Microcal Origin software package (Ver. 4.0, Microcal Software Inc., Northampton, MA).

2.2.2.10 Acrylamide Quenching Studies

For proteins in solution, 2.0 mL of a 10 μM monellin solution was titrated by adding a total of twenty-two 10 μL aliquots of 8.0 M acrylamide in buffer. A fluorescence spectrum was collected from the sample and an appropriate blank after each addition. Spectra were corrected for sample dilution and were integrated as described above. For monolith studies, 2.0 mL of buffer was added to the cuvettes containing the samples and the encapsulated proteins were then titrated as described above, with an equilibration time of 10 minutes after each addition of quencher. No dilution corrections were done for monolith titrations. All quenching data were analyzed using a form of the Stern-Volmer equation which accounted for both static and dynamic quenching, as well as the inaccessible fraction of entrapped protein as described in the Results and Discussion section.

2.3. Results and Discussions

2.3.1 Preparation of Sol-Gel Slides Containing Proteins

2.3.1.1 Hydrolysis and Gelation

All of our studies were done with TEOS derived gels. The major reason for this choice was that TEOS-based monoliths exhibited longer hydrolysis and gelation times compared to TMOS, which allowed a longer time for manipulation during monolith formation. In addition, it was determined that TEOS solutions had much lower levels of fluorescent impurities than TMOS. The initial hydrolysis times for the TEOS/water mixtures were approximately one hour to produce one-phase solutions. However, solutions were normally stored at -20°C for at least 7 days before the addition of the buffer solution containing monellin or NATA. This method has several advantages. Firstly, it allows the hydrolysis process to continue to completion. Secondly, low temperatures allow condensation and polycondensation to occur very slowly and controls the degree of cross-linking. Thirdly, low temperatures prevent gelation from starting, thus allowing sols to be stored for over one month before use. Lastly, allowing a few days to let the cross-linking proceed shortens the amount of time required for gelation after addition of buffer. Short gelation times are preferred when mixing the sol and protein solution to form the gel. The choice of waiting period was based upon evidence provided by ^{29}Si NMR, which showed that after 7 days there was no unreacted TEOS remaining in the solution (results not shown). These results agree with those of Zink,[6] who reported that TEOS must be either refluxed or allowed to stand for extended periods to achieve complete hydrolysis.

Our results also correlate with the rate constants for acid catalyzed hydrolysis of TEOS which were reported by Fyfe and Aroca.[24]

Following complete hydrolysis, the cold TEOS solution was mixed with an equal volume of cold buffer (with or without protein) and immediately transferred to polyacrylate cuvettes to allow gelation. The gelation times decreased dramatically with an increased concentration of phosphate buffer, most likely owing to the ability of phosphate to catalyze the condensation reaction.[25] The ability to control the gelation time by adjustment of the buffer concentration allowed us to select a gelation time which was very rapid (less than 5 minutes) so as to minimize the time which the protein spent in the ethanol-containing liquid silane and at room temperature.

Immediately after gelation, the gels were rinsed several times so that residual EtOH was diluted and removed from the gel. The rinsing steps also had the advantage of removing any fluorescent impurities. Blank slides which were not rinsed showed moderate fluorescence at 353 nm when excited at 295 nm.

2.3.1.2 Aging of the Slides

Sol-gel derived slides were aged by two different methods; a wet-aging method where the slides were aged in buffer, and a dry-aging method where slides were aged in a dry environment. The dry-aged slides decreased in both size and mass by 80% over a period of 25 days at 4°C, reaching a final size of 20 mm x 5 mm x 0.2 mm. The aging was done at 4°C to minimize the extent of protein denaturation during aging. The wet-aged gels decreased in size and mass by only about 20% over the 25 day period to dimensions of 35

mm x 8 mm x 1.5 mm, with most of the change occurring in the first 48 hours after gel formation. The smaller degree of shrinkage for wet-aged gels is consistent with the presence of a large amount of water shifting the equilibria for condensation and polycondensation, which should reduce the degree of crosslinking and the shrinkage of the gel. We speculate that the wet-aged gels may approximate the structure of the dry-aged slides during the first few days of drying. Therefore, the use of the wet-aged monoliths may allow for the investigation of the environment and accessibility of proteins during the early stages of the sol-gel formation.

2.3.2 Physical Characteristics of Sol-Gel Slides Containing Proteins

2.3.2.1 Pore Size Analysis

Pore size analysis was done on dry-aged gels both with and without protein present using two different outgassing temperatures. For both blank gels and those containing proteins, the average pore size was approximately 6.7 ± 0.7 nm in diameter for samples which were outgassed at 100°C. Outgassing at a higher temperature (200°C) resulted in a pore size distribution which was bimodal; 85% of the pores had a diameter of 6.5 ± 0.7 nm, with the remaining pores having diameters of 4.5 ± 0.6 nm. This clearly shows that the temperature used to outgas the slides was directly affecting the measured pore size, with the pore diameters decreasing as the outgassing temperature increased. The pore size of the dry-aged slides was expected to be higher than reported here since these samples should still contain a significant amount of entrapped water, thus the outgassing process

may have removed the internal water from the slides and caused the collapse of the pores. The need for drying of slides before pore-size analysis prevented a meaningful examination of wet-aged slides.

2.3.2.2 Elimination of Scattering from TEOS Derived Slides

Before attempting to collect fluorescence spectra from entrapped proteins, we examined methods for minimizing the background contribution arising from scattering from the slide. To determine optical clarity, a transmittance curve was obtained for TEOS derived slide with a thickness of *ca.* 0.2 mm which was dry-aged for 25 days at 4°C. The transmittance at 295 nm (the excitation wavelength used for Trp) was around 80%, which indicates that the slides were sufficiently transparent to allow excitation of fluorescence using this wavelength. The scattering of light at right angles to the excitation beam was then examined and indicated that the slides produced a large amount of light scattering. This scattering was found to be dependent mainly on the orientation of the slide within the cuvette, the excitation slit widths employed and the presence of buffer. The relative amount of scattering and fluorescence emission was tested for slides containing 10 μM NATA which had been dry-aged for 25 days. The curves, collected at 295 nm excitation with 4 nm excitation and emission bandpasses, are shown for various different sample orientations both with and without buffer in Figure 2.2. The optimal orientation was one wherein the slides were placed at 45° with respect to the excitation beam such that excitation light was reflected away from the emission PMT. The addition of buffer dramatically reduced the amount of scattering, likely due to the closer match of the

refractive indices of the slide and the solution. When the slide was oriented in any other direction the amount of scattering was substantially higher than the fluorescence signal observed. Even with the "optimal" orientation, a small amount of scattering was still observable at the blue end of the NATA spectrum for some samples. The spectra showed a consistent symmetry indicating that integration of half of the spectral contour would provide representative integrated intensity results. For this reason all integrated intensity values reported below were calculated by summing only the red half of the emission spectrum. Excitation bandpasses of 4 nm or less gave identical amounts of scattering, while bandpasses of 8 nm or more caused large increases in scattering. For this reason, all spectra were collected with 4 nm excitation and emission bandpasses. Wet-aged slides exhibited more scattering than dry-aged slides, likely due to larger diameters of the pores of the wet-aged slide which might be close to the excitation wavelength, causing the scattering of light inside the pores.

A sample holder (Figure 2.1) was designed to hold the slides at 45° to the excitation beam inside the cuvette and allowed about 0.5 cm of space between the slide and the bottom of the cuvette to allow insertion of a stirring flea.

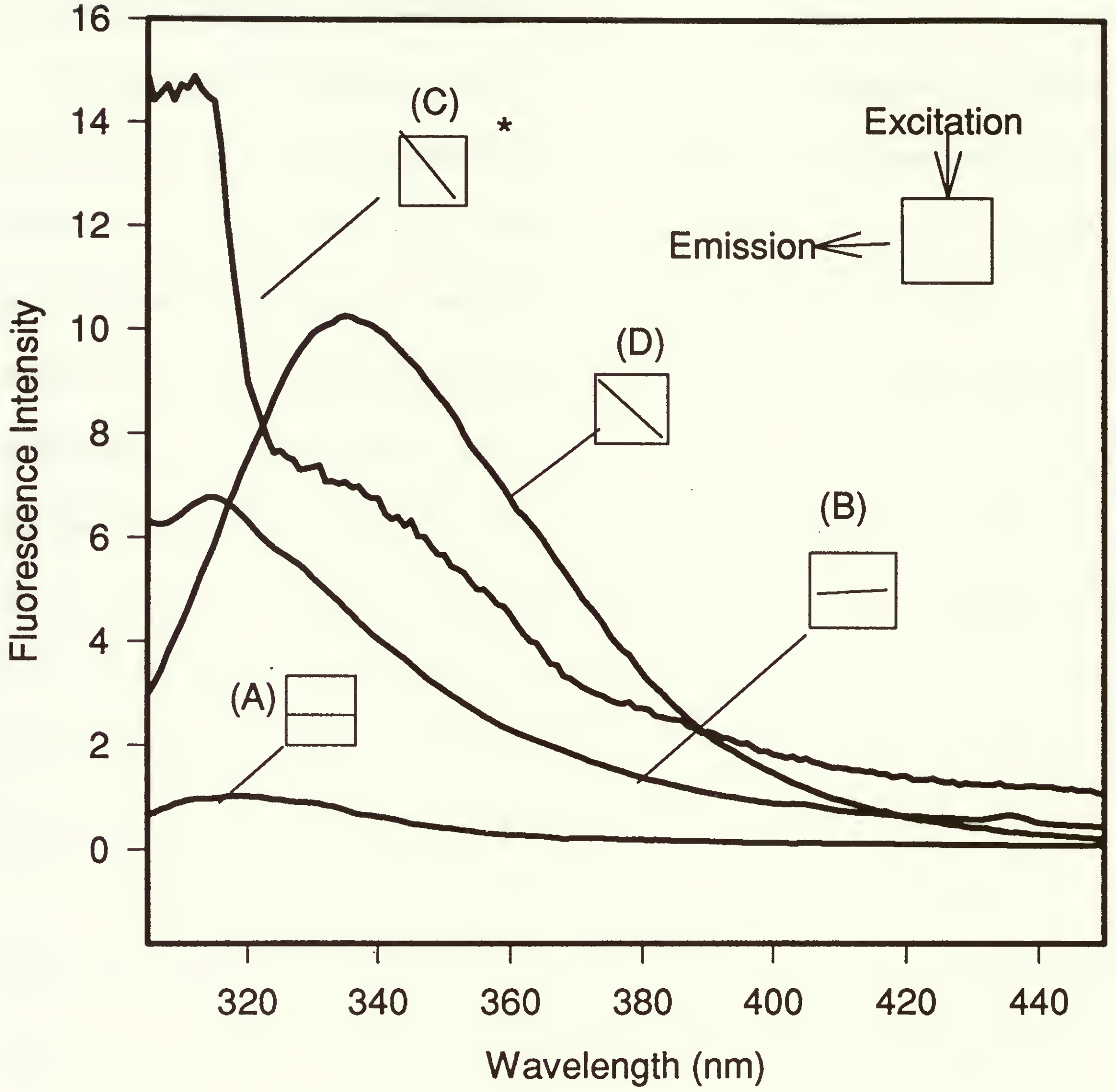

Figure 2.2 Scattering of light from sol-gel slides containing NATA in the presence and absence of buffer and as a function of different sample orientations. The sample orientation and buffer conditions are shown on the figure. The asterisk denotes the spectra which were collected in the absence of buffer.

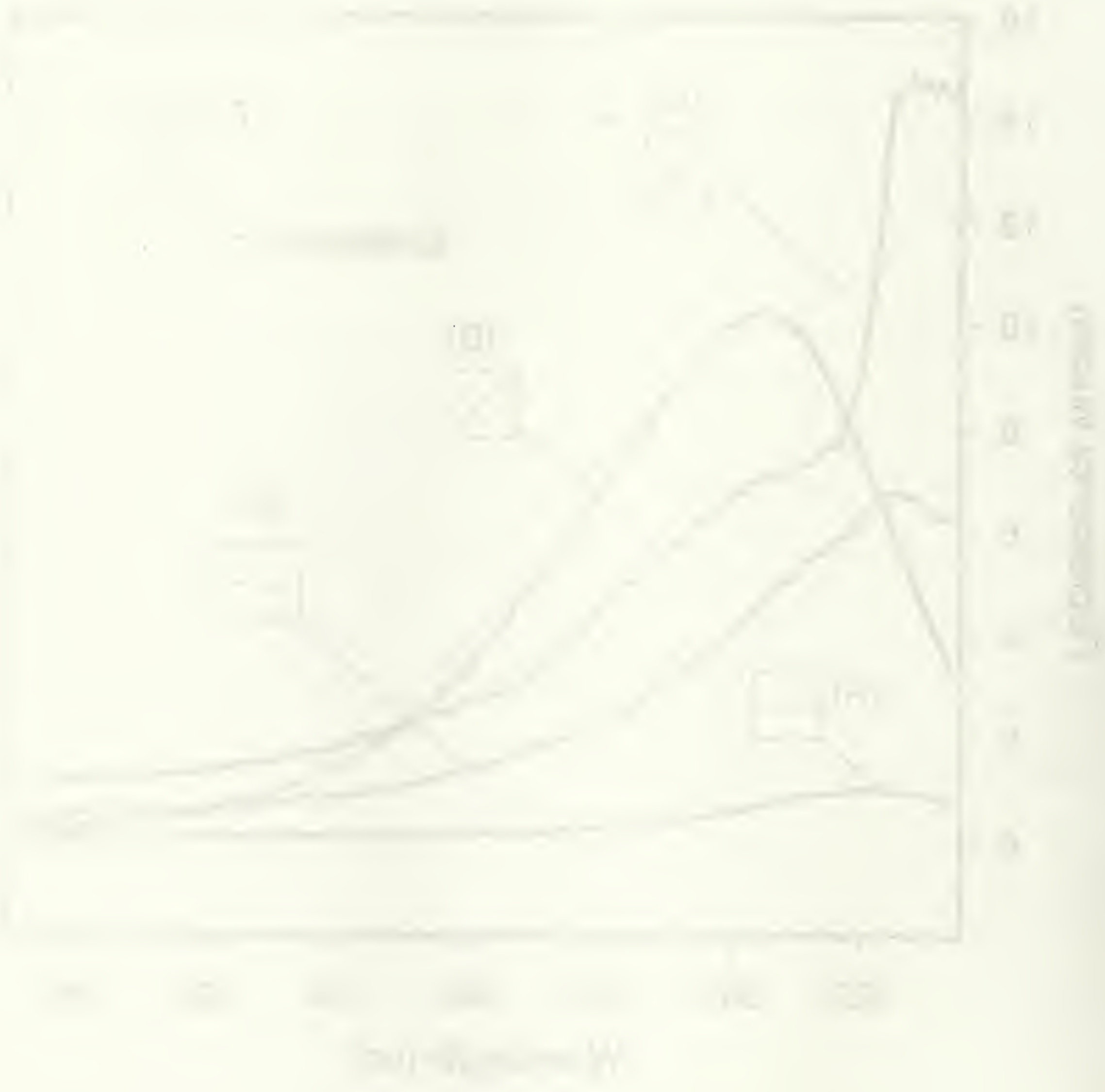

[illegible]

2.3.2.3 Photobleaching in Sol-Gel Slides

The photobleaching efficiency and signal-to-noise ratio for entrapped monellin were measured for various excitation monochromator slit widths, both with and without neutral density screens in the excitation path. The results indicated that the use of 4 nm excitation and emission slit widths with two neutral density screens (each providing 40% attenuation) provided sufficient attenuation of the excitation light to virtually eliminate photobleaching while still retaining an acceptable signal-to-noise (S/N) ratio. In this case, the photobleaching was less than 1% over a period of 15 minutes, and the S/N ratio was 33. Reduction of the excitation slit widths also resulted in a reduction in photobleaching. However, the signal recorded at the reference channel was also reduced, resulting in more noise from the reference channel and thus noisier spectra after division of the sample channel by the reference channel. In this case, the S/N ratio was 27 for less than 1% photobleaching over 15 minutes. The placement of neutral density screens after the beamsplitter attenuated the light after it had been detected by the reference channel, thus increasing the signal-to-noise level in the reference channel and in the final spectra recorded. For this reason, all fluorescence studies were performed with two neutral density screens present in the excitation path.

2.3.2.4 Limit of Detection for Measuring Protein Fluorescence in a Slide

The limit of detection (LOD) for fluorescence measurements of encapsulated monellin was examined using the optimal slide orientation and two neutral density screens to eliminate photobleaching, with all bandpasses set to 4 nm. This experiment indicated that the LOD for monellin was *ca.* 0.5 μM using the configuration described above (i.e. 300 μl of 0.5 μM of monellin was added to 300 μl of TEOS). When polarizers were placed into the excitation and emission paths the limit of detection rose to 5 μM, however when the integration time was increased 10-fold to 3 seconds, the limit of detection dropped to 1.5 μM. Naturally, increasing the integration time on the emission PMT will improve the limit of detection for spectra as well, but this also increases the collection time per spectrum by a factor of 10, produces a higher degree of photobleaching and makes the time required for some experiments unacceptably long. For most of the fluorescence studies described in this work the concentration of monellin within the monolith was approximately 10 μM for spectral studies and 30 μM for anisotropy studies. A concentration was chosen which was 20-fold higher than the LOD since many of the experiments done, such as addition of acrylamide, involved substantial quenching of the initial fluorescence indicating that higher initial intensity values had to be used so that the quenched fluorescence intensity remained above the LOD. The extremely good limits-of-detection allow for very small amounts of protein to be encapsulated into the slides, which may reduce aggregation effects for proteins at the higher concentrations required for absorbance measurements.[6] The ability to use small amounts of protein also extends the technique to proteins which have limited solubility in the silane solutions.

2.3.2.5 Fluorophore and Protein Leaching

Leaching of proteins from slides was also tested. We examined the leaching of both proteins and NATA from wet-aged and dry-aged TEOS slides. No leaching of monellin was observed from either type of slide. However, significant leaching was observed for NATA in both wet-aged and dry-aged slides. For wet-aged slides, complete leaching of the fluorophore occurred over a period of 8 hours. For dry-aged slides, 30% of the NATA leached over 8 hours, indicating that the relative pore diameter for the dry-aged slide was substantially smaller than that of the wet-aged slides. This shows that the pore size is dependent on the aging conditions used, as expected. A total of 4.5% of the probe leached out of the dry-aged slides over a period of 1 hour, which was the time required for quenching experiments. This suggested that quenching of entrapped NATA could still be examined in dry-aged slides with reasonable accuracy.

2.3.3 Kinetics of Reactions in Sol-gel Slides

2.3.3.1 Interaction of Neutral Analytes with Entrapped Monellin

The leaching results indicated that small molecules could exit the slide over a period of hours. For sensor development, it is also important to know the response time and overall kinetics for small molecules to enter into the slides and interact with encapsulated proteins. A neutral quencher acrylamide was first used for the kinetics study. The response curve for addition of acrylamide to monellin in solution and when entrapped are shown in Figure

2.3a. The responses were fit to first order, second order and to a sum of first order time constants. The quality of the fitting was determined by residual plots and by the value of the chi-squared parameter. The results of the fitting process and the average response times are shown in Table 2.1. The addition of acrylamide to monellin in solution resulted in response times of less than 5 seconds (the minimum time between the addition of reagent and the collection of data for our fluorescence system), and precluded a proper kinetic analysis of the response curve. The extremely rapid response time is expected since the rate of the interaction in solution is diffusion limited. The bimolecular quenching rate constant (k_q) for the interaction of acrylamide with monellin has previously been reported to be 2.0 x 10^9 $M^{-1}s^{-1}$.[26] Thus, the time-constant (t_q) for the reaction, which may be defined as $1/k_q$, is 5.0 x 10^{-9} M.sec.

The reaction of acrylamide with entrapped monellin was far slower, and provided unexpected results. In both wet-aged and dry-aged slides, the reaction occurred by a sum of two *first-order* (or pseudo-first-order) processes. For both wet-aged and dry-aged slides, there was a fairly fast process (40 sec for wet-aged slides and 52 sec for dry-aged slides) which represented 62 to 65% of the response signal, and a slower process (166 sec in wet-aged slides, 213 sec in dry-aged slides) which accounted for the remaining 35 to 38 % of the response. Analysis of the time constants showed that both the shorter and longer time constants, as well as the mean response time, were 1.28-fold greater in the dry-aged slides compared to the wet-aged slides, indicating that both processes were affected in a similar manner by the drying of the slides. The results clearly show that the presence of the

glass matrix causes a substantial decrease in the rate of diffusion of the quencher, causing the response time to be orders of magnitude slower than in solution.

Table 2.1. Response times, time constants and normalized pre-exponential factors for addition of GdHCl, acrylamide or iodide to monellin in solution, wet-aged and dry-aged slides.

Sample	A_1	t_1 (s)	A_2	t_2 (s)	mean response time[a] (s)	Final Intensity (%)[b]	χ^2
Acrylamide							
Solution	1	< 5	-	-	< 5	20	
Wet-Aged Gel [c]	0.647[d]	40[e]	0.353	166	84	35	2.8E-5
Dry-Aged Gel[c]	0.620	52	0.380	213	113	37	2.1E-5
Iodide							
Solution		< 5		36	< 5	10	
Wet-Aged Gel[f]					445	35	
Dry-Aged Gel[f]					110	29	
GdHCl							
Solution	0.25	< 5	0.75	316	237	78	
Wet-Aged Gel	0.503	59	0.497	379	379[b]	80	6.6E-5
Dry-Aged Gel	0.223	38	0.777	634	634[b]	85	4.4E-5

[a]defined as the time for the intensity to reach a value which was 37% (1/*e*) of the initial intensity, [b]the error in these values is less than 1%, [c]these values were obtained by fitting the response to the following equation: $I = I_0 + A_1 e^{(-t/t_1)} + A_2 e^{(-t/t_2)}$, [d]the errors on the pre-exponential factors were ±0.005, [e]the errors on the time constants were ± 1 second, [f]the complexity of these response curves made it impossible to obtain a reasonable fit of the curves by any kinetic rate equation.

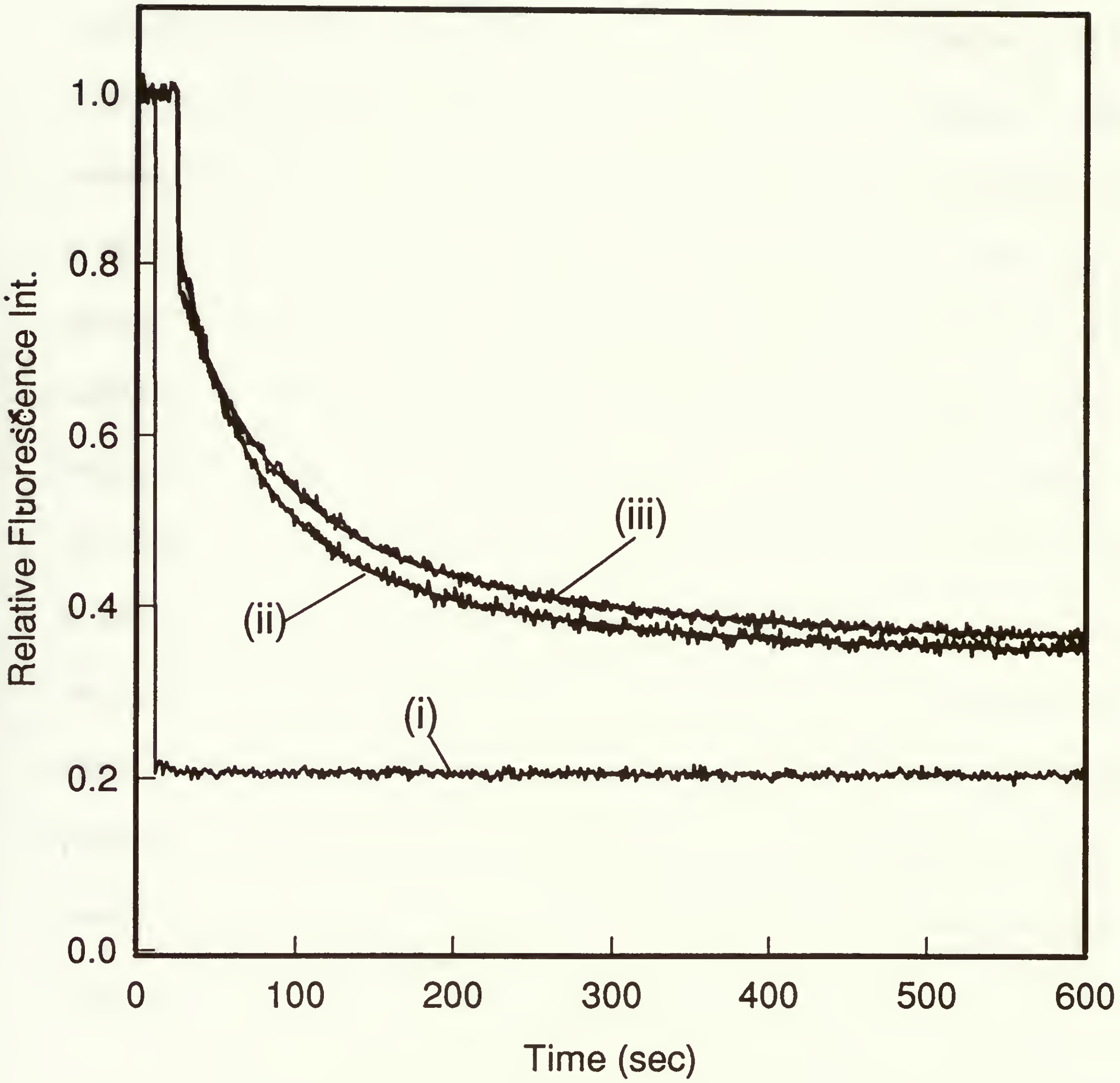

Figure 2.3a Response curves for the addition of various species to free and entrapped monellin. (A). Addition of acrylamide to monellin (i) in solution, (ii) in a wet-aged slide and (iii) in a dry-aged slide.

These results clearly indicate that two first-order processes occur in parallel to cause quenching of the entrapped protein. This is at first surprising, since fluorescence quenching is inherently a bimolecular, or second-order, process. However, the protein which is entrapped in the slides is unable to diffuse, and thus the kinetics of the interaction will be determined solely by the ability of the quencher to diffuse through the glass and reach the entrapped protein. Hence, under the conditions of our experiment the quenching should occur by a first-order process. There are numerous possible explanations for the presence of two discrete rate constants. For example, it is possible that there is a set of discrete environments for the protein which is determined by the distribution of pore sizes within dry-aged slides, as described above. Alternatively, two independent processes may be required for the quencher-fluorophore interaction to proceed. One may be the entry of the reagent into the glass followed by the diffusion through the pores. At this time, there is insufficient data on which to base an explanation of the observed behaviour. However, one possibility which can be discounted is electrostatic interactions between the quencher and the glass matrix and/or protein, since the quencher is neutral. The results suggest the presence of more complex reaction kinetics when entrapped species are involved, and this complexity may cause difficulties with sensors which rely on rapid signal development or which work in a flow injection or dynamic measurement mode.

2.3.3.2 Interaction of Charged Analytes with Entrapped Monellin

The fluorescence response of monellin was monitored after the positively charged denaturant GdHCl or the negatively charged quencher iodide were added to free and entrapped protein. The results indicated that the kinetics of the interaction of charged species with monellin was complicated, even in solution. For this reason, it was not possible to fit the responses to any form of rate equation. Thus, the average time to reach an intensity of 1/*e* of the total response (37%) was determined. This was done so that direct comparisons to the time constants for acrylamide quenching of monellin could be done.

The interaction of iodide with monellin in solution showed a very rapid initial response, followed by a much slower response which caused the total time for the interaction to be 100 seconds (for 100% signal development). This may be the result of electrostatic interactions between the negatively charged quencher and the protein which has a net charge of -1 at pH 7.2.[27] The average response times for the interaction of iodide with entrapped monellin were slower than in solution for both wet-aged and dry-aged slides. However, the wet-aged slides provided *longer* response times and higher final intensity values than the dry-aged slides, which was opposite to the responses obtained using the neutral quencher acrylamide. These results suggested that the iodide was not able to enter the wet-aged slides as easily as for dry-aged slides.

The basis of this behaviour is not fully understood at this time, however it is very likely that there are electrostatic interactions between the negatively charged silicate and the

negatively charged quencher, which may be complicated further since the protein is also negatively charged at pH 7.2.[25] The reaction rate is further complicated by fact that the wet-aged slides were thicker than the dry-aged slides, and by the factors described above for the interaction of acrylamide with entrapped monellin. The unexpected decrease in both of the response times on going from the wet-aged to the dry-aged slides suggests that the interaction between the negatively charged iodide and the negatively charged siloxide groups of the glass may play an important role in the kinetic behaviour.[28] The overall charge of these two types of slides would be expected to be quite different based on the different degrees of crosslinking and the changes in the number of free siloxide groups. The longer response times in the wet-aged slides strongly suggest that these glasses undergo more electrostatic interactions with iodide, and may exclude the iodide from the internal region of the glass, increasing the response times.[13]

The responses for the addition of GdHCl to free and entrapped monellin are shown in Figure 2.3b. The rate of interaction of GdHCl with monellin was quite slow for both the free and entrapped proteins. In solution, there was a small initial response that took less than 5 seconds. This was combined with a much slower response which could be fit to a first order time constant (t_1 = 316 sec). The addition of GdHCl to monellin in wet-aged and dry-aged slides provided slightly longer response times compared to those in solution. Interestingly, in each case there was an initial *increase* in intensity followed by a stage of rapid decrease and then a stage of slower decrease in intensity. The initial increase suggests that the initial stages of unfolding are observable in the slides. This increase is expected based on the results obtained for GdHCl titrations of monellin in solution and in

slides (See Chapter 3). The fact that this step is observable only in slides suggests that the response of the slides is again slower than that of solution, as expected.

The kinetics for the interaction of GdHCl with entrapped monellin were complicated. However, reasonable time constants could be obtained by fitting only the decrease in intensity after the initial rapid rise. The results are shown in Table 2.1. The results indicated that the reaction occurred significantly faster in wet-aged slide than in dry-aged slides. This would be expected based on both the larger pores and the greater overall charge of the wet-aged slides, as proposed above. It is expected that the positively charged GdHCl would be attracted into the slide, and would thus react faster if the slide was more negatively charged.

Overall, it appears that the rate of interaction of charged species with entrapped proteins is dominated by both the pore size and the overall charge on the glass matrix. This has serious ramifications in cases where glasses which have not been aged are used, but becomes much less of a problem when fully aged matrices are used for sensor development. A key observation is that the responses all require at least several hundred seconds for complete interaction of the analyte with the entrapped protein, even though the slides are only 200 µm thick. This indicates that extremely thin films (likely less than 1 µm in thickness) will be required if response times on the order of seconds are desired.

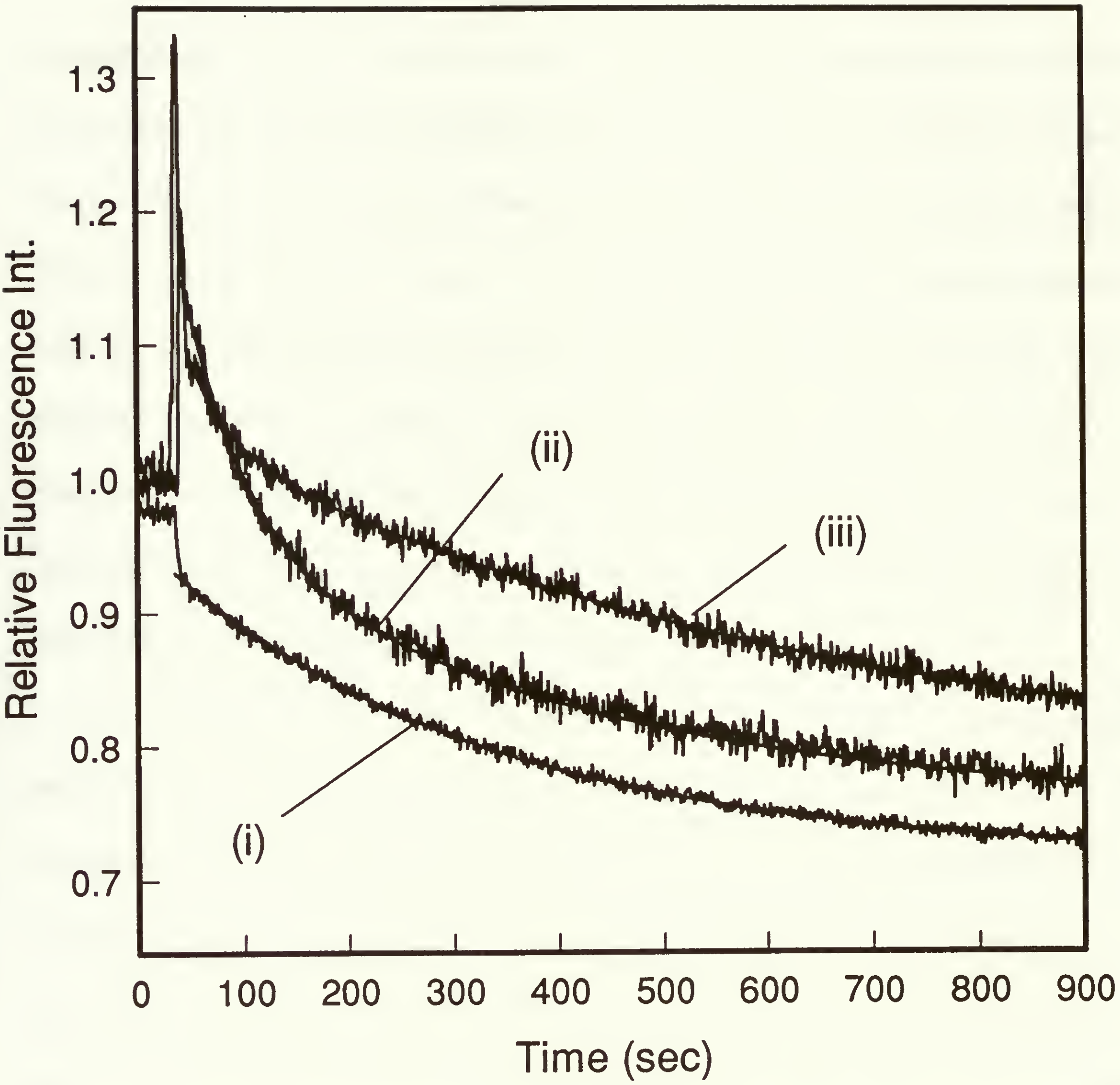

Figure 2.3b Response curves for the addition of various species to free and entrapped monellin. (B) Addition of GdHCl to monellin (i) in solution (ii) in a wet-aged slide and (iii) in a dry-aged slide.

2.3.4 Internal Environment of Protein Doped Gels

2.3.4.1 Acrylamide Quenching Studies

One observation from the kinetic studies of the interaction of acrylamide with entrapped monellin was that the final fluorescence intensity of the protein in the two slides was similar, but both values were higher than the values in solution, indicating that there was a lower degree of quenching for the protein when present in the slides. This could be due to at least three factors; a lower concentration of quencher in the slides compared to solution, an inaccessible fraction of protein,[9,10] or a lower bimolecular quenching constant. Previous studies by Shen and Kostic[13] have shown that the concentration of neutral species in TMOS derived slides is identical to that in solution for ionic strengths above 300 mM, as was the case in this study. This suggests that the differences in quenching efficiency were not the result of a lower concentration of quencher in the slides.

The quenching of monellin by acrylamide was examined in solution and in the sol-gel derived matrices to address the remaining possibilities. This study also allowed an examination of the nature and distribution of protein environments. Acrylamide was chosen for these studies for several reasons. The response time studies indicated that acrylamide was able to enter the pores of both wet-aged and dry-aged slides and could interact with entrapped species. Another reason for using acrylamide was that we wanted to avoid any effects which may have arisen due to interaction of charged quenchers with the negatively charged siloxides that are known to exist at pH 7.[12,13] Such interactions can result in non-linear Stern-Volmer plots, and may produce alterations in K_{SV} values. There is some controversy regarding the possibility for binding of acrylamide to proteins.[29]

However, the most recent discussion of this topic, which concentrates on the interaction of acrylamide with monellin, favors the view that there is no specific binding of acrylamide to proteins.[30]

Figure 2.4 shows Stern-Volmer (SV) plots of the acrylamide quenching of monellin in solution, in wet-aged slides and in dry-aged slides. Fitting of the data to a standard SV plot always resulted in an upward curvature owing to the presence of both static and dynamic quenching. Eftink and co-workers have done extensive studies on the quenching of proteins by acrylamide,[31] and have shown that a correction for static quenching can be applied which results in the ability to accurately fit the dynamic quenching contribution.[30] In addition, the fraction of inaccessible species can be described by including a parameter f_i, which varies from 0 (all species accessible) to 1 (all species in accessible). The data were analyzed using the modified version of the SV equation which accounts for both dynamic and static quenching of Trp fluorescence, as given in equation (2.1):

$$\frac{F_0(1-f_i)}{(F-F_0 f_i)e^{V[Q]}} = 1 + K_{SV}[Q] \qquad (2.1)$$

where F_0 is the fluorescence intensity in the absence of the quencher, F is the fluorescence intensity at a given molar concentration of quencher [Q], K_{SV} is the Stern-Volmer quenching constant (M^{-1}), and V represents the volume (in M^{-1}) of the active quenching sphere within which the quenching of the fluorophore is instantaneous. In all cases we were able to obtain excellent fits to the quenching data using the above equation. The results of the Stern-Volmer analysis are shown in Table 2.2.

The quenching of monellin in solution showed a K_{SV} value of 3.3 M^{-1} and a quenching sphere volume of 0.4 M^{-1}. The K_{SV} and V values indicate that the Trp in monellin is

reasonably inaccessible. Encapsulation of monellin or NATA into wet-aged or dry-aged gels caused the K_{SV} values to drop and the inaccessible fractions to increase, although the volume of the active quenching sphere remained relatively constant. A decrease in K_{SV} is usually interpreted as a decrease in accessibility. However, the lower K_{SV} could also be the result of a decrease in either the diffusion-dependent bimolecular quenching constant (k_q) or the environment-dependent lifetime (τ_0). Unfortunately, an instrument for measuring fluorescence lifetime is not available in our lab, so the τ_0 values could not be obtained. However, the fluorescence lifetime of monellin can be assumed to either remain constant or increase upon encapsulation based on the lower solvent mobility within the slides. Therefore, the decrease in the K_{SV} values likely reflect a decrease in k_q which would result from a lower rate of diffusion of the quencher. The possibility of a lower k_q values agrees with the results from Shen and Kostic,[13] who showed that there is a 5-fold decrease in the rate of diffusion of small molecules in TMOS derived matrices compared to diffusion rates in solution.

The value of the inaccessible fraction for entrapped species ranged from 0.06 for NATA to 0.15 for monellin, and suggested that there could be up to 15% of the entrapped proteins which are inaccessible to the quencher. However, the number of variables in equation (2.1) make it difficult to conclusively determine whether an inaccessible fraction of protein exists. The possible presence of an inaccessible fraction of protein supports the results of Saavedra's group[9,10] and suggests a distribution of environments, in agreement with the results from the response time studies. The existence of a distribution of environments is extremely important for sensor development when using this

encapsulation format. It will likely result in mixed signals from different parts of the sensing matrix, causing complicated responses and difficult calibration.

Table 2.2. Stern-Volmer analysis of acrylamide quenching for NATA and monellin in solution, wet-aged and dry-aged TEOS slides.

Sample[a]	K_{SV} (M^{-1})	V (M^{-1})	*f*	constant	r^2
Monellin in solution	3.3 ± 0.1	0.4± 0.1	0	1.01 ± 0.01	1.00
Monellin (wet-aged monolith)	2.0 ± 0.1	0.3 ± 0.1	0.15 ± 0.03	0.96 ± 0.04	0.98
Monellin (dry-aged monolith)	2.6 ± 0.1	0.4 ± 0.1	0.08 ± 0.02	0.97 ± 0.01	1.00
NATA in solution	17.4 ± 0.1	1.8 ± 0.2	0	1.00 ± 0.01	1.00
NATA (dry monolith)	8.2 ± 0.2[b]	2.0 ± 0.2	0.06 ± 0.02	0.97± 0.03	0.99

[a] NATA in a wet-aged monolith could not be examined due to severe leaching of the probe.

[b] NATA slowly leaches from dry-aged monoliths. The acrylamide titration was done over a period of 20 minutes, thus there could be a small contribution from the quenching of NATA in solution which would lead to an increase in the K_{SV} value.

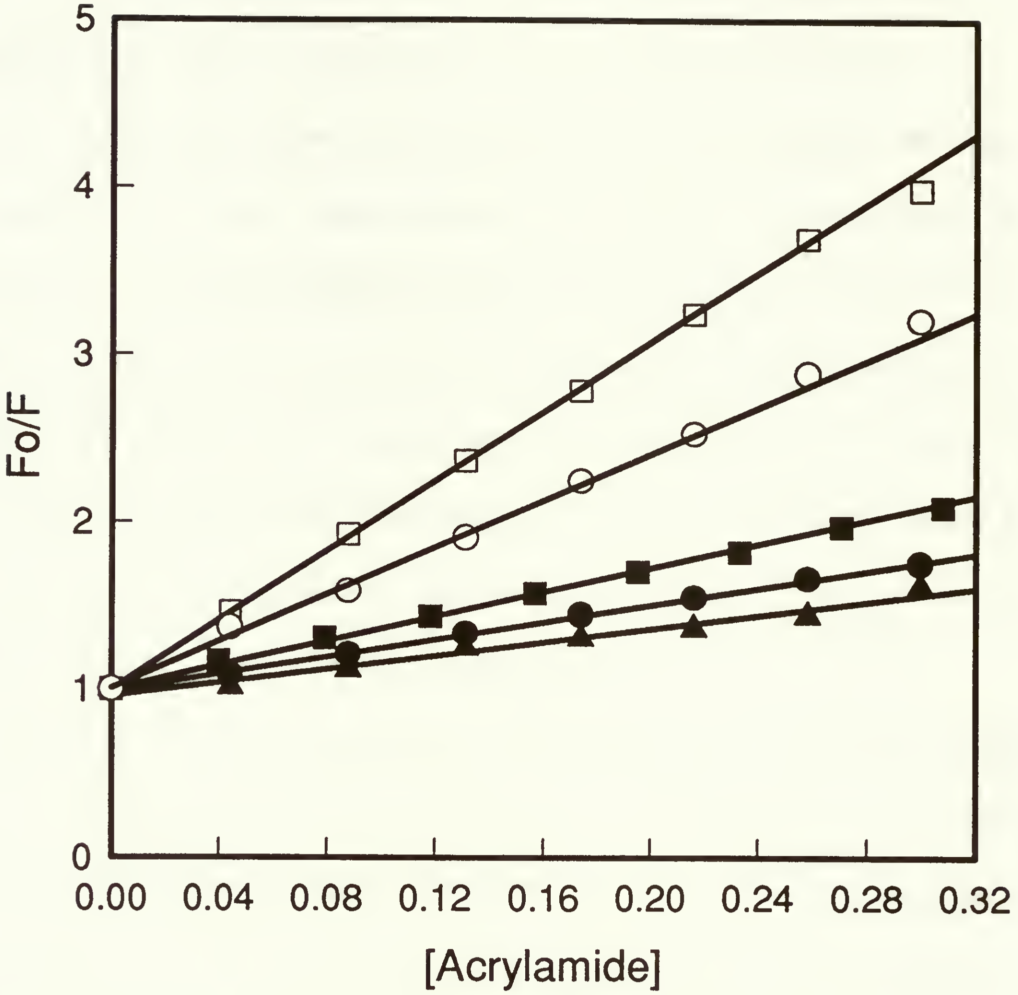

Figure 2.4 Stern-Volmer plots for acrylamide quenching of NATA (open symbols) and monellin (closed symbols) in solution (■), wet-aged slides (▲), and dry-aged slides (●) derived from TEOS. The data was plotted according to equation (2.1) and was fit as described in Table 2.2. Reliable quenching data for NATA in wet-aged slides was not obtained due to extensive leaching of NATA from such matrices.

2.3.4.2 Fluorescence Spectra of Entrapped Species

To further probe the internal environment of sol-gel derived matrices, the fluorescence spectra of NATA and monellin were measured in the sol-gel slides using the sample orientation shown in Figure 2.1. The results are shown in Figures 2.5 and 2.6, respectively. The spectrum of the encapsulated monellin in either wet-aged or dry-aged slides was effectively identical to that of the free protein, with an emission maximum of 334 ± 1 nm and a half-width-at-half-maximum (HWHM) of 32 nm in each case. The emission maximum of monellin was also determined in ethanol:buffer mixtures ranging from 0 % to 50% ethanol. In this case, the emission maximum was 334 ± 1 nm up to 30% ethanol, and shifted slightly to the red with increasing ethanol concentration, reaching a value of 341 ± 1 nm at 50% ethanol owing to partial denaturation. These results indicate that the monellin in wet-aged or dry-aged monoliths had almost the same native fluorescence spectral properties as monellin in solution, suggesting that our encapsulation method did not seriously alter the structure of the native monellin. Care was taken during encapsulation to ensure that a minimal amount of ethanol was present when the protein was entrapped, since ethanol is known to cause substantial changes in the structure of monellin.[17] In our protocol, no ethanol was used as a co-solvent during the hydrolysis of TEOS. This was possible since sonication of the hydrolysis mixture resulted in sufficient release of ethanol (via hydrolyzed ethoxy groups) to promote miscibility of all components in the mixture. The results indicated that the ethanol concentration inside the pores of the monoliths did not exceed 30% (by volume). Hence, the sol-gel processing conditions used in our studies did not damage the protein.

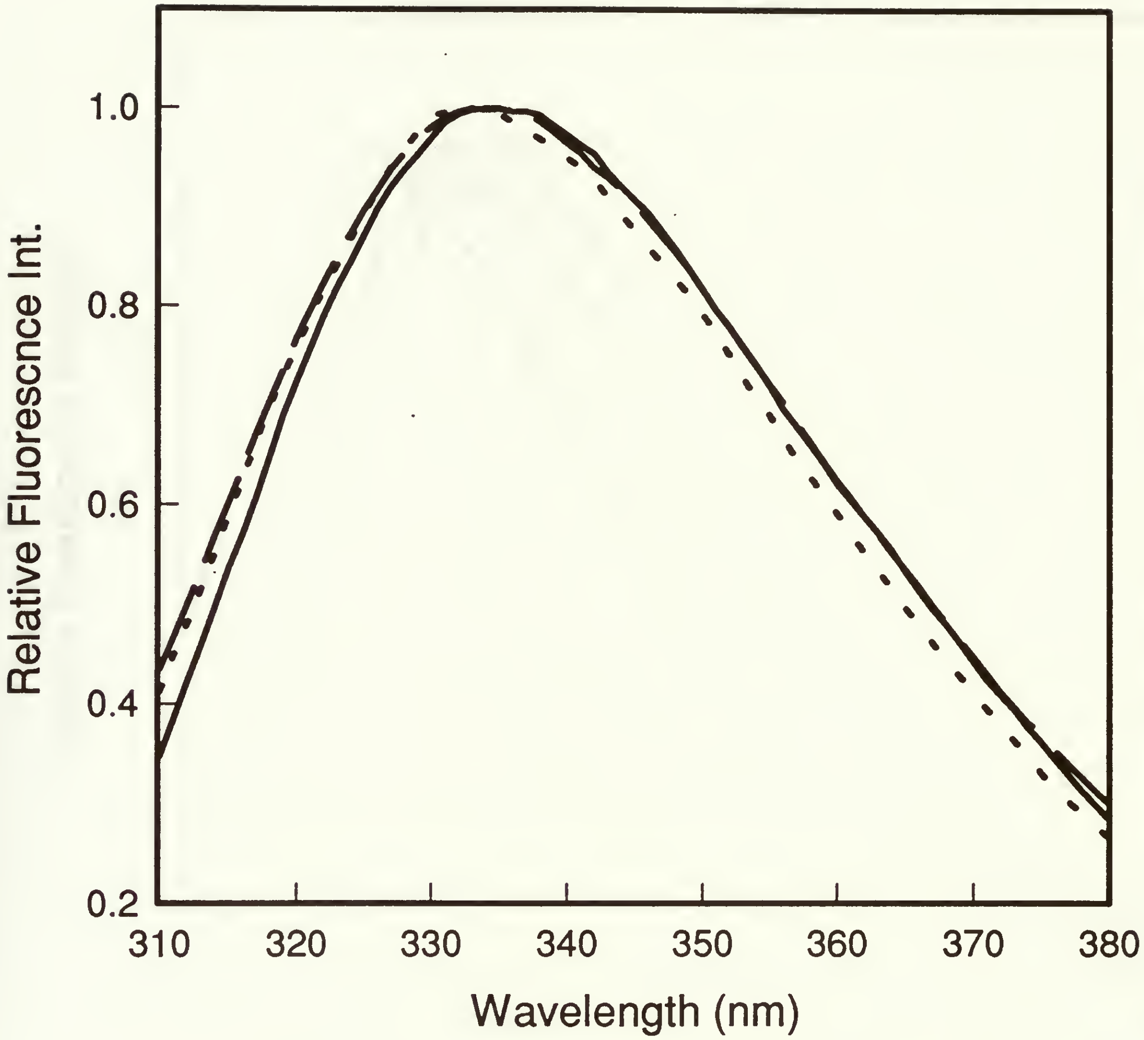

Figure 2.5 Fluorescence spectra of 10 µM monellin in 100 mM phosphate buffer solution, pH 7 (solid line), in a wet-aged slide present in 100 mM phosphate buffer (dashed line), and in a dry-aged slide present in 100 mM phosphate buffer (dotted line). All spectra have been normalized.

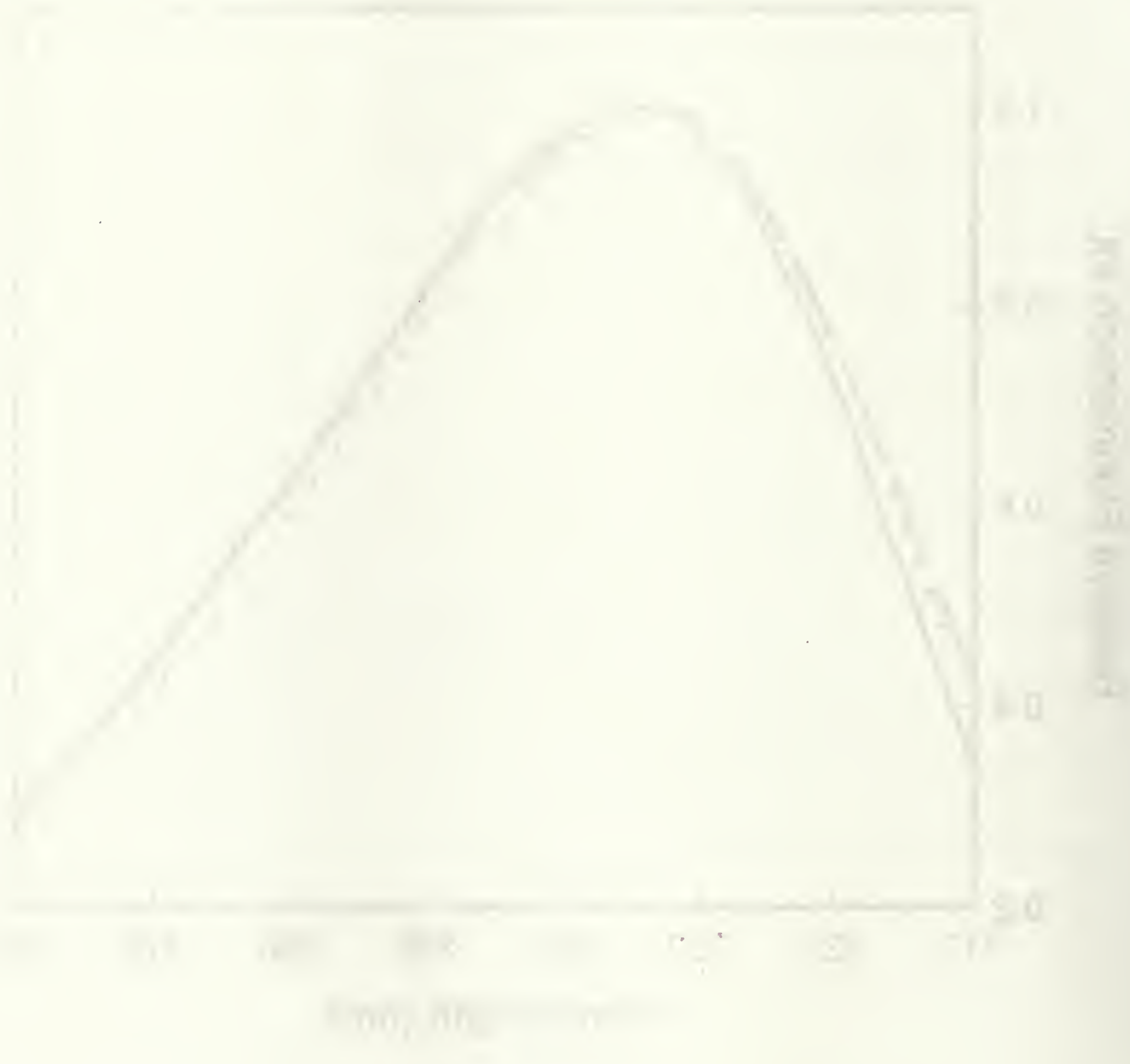

[illegible]

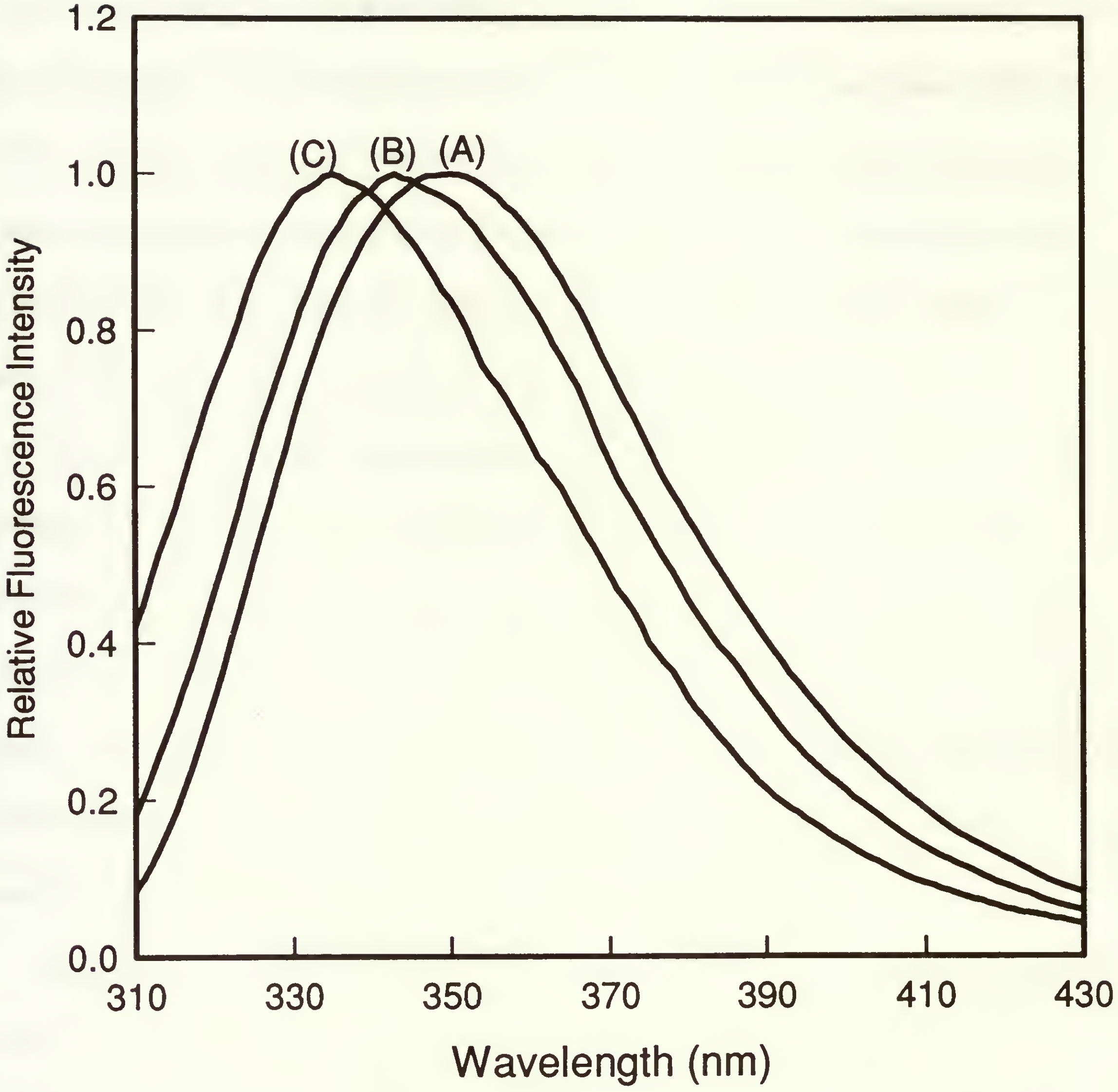

Figure 2.6 Fluorescence spectra of 10 μM NATA. (A) in 100 mM phosphate buffer solution at pH 7, (B) in a wet-aged slide present in 100 mM phosphate buffer, (C) in a dry-aged slide present in 100 mM phosphate buffer. All spectra have been normalized.

In contrast to monellin, the spectral characteristics of NATA in solution, wet-aged slides and dry-aged slides were quite different. In solution, the emission maximum for NATA was 348 nm with a HWHM value of 34 nm. The emission maximum shifts to 343 nm for wet-aged slides (HWHM of 34 nm) and to 335 nm for dry-aged slides (HWHM of 34 nm). These results suggest that the environment of the dry-aged slides is either less polar or less mobile than that of the wet-aged slides, which is slightly less polar or less mobile than that of an aqueous environment. The results suggest that the internal environment of the slides is dependent on the aging method employed.

There are several possible explanations for differences in the NATA emission maximum in solution, wet-aged and dry-aged gels. The first is that there may be a substantial amount of EtOH or unhydrolyzed ethoxy groups in the wet-aged gels, which increases as the gels dry. However, the TEOS solutions were allowed to hydrolyze for at least 7 days, removing the possibility of unreacted ethoxy groups altering the local polarity (^{29}Si NMR of the hydrolyzed TEOS solutions showed no evidence of ethoxysilane species).

Another possibility for the blue shift is that the environment in the region of NATA is dehydrated, leaving the silane as the solvent. Dehydration should cause the NATA to adsorb onto the silica surface. This would alter the emission wavelength since it would make the probe less susceptible to solvent relaxation effects.[32] While this may be possible in the case where the slides are present in air, it is less likely when the slides are present in buffer solution. The external water should be able to enter the pores of the slide and hydrate the encapsulated fluorophore. In addition, it would be expected that the HWHM

for the spectra should have broadened owing to a distribution of free and adsorbed NATA contributing to the spectra. The similarity of the HWHM in slides to that obtained in solution suggests that the NATA is likely in a single environment, thus it is either all adsorbed or all free (assuming that the spectra for the free and adsorbed NATA are different). This suggests that adsorption may not have been a large contributor to the observed blue shift in the emission maximum.

A final possibility is that the shift in emission wavelength may be the result of a reduction in the rate of dipolar relaxation of the probe by the entrapped water. Bright *et al.*[2,3,5b,33] have used steady-state anisotropy and time-resolved emission spectra to show that the dipolar relaxation time for fluorescent probes in TMOS derived slides is slower than that found in solution. This suggests that the internal water may be less able to stabilize the energy of the excited state of the entrapped probes, reducing the extent of the solvent induced red-shift. There have also been a number of studies which show that NATA undergoes both a blue shift in emission wavelength[34] and a decrease in K_{SV}[29,30] as the viscosity of the local environment increases. These results therefore indicate that the mobility of the internal environment is likely substantially reduced compared to that of aqueous solution.

2.3.4.3 Steady-State Anisotropy of Entrapped Species

In order to obtain additional information about the environment of entrapped NATA and monellin, we monitored the steady-state anisotropy of the entrapped protein. It was necessary to first characterize the contribution of scattering to the observed anisotropy,

since scattering tends to produce increases in anisotropy.[35] Three experiments were done to characterize the effect of scattering on the measured anisotropy values. The intensity at each of the four polarizer orientations was measured for the slides with and without entrapped monellin. At each setting, the intensity of the blank was less than 1% that of the sample, indicating that scattering was likely not a major problem. The anisotropy of entrapped monellin was measured at three different concentrations of protein; 10 μM, 20 μM and 30 μM. In each case the anisotropy values were within 5% of each other, again indicating that contributions from scattering were not affecting the measured anisotropy value. The anisotropy of the protein was also measured when entrapped in sol-gel derived blocks with dimensions of 8 mm x 8 mm x 20 mm, which showed no light scattering whatsoever. Again, the anisotropy results were identical to those obtained in the thin slides used for all other experiments. These results indicated that steady-state anisotropy could be reliably measured for entrapped proteins using the ultrathin slides which were oriented as shown in Figure 2.1. These results are in agreement with the results of Bright and co-workers,[5b] who have shown that TMOS derived matrices are not birefringent, and thus are suitable for studies of time-resolved anisotropy.

Additionally, anisotropy values at different emission wavelengths were obtained to select a optimal wavelength for single point anisotropy measurements. Results showed that emission wavelength values between 340 to 355 nm gave the most reliable results. Anisotropy values collected below this wavelength range were substantially affected by light scattering while at longer wavelengths, more concentrated proteins were required

because of the decrease of the intensity when the emission wavelength was far removed from the emission maximum.

It was observed that the anisotropy of the protein increased moderately upon encapsulation, increasing from 0.134 ± 0.002 in solution to 0.18 ± 0.01 in both wet-aged and dry-aged slides. The higher level of error in the anisotropy values for slides may reflect small differences in sample orientation, aging conditions, or light scattering. Overall, the anisotropy values indicate that the mobility of the protein was reduced upon encapsulation. This may be due to either a steric restriction of protein movement, or a somewhat higher viscosity for the solvent (water) inside the pores of the slide, or a combination of both. The protein is not fully restricted in its motion, otherwise an anisotropy value approaching 0.4 would be observed.[33] It may be the case that the protein motion is severely restricted but that the Trp residue itself is able to rotate sufficiently to provide an anisotropy value which is not representative of the global motion of the protein.

To examine the mobility of a fully exposed Trp residue, we measured the anisotropy of NATA in solution and in dry-aged slides (NATA leaching from wet-aged slides prevented meaningful anisotropy measurements). The anisotropy increased from a value of zero in solution (complete randomization of polarization) to a value of 0.05 ± 0.01 when encapsulated. The results clearly indicated that the mobility of NATA was significantly reduced in the dry-aged slides, in agreement with previous studies which utilized probes such as prodan.[3] The increase in anisotropy is most likely the result of an increase in solvent viscosity, since the alternative possibility of adsorption of NATA onto the surface

of the silane would be expected to have resulted in a broadening of the HWHM. The measurement of time-resolved decays of anisotropy are required to further explore this issue.

The quenching, spectral and anisotropy results all indicate that the environment of the entrapped protein is likely one which has a lower mobility than that of free solution, and that this lowers the accessibility of small molecules which enter the pores of the slides to interact with the entrapped protein. The lower mobility is to be expected given the pore size of the dry-aged slides, which was ~6.5 nm. It would be expected that the internal water would have a strong association with the highly polar internal surfaces of the slide, which could promote a more ordered hydrogen bonded network within the solvent than would occur in bulk solvent, as has been suggested by others.[12,13] The result would be a lower mobility for the entrapped solvent which could cause the alterations in the spectroscopic parameters which were observed. The unique environment experienced by entrapped species also has a dramatic effect on the stability of entrapped monellin, as is described in the following chapter.[36]

2.4 Conclusions

The extremely thin sol-gel slides described in this chapter provide the ability to do "real-time" studies such as quencher and denaturant titrations which can provide a wealth of information about the characteristics of entrapped proteins. These slides have a number of uses in cases where information about the interaction of an analyte with an entrapped

biomolecule is desired either for characterization of the biomolecule and/or matrix, or in cases where fluorimetric sensing of the analyte is desired.

In this work, we demonstrated that the single Trp protein monellin can be encapsulated into a TEOS derived matrix without altering the structure of the protein. The entrapped proteins were able to interact with different species such as acrylamide, GdHCl and KI. However, many questions arose concerning the application of this encapsulation format for biosensor development. For example, the effect of the negatively charged silicate matrices on the protein-analyte interaction, the distribution of environments inside the sol-gel matrices and the possibility of an inaccessible fraction of the entrapped protein can all affect the signals obtained from the sol-gel based biosensor. Obviously, a large amount of work needs to be done to characterize and understand this encapsulation method as it pertains to further biosensor development.

2.5 References for Chapter 2

1. Braun S.; Rappoport, S.; Zusman, R.; Avnir, D.; Ottolenghi, M. *Mater. Lett.* **1990**, *10*, 1.
2. Lundgren, J.S.; Bright, F.V. *Anal. Chem.* **1996**, *68*, 3377.
3. Narang, U.; Jordan, J.D.; Bright, F.V.; Prasad, P.N. *J. Phys. Chem.* **1994**, *98*, 8101.
4. a) Nishida, F.; McKiernan, J.M.; Dunn, B.; Zink, J.I.; Brinker, C.J.; Hurd, A.J. *J. Amer. Ceram. Soc.* **1995**, *78*, 1640., b) Narang, U.; Bright, F.V.; Prasad, P.N. *Appl. Spec.* **1993**, *47*, 229., c) Matsui, K.; Matsuzuka, T.; Fujita, H. *J. Phys. Chem.* **1989**, *93*, 4991.
5. a) Dave, B.C.; Soyez, H.; Miller, J.M.; Dunn, B.; Valentine, J.S.; Zink, J.I. *Chem. Mater.* **1995**, *7*, 1431., b) Jordan, J.D.; Dunbar, R.A.; Bright, F.V. *Anal. Chem.* **1995**, *67*, 2436.
6. a) Yamanaka, S.A.; Nishida, F.; Ellerby, L.M.; Nishida, C.R.; Dunn, B.; Valentine, J.S.; Zink, J.I. *Chem. Mater.* **1992**, *4*, 495., b) Braun, S.; Shtelzer, S.; Rappoport, S.; Avnir, D.; Ottolenghi, M. *J. Non-Cryst. Solids* **1992**, *147*, 739., c) Wang, R.; Narang, U.; Prasad, P.N.; Bright, F.V. *Anal. Chem.* **1993**, *65*, 2671., d) Narang, U.; Prasad, P.N.; Bright, F.V.; Ramanathan, K .; Kumar, N.D.; Malhotra, B.D.; Kamalasanan, M.N.; Chandra, S. *Anal. Chem.* **1994**, *66*, 3139. e) Yamanaka, S.A.; Dunn, B.; Valentine, J.S.; Zink, J.I. *J. Am. Chem. Soc.* **1995**, *117*, 9095.
7. Miller, J.M.; Dunn, B.; Valentine, J.S.; Zink, J.I. *J. Non-Cryst. Solids* **1996**, *220*, 279.
8. a) Dave, B.C.; Dunn, B.; Valentine, J.S.; Zink, J.I. *Anal. Chem.* **1994**, *66*, 1120A., b) Avnir, D.; Braun, S.; Lev, O.; Ottolenghi, M. *Chem. Mater.* **1994**, *6*, 1605.

9. Edminston, P.L.; Wambolt, C.L.; Smith, M.K.; Saavedra, S.S. *J. Coll. Int. Sci.* **1994**, *163*, 395.

10. Wambolt, C.L.; Saavedra, S.S. *J. Sol-Gel Sci. Tech.* **1996**, *7*, 53.

11. Samuel, J.; Polevaya, Y.; Ottolenghi, M.; Avnir, D. *Chem. Mater.* **1994**, *6*, 1457.

12. a) Xu, S.; Ballard, L.; Kim, Y.J.;Jonas, J. *J. Phys. Chem.* **1995**, *99*, 5787, b) Korb, J.-P.; Delville, A.; Xu, S.; Demeulenaere, G.; Costa, P.; Johas, J. *J. Chem. Phys.* **1994**, *101*, 7074.

13. Shen, C.; Kostic, N.M. *J. Amer. Chem. Soc.* **1997**, *119*, 1304.

14. Eftink, M.R. In *Methods of Biochemical Analysis: Vol. 35, Protein Structure Determination*; Suelter, C.H., Ed.; John Wiley and Sons Inc.: New York, 1991; pp 127.

15. Demchenko, A.P.; Gryczynski, I.; Gryczynski, Z.; Wiczk, W.; Malak, H.; Fishman M. *Biophys. Chem.* **1993**, *48*, 39.

16. Hargrove, M.S.; Krzywda, S.; Wilkinson, A.J.; Dou, Y.; Ikeda-Saito, M.; Olson, J.S. *Biochem.* **1994**, *33*, 11767.

17. Eftink, M.R. *Biophys. J.* **1994**, *66*, 482.

18. a) Dahms, T.E.S.; Willis, K.J.; Szabo, A.G. *J. Am. Chem. Soc.* **1995**, *117*, 2321., b) Dahms, T.E.S.; Szabo, A.G. *Biophys. J.* **1995**, *69*, 569.

19. Frieden, C.; Jiang, N.; Cistola, D.P. *Biochem.* **1995**, *34*, 2724.

20. Beechem, J. M. Proc. *SPIE* **1992**, 1640, 676.

21. Chen, R.F. *Biochem. Biophys. Res. Comm.* **1964**, *17*, 141.

22. Barrett, E.P.; Joyner, L.G.; Halenda, P.H. *J. Amer. Chem. Soc.* **1951**, *73*, 373.

23. Fan, P.; Bracken, C.; Baum, J. *Biochem.* **1993**, *32*, 1574.

24. Fyfe, C.A.; Aroca, P.P. *Chem. Mater.* **1995**, *7*, 1800.

25. a) Brinker, C.J.; Scherer, G.W. *Sol-Gel Science*, Academic Press: New York, 1989. b) Hench, L.L.; West, J.K. *Chem. Rev.* **1990**, *90*, 33.

26. Eftink, M.R.; Ghiron, C.A. *Biochem.* **1976**, *15*, 672.

27. Morris, J.A.; Martenson, R.; Deibler, G.; Cagan, R.H. *J. Biol. Chem.* **1973**, *248*, 534.

28. Ramsden, J.T. *Chem. Soc. Rev.* **1995**, *24*, 73.

29. Blatt, E.; Hussain, A.; Sawyer, W.H. *Biochim. Biophys. Acta* **1986**, *861*, 6.

30. Eftink, M.R.; Ghiron, C.A. *Biochim.* Biophys. Acta **1987**, *916*, 343.

31. a) Eftink, M.R.; Ghiron, C.A. *Biochem.* **1977**, *16*, 5546, b) Eftink, M.R.; Ghiron, C.A. *J.Phys.Chem.* **1977**, *5*, 486.

32. C.M. Ingersoll, J.D. Jordan and F.V. Bright, *Anal. Chem.* **1996**, *68*, 3194.

33. R. Wang, S. Sun, E.J. Bekos and F.V. Bright, *Anal. Chem.* **1995**, *67*, 149.

34. Lakowicz, J.R. *Principles of Fluorescence Spectroscopy,* Plenum Press: New York, 1983.

35. Price, J.M.; Kaihara, M.; Howerton, H.K. *Appl. Optics* **1962**, *1*, 521.

36. Zheng, L.; Brennan, J.D.. *Anal. Chem.* submitted.

Chapter 3 Conformational Flexibility and Stability of Monellin Entrapped in the Sol-Gel Matrix

3.1 Introduction

In the past few years, the low temperature sol-gel processing method has been used by several groups for the development of analytical devices utilizing biological components.[1,2,3] It has been found that biomolecules were usually entrapped with the retention of a substantial fraction of their initial activity by the utilization of these materials.[3] In addition, many reports suggested that protein stability was actually improved upon entrapment.[1,4] These findings resulted in several studies which were aimed at understanding the structure and dynamics of entrapped proteins,[5] the internal environment of sol-gel derived matrices,[6] and the overall basis for the enhancement in long-term protein stability.[3] In spite of the amount of work done, the structure and environment of entrapped proteins and the basis for the improved stability are still not well understood.

As mentioned previously, the measurement of the fluorescence of tryptophan (Trp) residues can be utilized to monitor several parameters, including protein structure,[7,8] dynamics,[9] stability,[10] and folding and unfolding phenomena.[11] A standard method for examining protein stability in solution is to measure the changes in the fluorescence from intrinsic tryptophan residues as a function of temperature or denaturant concentration.[11] Proteins which contain a single Trp residue are generally used for such studies since they allow for unambiguous investigation of the region being probed, provide a simple system

for examining fluorescence lifetimes, and also provide a simpler system for probing rotational anisotropy or exposure of Trp to quenchers. Additionally, Trp fluorescence has also been used to examine the conformational motions and accessibility of entrapped proteins.[12]

In chapter 2, we described a method for preparing optically clear monoliths which were suitable for monitoring the fluorescence of Trp residues within encapsulated proteins. These sol-gel slides were sufficiently thin to permit titrations of an entrapped protein to be done, and allowed for an examination of the interaction between the entrapped single tryptophan protein monellin and external reagents. In this section, we extend these studies to investigate the thermal and chemical stability of monellin when entrapped in such sol-gels by performing equilibrium denaturation studies. Monellin was chosen for this study for a number of reasons. Firstly, the protein is small, with a molecular weight of 10.7 kDa and a diameter of 3.5 nm.[13,14] Thus, it is similar in size to a number of small proteins such as cytochrome-*c*[2,3a] and myoglobin[14] which have been studied previously in sol-gel derived monoliths. Secondly, the protein is highly structured, but has no disulfide bridges,[15] indicating that it should be possible to fully unfold the protein using either high temperatures or a high concentration of denaturant. Thirdly, monellin contains only one Trp residue per protein, located in a moderately hydrophobic region near the end of a β-sheet. This makes the interpretation of fluorescence data much simpler since a single segment of the protein can be monitored. Lastly, previous studies of monellin have shown that the intrinsic Trp fluorescence is sensitive to the unfolding of the

protein in solution,[16] thus intrinsic fluorescence should be useful for monitoring the stability, structure and conformational motions of the entrapped protein.

This study shows that the fluorescence spectra, steady-state anisotropy and acrylamide quenching of the single Trp residue within monellin can be used to provide useful information about a number of parameters. These include the ability of entrapped proteins to undergo large scale conformational changes; the changes in thermal, chemical and long term stability which occur upon encapsulation; and the effects of aging the sol-gel derived matrix on the distribution of protein environments. These results are able to provide useful insights into the basis for the changes in protein stability which are observed upon entrapment.

3.2 Experimental

3.2.1 Chemicals and Equipment

The chemicals and equipment used in this chapter were the same as those described in chapter 2.

3.2.2 Procedures

3.2.2.1 Preparation and Fluorescence Measurements of Protein Doped Sol-Gel Slides

Procedures for hydrolysis of the sol and preparation of the monellin doped sol-gel thin slides were the same as described in the previous chapter. In addition, the equipment and procedures for the fluorescence intensity and anisotropy measurements of monellin in

solution and when entrapped in the wet-aged and dry-aged slides were the same as described in the previous chapter.

3.2.2.2 Thermal Denaturation Studies

For solution-based studies, a volume of 2.0 mL of monellin in a buffer consisting of 100 mM sodium phosphate, 100 mM KCl, pH 7.2 was placed into a quartz fluorimeter cuvette. For studies of sol-gel slides, 2.0 mL of the buffer was placed into the cuvettes containing the slide. All the buffers used were purged with a nitrogen stream for 15 minutes before preparing the samples. The air space in the cuvette was filled with nitrogen gas to remove dissolved oxygen and the cuvette was immediately capped. Oxygen was shown to cause irreversible alterations in the fluorescence signals from thermally unfolded proteins.

The temperature was raised in *ca.* 5°C increments starting at 20°C and going to 70°C for solution or wet-aged slides and to 80°C for dry-aged slides. The temperature was controlled using a Neslab R110 recirculating water bath, and the temperature of the solution in the cuvette was measured directly using a thermistor probe (Hanna Instruments model 9043A) to account for loss of heat through the tygon tubing connecting the sample holder and the water bath. The samples were allowed to equilibrate for at least ten minutes at each temperature with no stirring. A fluorescence spectrum or anisotropy value was then collected from the sample and an appropriate blank at each temperature. The corrected spectra were integrated from 310 nm to 450 nm and the intensity at each point was normalized to the intensity at the beginning of the experiment to generate intensity-based unfolding curves. Alternatively, anisotropy values were plotted directly

against temperature to generate anisotropy-based unfolding curves. The unfolding curves were analyzed by non-linear fitting to equations 1.14 and 1.15.

The differential heat capacity $\Delta C_{p,un}$ for equation 1.16 was measured by the following procedure: the unfolding curve of monellin was measured in solution at pH 3, 5 and 7, and the values of ΔH^0_{un} and T_{un} were calculated by fitting of equation (1.15). $\Delta C_{p,un}$ was calculated by dividing the difference in ΔH^0_{un} at two different pH values by the difference in T_{un} at these pH values. The average of $\Delta C_{p,un}$ was used for further calculations of $\Delta G_{un}(T_r)$.

3.2.2.3 Chemical Denaturation Studies

For solution based studies, a volume of 1.30 mL of monellin in buffer was added to a quartz cuvette. A total of twenty-nine aliquots of 8.0 M GdHCl in buffer were added (4 x 30 μL, 12 x 60 μL, 13 x 100 μL) with constant stirring and a minimum of 10 minutes was allowed for equilibration (with a shutter blocking the excitation light). A fluorescence spectrum or a steady state anisotropy value was collected at each point from both the sample and a blank containing an identical concentration of GdHCl. For sol-gel slide studies, the rehydrated slides (wet-aged or dry-aged) were mounted into a quartz cuvette and 1.30 mL of buffer was added. The 8.0 M GdHCl solution was added into the buffer as described above. After each addition, the solution was gently stirred for 20 minutes to allow for equilibration. Once again, a fluorescence spectrum or a steady-state anisotropy value was collected at each point for both the sample and a blank containing an identical concentration of GdHCl. The solution-based spectra were corrected for dilution factors.

No dilution correction was necessary for slides containing protein. The intensity-based and anisotropy-based unfolding curves for these experiments were obtained as described for the thermal denaturation experiments.

The unfolding curves were fit using equation 1.13.[17]

3.2.2.4 Acrylamide Quenching Studies

Acrylamide quenching studies were done for monellin in solution and in slides in the presence of varying amounts of GdHCl. For proteins in solution, 2.0 mL of a 10 μM monellin solution was titrated by adding a total of twenty-two 10 μL aliquots of 8.0 M acrylamide in buffer with continuous stirring. A fluorescence spectrum was collected from the sample and an appropriate blank after each addition. Spectra were corrected for sample dilution and were integrated as described above. For sol-gel slide studies, 2.0 mL of buffer (with or without 4.5 M GdHCl) was added to the cuvettes containing the samples and the encapsulated proteins were then titrated as described above, with an equilibration time of 10 minutes after each addition of quencher. No dilution corrections were done for slide titrations. All quenching data were analyzed using equation 2.1.[14,18]

3.3 Results and Discussions

3.3.1 Thermal Stability Studies

Steady-state fluorescence spectra and fluorescence anisotropy were measured at various temperatures for monellin in solution, in wet-aged slides and in dry-aged slides. The spectral characteristics at 20°C and 70°C are given in Table 3.1. The spectral

characteristics of free and entrapped monellin at 20°C were similar, although the anisotropy of the entrapped monellin was higher than in solution, likely owing to the higher viscosity of solvents within sol-gel derived matrices.[5b,6a,19] This suggests that encapsulation did not induce substantial conformational changes in the native protein, and agrees with results reported for other proteins.[2,3,14a]

The spectral characteristics of the denatured protein were quite different in sol-gel derived matrices when compared to the protein in solution. The spectral changes in solution were consistent with the movement of the Trp residue from a moderately hydrophobic region, which was fairly well protected from the solvent, to a more exposed and more polar environment as monellin was heated.[7] Cooling the protein to 20°C did not result in a full recovery of the native spectral characteristics. This was likely due to a small amount of aggregation, which was evident from the increase in light scattering at 330 nm observed for the cooled protein.

Table 3.1. Fluorescence spectral and steady-state anisotropy data for thermal denaturation of monellin.

Matrix	Intensity Change (± 2%)[a]	λ_{max} native (nm)	λ_{max} change (nm)[a,b]	FWHM change[a,c] (nm)	Initial anisotropy	Change of anisotropy[d]
Solution	53% decrease	335[c]	9[c]	10[c]	0.134 ± 0.002	0.046 ± 0.004[d]
Wet-Aged	80% decrease	334	4	6	-	
Dry-Aged	60% decrease	335	4	3	0.202 ± 0.002	0.031 ± 0.004[d]

[a]Changes reported refer to a change in temperature from 20°C to 70°C for monellin in solution or wet-aged slides, or from 20°C to 70°C for monellin in dry-aged slides, [b]the error is each value is ±1 nm, [c]FWHM is full-width-at-half-maximum, [d]this is the difference in anisotropy values between 45°C and the point where aggregation begins, taken at ~ 65°C.

Upon encapsulation, the shifts in both the emission maximum and anisotropy values upon unfolding were significantly smaller than in solution. This is consistent with a restriction in conformational motion, and suggests that the protein either did not unfold completely or unfolded to a state which was different than that in solution. Interestingly, the decrease in intensity was greater for entrapped proteins compared to the protein in solution. Given the smaller changes in emission wavelength and anisotropy upon unfolding of entrapped proteins, the larger decreases in intensity for entrapped proteins

suggest that the monoliths retained a large amount of entrapped O_2 even after purging with nitrogen, leading to an increase in the quenching of the exposed Trp residue.[20]

Figures 3.1 and 3.2 show the plots of normalized integrated intensity and steady-state anisotropy at different temperatures for monellin in solution and when encapsulated. The intensity and anisotropy changes observed in the initial and final portions of the unfolding curves are due to thermally induced effects on the quantum yield and mobility of the Trp residue, and are normally observed during thermal denaturation of proteins.[21] The anisotropy curve for monellin in dry-aged slides did not show substantially sloping baselines, suggesting that increases in temperature did not affect the global motion of the folded protein when entrapped. This provides further evidence that the motions of entrapped monellin were restricted upon entrapment. In most cases, the main unfolding transition could be detected by both intensity and anisotropy changes. However, the wet-aged monoliths produced a significant degree of light scattering which could be observed using both fluorescence and absorbance measurements. The polarized nature of the scattered light resulted in extremely high anisotropy values from wet-aged monoliths[22] especially at high temperature when the intensity of the protein was substantially quenched. For this reason, it was not possible to obtain meaningful data from anisotropy measurements of monellin in wet-aged slides during thermal denaturation.

An interesting aspect of the intensity-based thermal unfolding curves is that encapsulation of monellin into dry-aged slides resulted in a broadening of the unfolding transition, as shown in Figure 3.1. The unfolding range was approximately 18°C for monellin in dry-aged slides, while the unfolding range for monellin in solution and wet-

aged slides was only 14°C. This suggests that there was a distribution of microenvironments for the entrapped protein in dry-aged slides, each with a slightly different thermodynamic stability. This agrees with previous studies by Bright and co-workers[6a] and our own group,[13] which suggest that a distribution of environments likely exists within sol-gel derived matrices.

The intensity-based unfolding curves for free and entrapped monellin were analyzed using equation (1.14). The results are given in Table 3.2 for the protein at pH 7.2. Attempts to fit the anisotropy-based unfolding curves were unsuccessful, likely owing to the large increase in anisotropy above 65°C for both free and entrapped monellin. For the free protein, it was assumed that the unfolding was a two-state reaction from a native state (N) to an unfolded state (U), and that complete unfolding occurred. In the case of entrapped proteins, it was assumed that the protein unfolded to some intermediate state (I) which may or may not be identical to the completely unfolded state obtained in solution. This intermediate state represents the final state for the denatured protein within the monoliths, and thus allows the unfolding to be treated as a two-state unfolding process. It is realized that the values calculated for entrapped proteins using equation (1.14) likely represent the average over a distribution of environments. However, these values are still useful for the purposes of comparisons to solution values.

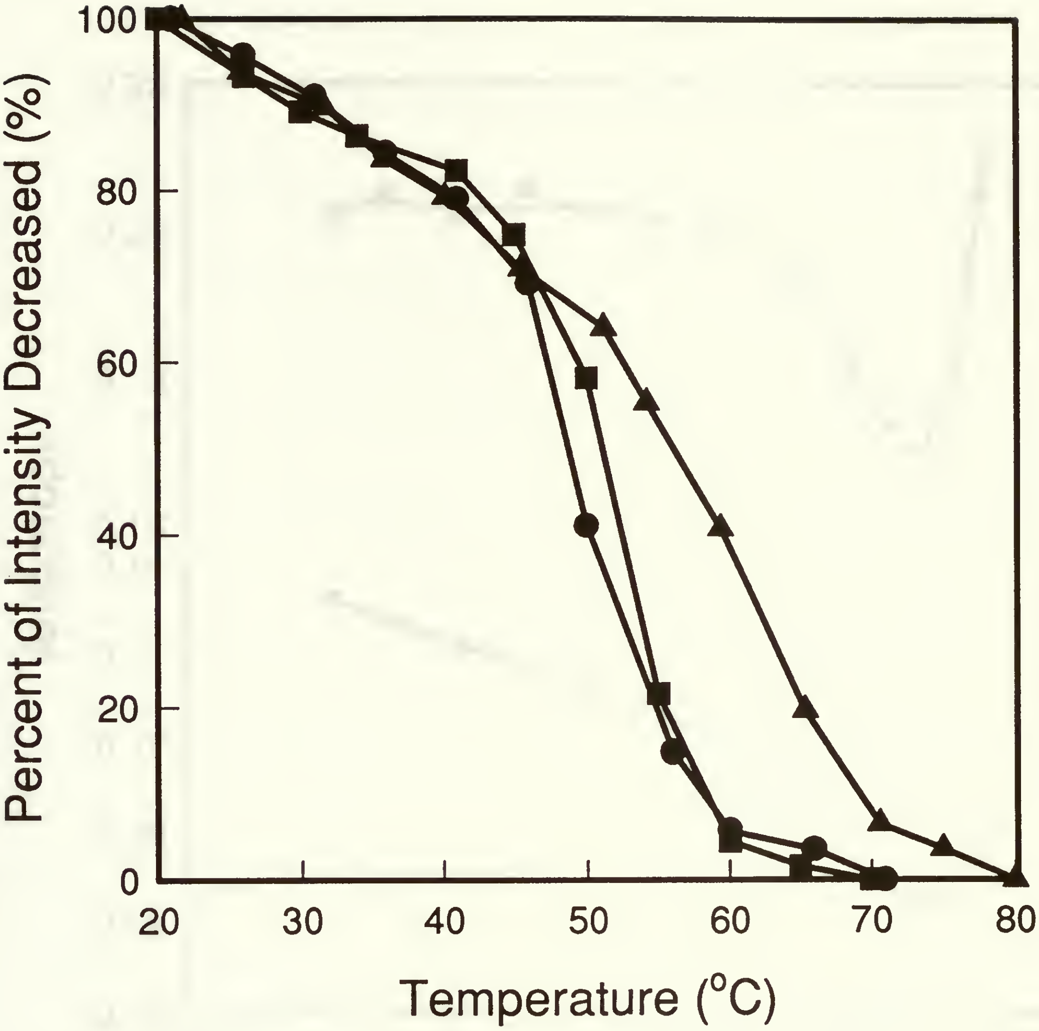

Figure 3.1 Changes in fluorescence intensity for monellin as a function of temperature in solution (●); in a wet-aged slide (■); and in a dry-aged slide (▲). The symbols are the experimentally derived data points. The solid lines are the lines-of-best-fit as determined by fitting to equation 1.14. The data was normalized by setting the initial intensity to a value of 100 and the final intensity to a value of 0 to provide an overlap of each unfolding curve.

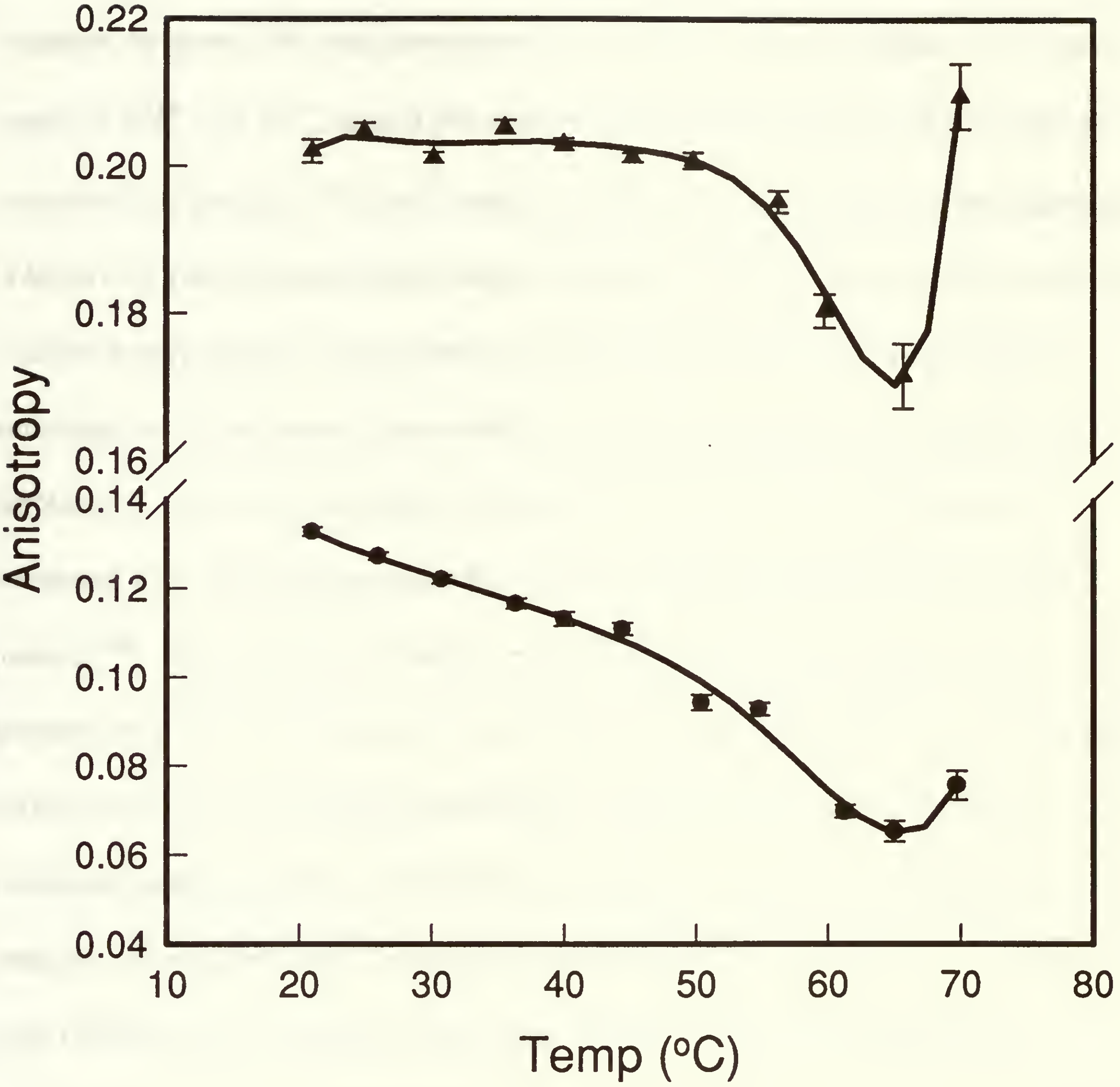

Figure 3.2 Changes in fluorescence anisotropy for monellin as a function of temperature in solution (●); and in a dry-aged slide (▲). The symbols are the experimentally derived data points.

Two comparisons can be made to better understand the meaning of the thermodynamic data. The first is a comparison of solution values to those obtained in wet-aged sol-gel slides. Here, the T_{un} value increased by 3°C while both ΔH^0_{un} and ΔS^0_{un} decreased by about 15% upon entrapment of monellin into wet-aged slides. The lower values of ΔH^0_{un} and ΔS^0_{un} suggest that monellin unfolded to a different state in solution as compared to in the slide. The lower value for the enthalpy of unfolding can be interpreted in terms of a lower amount of heat energy being absorbed by the protein during unfolding in slides when compared to the protein in solution. The difference in the entropy of unfolding can be interpreted in terms of the change in the solvation of the protein upon unfolding. Generally, the unfolding of a protein will result in a large increase in the amount of water molecules required for solvation of the polypeptide backbone of the protein.[23,24] The smaller total change in entropy for monellin in a wet-aged slide can therefore be interpreted in terms of a lower degree of exposure of the protein backbone to solvent, which is consistent with a restriction in the conformational motions of the entrapped protein and thus a smaller degree of unfolding. The smaller changes in the enthalpy and entropy of unfolding strongly suggests that the unfolding behaviour was quite different upon entrapment, and is likely indicative of incomplete unfolding.

In order to properly calculate the free energy of the unfolding transition using equation 1.15, it was first necessary to determine the change in heat capacity between the folded and unfolded states of the protein. This value was determined by monitoring the thermal unfolding of monellin in solution at different pH values and calculating ΔH^0_{un}, ΔS^0_{un} and T_{un} in each case. The change in heat capacity ($\Delta C_{p,un}$) was determined from a plot of $\Delta(\Delta H^0_{un})$

vs. ΔT_{un}, and had an average value of 10600 ± 1500 J.(mol.deg)$^{-1}$. This value is in reasonable agreement with values determined for other proteins of a similar size.[25] It was assumed that this value was similar in wet-aged and dry-aged slides, based on the fact that this parameter is not very solvent dependent.[26]

The value of ΔG_{un} was determined for free and encapsulated monellin equation 1.16, and the values are given in Table 3.2. Again comparing the values obtained for monellin in solution and in wet-aged gels, it is apparent that the value of ΔG_{un} was lower for the entrapped protein. This is expected given the lower values of both ΔH^0_{un} and ΔS^0_{un} for the entrapped protein, and is a further indication that the entrapped protein did not unfold completely. Given the possibility of incomplete unfolding for the entrapped protein, the free energy change may not be able to correctly indicate the stability differences upon encapsulation. However, the unfolding temperature calculated from equation 1.15 does seem to provide a useful indication of protein stability, and suggests an overall increase in protein stability upon encapsulation into dry-aged slides.

The second comparison that can be made is between the thermodynamic values obtained in wet-aged slides and those obtained in dry-aged slides. In this case, the ΔH^0_{un} decreased by about 30% while the ΔS^0_{un} value decreased by 33% compared to the values obtained from monellin in wet-aged slides. This has the effect of increasing the T_{un} by 11°C, suggesting that the protein has increased thermal stability in dry-aged slides. The further decrease in the values of ΔH^0_{un} and ΔS^0_{un} for unfolding for monellin in dry-aged slides compared to wet-aged gels suggests that the amount of heat absorbed and the solvation of the protein by the entrapped solvent is altered, and suggests that the protein is

less capable of unfolding as the gel aged. This lower entropy value is likely a manifestation of the higher overall rigidity of solvents within dry-aged slides.[3a,13] A more rigid solvent will not undergo as large a change in entropy upon ordering of the solvent around the unfolded protein, and thus the entropy change is smaller for unfolding of the protein in dry-aged gels compared to wet-aged slides.

Table 3.2. Thermodynamic parameters for thermal unfolding of monellin in solution and in wet-aged or dry-aged slides.

Sample	ΔH^0_{un} (kJ.mol^{-1})^a	ΔS^0_{un} (J.K^{-1}.mol^{-1})^a	T_{un} (°C)^b	ΔG^0_{un} (kJ.mol^{-1})^c	$\chi^{2(e)}$
Monellin in Solution	504 ± 50^f	1560 ± 125^f	50 ± 1	32.9 ± 4.5	0.98
Monellin in a Wet-Aged slide	434 ± 45^f	1330 ± 120^f	53 ± 1	26.7 ± 3.5	0.99
Monellin in a Dry-Aged slide	300 ± 28^f	890 ± 70^f	64 ± 1	9.0 ± 1.3	0.99

[a]These values were obtained by fitting of unfolding curves to equation 1.14,
[b]calculated from $\Delta H^0_{un} / \Delta S^0_{un}$,
[c]the value of ΔG^0_{un} was determined using a value of $\Delta C_{p,un}$ = 10600 cal.(deg.mol)$^{-1}$,
[e]determined from non-linear curve fitting using SigmaPlot 1.02 for Windows,
[f]derived from intensity measurements,
[g]derived from anisotropy values.

The value of ΔG_{un} for the dry-aged slide was significantly lower than the value obtained either in solution or in wet-aged slides. Given the obvious increase in the temperature of the unfolding transition, it would appear that the calculated free energy

value may be significantly lower than the actual value. The value of ΔG_{un} was calculated based on the assumption that $\Delta C_{p,un}$ was similar in solution, wet-aged and dry-aged slides. Clearly, if the protein is not fully unfolding then the differential heat capacity of the folded and unfolded states will be significantly reduced. The value of ΔG_{un} was recalculated at several values of $\Delta C_{p,un}$, and increased as the value of $\Delta C_{p,un}$ decreased, reaching a value of 39 kJ.mol^{-1} for a $\Delta C_{p,un}$ value of 0 J.(deg.mol)^{-1}. Since the value of $\Delta C_{p,un}$ was not known for monellin in dry-aged slides, we were not able to reliably calculate a free energy value. For this reason, a second method of obtaining ΔG_{un} was used which had no reliance on temperature, and thus did not depend on the value of $\Delta C_{p,un}$. This is described in the next section.

Overall, the thermodynamic analysis of the unfolding of monellin in solution and in wet-aged or dry-aged slides provided several useful pieces of information. The lowering of the enthalpy and entropy values upon entrapment clearly show that the unfolding of the entrapped protein results in a different final state compared to the free protein in solution. The thermodynamic analysis also showed that the unfolding temperature (T_{un}) of monellin was only slightly affected by encapsulation in wet-aged slides, but was increased by 14°C upon entrapment in dry-aged slides. These results indicate that the initial stages of sol-gel formation did not substantially alter the stability of the protein, at least in the case of monellin. The lack of a large improvement of thermal stability in wet-aged gels is not unexpected since the wet-aged gels are still fairly loosely crosslinked.[27] The viscosity of the entrapped solvent within such gels is similar to that in solution,[6a] thus the protein appears to behave as if it were in solution, although it is not able to fully unfold. The values may be significantly lower than the actual values. The values of [illegible] were calculated based on the assumption that [illegible] was similar in solution and [illegible] dry aged films. Clearly, if the protein is not fully unfolding then the difference [illegible] of the folded and unfolded states will be significantly reduced. The value of [illegible] will be sensitive to different values of [illegible] and decreased as the value of [illegible] decreased [illegible] kJ mol [illegible] for a [illegible] value of [illegible]. Since the value of [illegible] for unfolding in the aged films [illegible] we have no way to reliably calculate a [illegible] value. For this reason, a second method of [illegible] was used which had [illegible] temperature, and thus did not depend on the value of [illegible]. This is described in the next section.

Overall, the thermodynamic analysis of the unfolding of [illegible] and aged as dry aged slides provided several useful pieces of information. The [illegible] the enthalpy and entropy values [illegible] clearly show that the [illegible] of the unaged protein results in a [illegible] the [illegible]. The thermodynamic analysis also showed that the unfolding temperature [illegible] was only slightly affected [illegible] in unaged slides, but [illegible] in the aged [illegible]. These [illegible] formation did not substantially [illegible] the stability of the protein, at least [illegible] transition. The lack of a large improvement of thermal stability [illegible] short period [illegible] fairly lengthy [illegible] the [illegible] within each [illegible] appears to [illegible] although it is not [illegible].

substantial increase in the unfolding temperature for monellin in dry-aged gels provides solid evidence that the sol-gel derived matrix dramatically alters the behaviour of the entrapped protein. This indicates that the internal environment of dry-aged slides is substantially different than that of aqueous solution, in agreement with our previous study described in chapter 2.

3.3.2 Chemical Stability Studies

Table 3.3 shows the spectral characteristics and steady-state fluorescence anisotropy values obtained from monellin in solution, wet-aged monoliths and dry-aged monoliths at different levels of the chemical denaturant GdHCl. The spectral characteristics of native monellin (no denaturant) were identical to those obtained during thermal denaturation studies. Once again, the shifts in the spectral emission maxima and anisotropy were smaller for unfolding of entrapped monellin than for the protein in solution, in agreement with the results from the thermal denaturation studies. The change in the emission maximum upon unfolding of the protein in wet-aged slides was slightly larger than in dry-aged slides, suggesting that the conformational motion of the protein was reduced upon drying, which is again in agreement with the results from the thermal denaturation study.

Figures 3.3 and 3.4 show the integrated intensity and steady-state anisotropy at different levels of denaturant for monellin in solution and when encapsulated. In all cases, there was an initial *increase* in intensity. In solution, the increase was 30% during the addition of the first 1.5 M of GdHCl, while the increase was roughly half as large for the encapsulated protein. This increase was accompanied by a decrease in the accessibility of

the Trp residue to the quencher acrylamide (described below), indicating that the presence of GdHCl resulted in a conformational change in the region of the Trp residue. This type of behavior has been observed for other proteins such as ribonuclease T_1 and barnase, and has been interpreted in terms of the specific binding of guanidine to the protein, with the induction of a change in fluorescence properties.[28] The smaller increase of intensity for the encapsulated protein suggests that either not all of the protein was accessible to GdHCl, or that the interaction of GdHCl with the entrapped protein was not able produce as large a conformational change as was possible in solution.

Table 3.3. Spectral data for chemical denaturation of monellin in solution, wet-aged slides and dry-aged slides.

Matrix	Intensity Change (± 2%)	λ_{max} native (nm)	λ_{max} change[a] (nm)	FWHM change[b] (nm)	Initial anisotropy	Change of anisotropy[a]
Solution	30% increase[c] 38% decrease[d]	334[e]	11[e]	5[e]	0.134 ± 0.004	0.079± 0.007
Wet-Aged Monolith	15% increase 40% decrease	333	7	5	0.195 ± 0.006	0.024 ± 0.008
Dry-Aged Monolith	13% increase 20% decrease	334	5	4	0.20 ± 0.02	0.023 ± 0.008

[a] Total change in emission wavelength or anisotropy between 0 M and 4.5 M GdHCl, [b] FWHM is full-width-at-half-maximum [c] for addition of first 1.5 M GdHCl, [d] for addition of the next 2.5 M GdHCl, [e] the error is each value is ±1 nm.

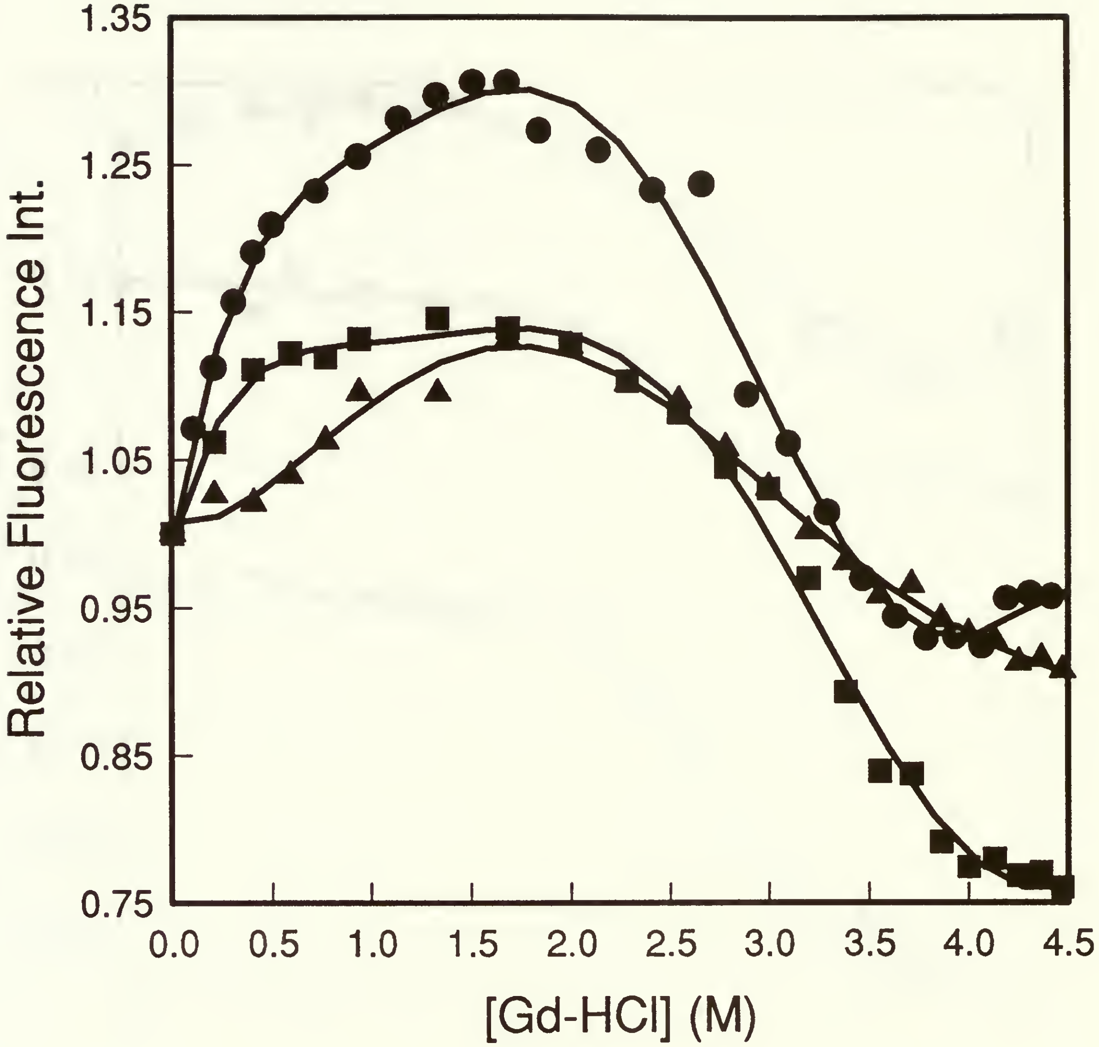

Figure 3.3 Changes in fluorescence intensity for monellin as a function of GdHCl concentration in solution (●); in a wet-aged slide (■); and in a dry-aged slide (▲). The symbols are the experimentally derived data points. The solid lines are the lines-of-best-fit as determined by fitting to equation 1.13.

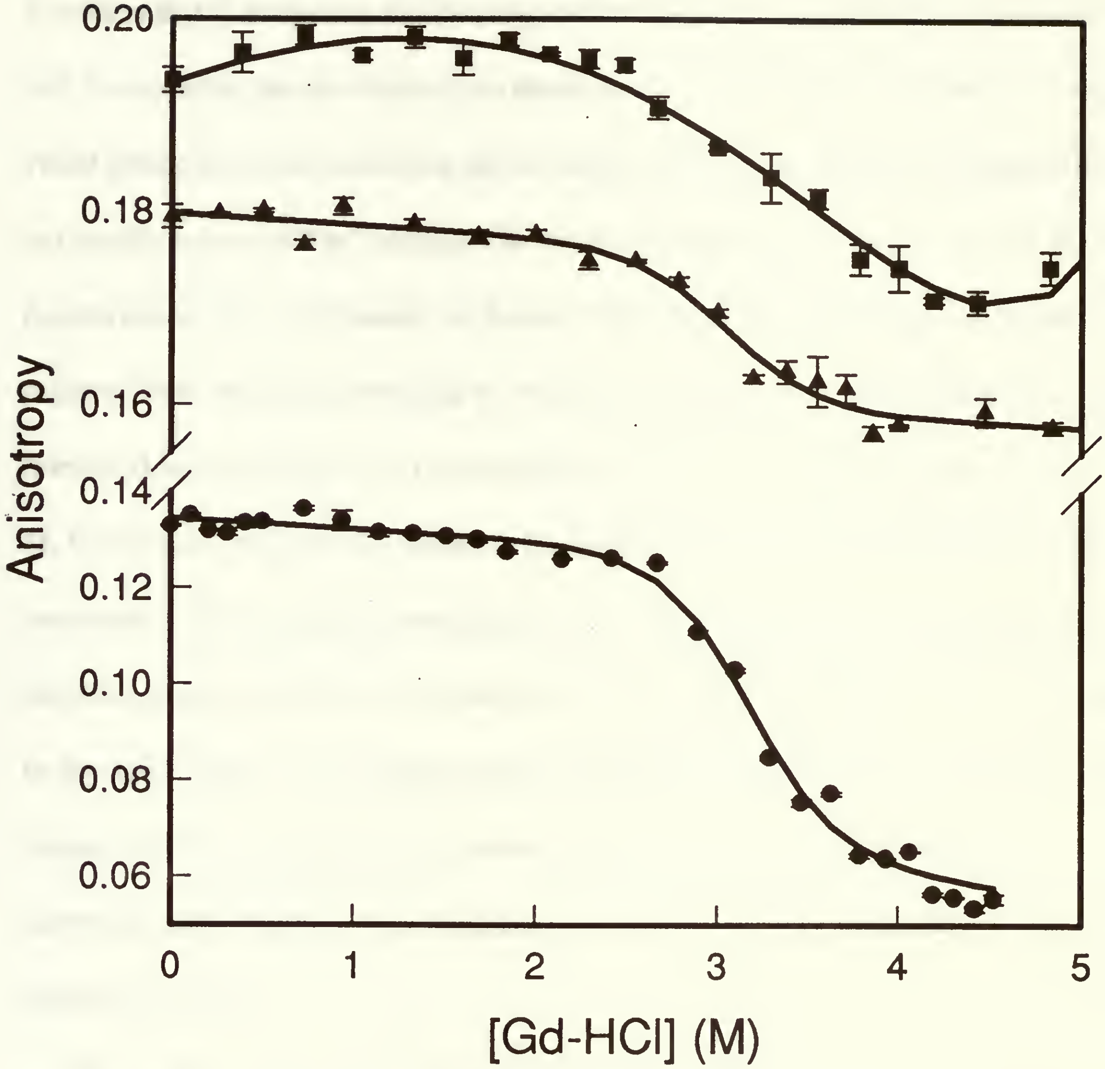

Figure 3.4 Changes in fluorescence anisotropy for monellin as a function of GdHCl concentration in solution (●); in a wet-aged slide(■); and in a dry-aged slide (▲). The symbols are the experimentally derived data points. The solid lines are the lines-of-best-fit as determined by fitting to equation 1.13.

Between roughly 1.5 M and 4.0 M a large decrease in intensity was observed for monellin in solution and in wet-aged gels. Using the intensity at 1.5 M as a basis point, it is evident that in both cases the intensity decreased by approximately the same amount, and it is apparent that the slope of the denaturation curves are quite similar. A simple visual inspection of the unfolding curves suggests that the monellin in wet-aged gels was not significantly stabilized compared to monellin in solution, in agreement with the thermal denaturation study. The results for denaturation of monellin in dry-aged gels were quite different from the results obtained in solution or wet-aged gels. In this case, the intensity decreased by only 20% as the concentration of GdHCl was increased from 1.5 M to 4.5 M. In addition, the intensity values never became constant even when 5.0 M of GdHCl was present. This supports the suggestion that the protein may not have completely unfolded in dry-aged slides. The most striking aspect of the unfolding curve for monellin in dry-aged slides is the broadness of the unfolding transition. This clearly shows that the protein exists in a distribution of environments, each with a slightly different thermodynamic stability, and again agrees with the results obtained from the thermal denaturation study.

The steady-state anisotropy values measured during chemical denaturation of free and entrapped monellin (Fig. 3.4) provided further evidence that the environment of the entrapped proteins was substantially different from a normal aqueous environment. Once again, the average anisotropy of the native protein in wet-aged and dry-aged slides was substantially higher than the value obtained in solution, as was observed during the

Between roughly 1.5 M and 3.0 M, a large decrease in viscosity was observed for myosin in solution and in wet-aged fish. Using the viscosity at 1.5 M as a base point, it is evident that in both cases the viscosity decreased by approximately the same amount, and it is apparent that the shape of the denaturation curves are quite similar. A visual inspection of the unfolding curves suggests that the myosin in wet-aged fish is only slightly more stabilized compared to myosin in solution, in agreement with the thermal denaturation study. The results on denaturation of myosin in dry-aged fish were quite different from the results obtained in solution or wet-aged fish. In this case, the viscosity decreased by only 20% as the concentration of GdnHCl was increased from 1.5 M to 3.0 M. In addition, the viscosity could not be measured even when 5.0 M of GdnHCl was present. This supports the suggestion that the protein was less completely unfolded in dry-aged fish. The most striking aspect of the unfolding curves for myosin in dry-aged fish is the broadness of the unfolding transition. This clearly shows that the protein exists in a distribution of conformations, each with a slightly different conformational stability, and again agrees with the results obtained from the thermal denaturation study.

The steady-state fluorescence values measured during chemical denaturation of fish and [illegible] (Fig. 5.9) provided further evidence that the conformation of the wet-aged protein was homogeneous. [illegible] there, a [illegible] suggests [illegible]. Once again, the average [illegible] of the [illegible] of wet-aged and dry-aged [illegible] was substantially higher than [illegible] in solution, as was observed during the thermal denaturation studies. In both solution and slides, the anisotropy of monellin remained relatively constant over a range of 0 M to 2.5 M GdHCl. The insensitivity of anisotropy to GdHCl concentration over this range indicates that the overall mobility of the protein in the region of the Trp residue remained constant. Further addition of GdHCl caused the anisotropy of free monellin to decrease substantially, which is indicative of an unfolded protein where the local motion of the Trp residue dominates the depolarization behaviour. For monellin in wet-aged and dry-aged monoliths, addition of GdHCl caused an obvious decrease in the anisotropy, which clearly showed the unfolding transition. However, in both cases, the change in anisotropy was significantly smaller than that obtained in solution. This result can be interpreted in several ways; incomplete unfolding of the protein, a contribution from an inaccessible fraction of protein, an environment of higher local viscosity compared to solution, or a large contribution from scattering which leads to an apparent increase in anisotropy. Given the results presented up to this point, it is most likely that the smaller changes in anisotropy reflected a restriction of the conformational motions of the entrapped proteins, and resulted from incomplete unfolding of the entrapped protein.

To obtain quantitative information on the changes in stability upon encapsulation, the intensity and anisotropy-based unfolding curves for free and entrapped monellin were analyzed using equation 1.13. The thermodynamic data is shown in Table 3.4. The unfolding free energy values obtained from anisotropy data were significantly larger than those obtained from intensity data. This trend is likely the result of the inability to properly fit equation 1.13 to the intensity-based unfolding curve, owing to the initial intensity rise.

This is apparent from the poor chi-squared values for the intensity- based data. The free energy change for the unfolding transition of free protein (calculated from anisotropy-based unfolding curves owing to the better correlation co-efficients) provides values which are in excellent agreement with the values obtained from thermal denaturation data. However, the free energy value obtained from chemical denaturation studies of monellin in dry-aged gels increased slightly (compared to the value obtained for monellin in wet-aged gels), and is substantially higher than the value obtained from thermal denaturation experiments. This strongly suggests that the free energy value calculated for monellin in dry-aged gels from thermal denaturation data was significantly affected by the use of an incorrect value for $\Delta C_{p,un}$. The slight increase in the value of ΔG_{un} for monellin as the monolith aged is in qualitative agreement with the increase in the unfolding temperature. The lower values of ΔG_{un} for entrapped monellin as compared to monellin in solution again suggests that the protein was not able to fully unfold when entrapped, and agrees with the data obtained from the thermal denaturation study.

The other important piece of information from the chemical denaturation curves is that the midpoint of the unfolding transition is similar for free and entrapped proteins. This is likely true for the protein in solution and wet-aged slides, given the similarity in the denaturant indices (m_G values) and the slopes of the unfolding transition, but is probably not valid in the case where monellin is encapsulated in dry-aged monoliths. In the latter case, there is obviously a much broader unfolding transition and a higher value for the denaturant index, likely signifying a distribution of environments for the protein, each of which likely has a different thermodynamic stability. However, the fitting was done with

This is expected from the good chi-squared values for the two-state model data. The free energy change for the unfolding transition of the protein [illegible] and its pattern based unfolding curves using urea [illegible] denaturation conditions [illegible] values are in excellent agreement with the values obtained from thermal denaturation [illegible]. However, the free energy value obtained from chemical denaturation curves of [illegible] dry-taped state [illegible] slightly [illegible] of the value obtained for [illegible] gels, and is substantially higher than the value obtained from thermal denaturation experiments. This strongly suggests that the free energy value calculated for unfolding of dry-taped gels from thermal denaturation is not significantly affected by the lack of a baseline value for ΔC_p. The slight increase in the value of ΔG [illegible] essentially equal is in qualitative agreement with the increase in the melting temperature. The lower values of ΔG_u for the [illegible] as compared to [illegible] again suggests that the protein [illegible] in agreement with the data obtained from the thermal denaturation study.

The most important piece of information from the chemical denaturation curves is that the mechanism of the unfolding transition is similar for the gel and solution conditions. This is likely true for the protein in solution and [illegible] gels, given the similarity of their denaturant-induced transitions and the shapes of the unfolding curves, but it is likely not valid in the case where [illegible] is compared to dry-taped [illegible] state, which is definitely a much broader unfolding transition and a higher [illegible] denaturation curve, likely suggesting a mechanism of [illegible] for the protein, and which likely has a different thermodynamic stability. However, [illegible] the assumption of a single type of environment, which is certainly too simplistic based on the breadth of the unfolding transition in dry-aged slides.

Table 3.4. Thermodynamic parameters for the GdHCl induced unfolding of monellin.

SAMPLE	ΔG_{UN} (kJ.mol^{-1})^{a,b}	$-m_G$ (kJ.L.mol^{-2})^{a,b}	$D_{1/2}$ (M)^{a,c}	$\chi^{2(d)}$
Monellin in Solution	24 ± 3 34 ± 2	6.8 ± 0.7 8.0 ± 0.8	3.0 ± 0.4 3.2 ± 0.3	0.90 0.99
Monellin in a Wet-Aged Monolith	22 ± 2 27 ± 1	6.7 ± 0.9 8.2 ± 0.8	3.2 ± 0.5 3.3 ± 0.3	0.98 0.99
Monellin in a Dry-Aged Monolith	20 ± 2 29 ± 1	6.1 ± 0.5 9.4 ± 0.8	3.2 ± 0.3 3.1 ± 0.2	0.95 0.99

[a] The first value is that obtained from measurements of integrated intensity. The second is that obtained from measurements of steady-state anisotropy,
[b] These values were obtained by fitting of unfolding curves to equation 1.13,
[c] this value was obtained by dividing ΔG_{un} by $-m_G$,
[d] determined from non-linear curve fitting using SigmaPlot 1.02 for Windows.

The thermal and chemical unfolding curves for free and entrapped monellin both suggest that the protein is conformationally restricted upon entrapment and that this may lead to incomplete unfolding of the entrapped protein. These results are very interesting when one considers that chemical denaturation relies on the ability of a denaturing species to reach different parts of the protein, and thus should rely on accessibility of denaturant to different regions of the monolith, while thermal denaturation should have no dependence on protein accessibility since temperature changes should affect all proteins equally. The similarity in unfolding behaviour suggests that the ability of GdHCl to access and thus denature the protein was not significantly affected by encapsulation in wet-aged

or dry-aged slides. These results argue against an substantial inaccessible fraction of protein in the either wet-aged or dry-aged slides.

3.3.3 Acrylamide Quenching

To further explore the accessibility of the folded and unfolded protein, acrylamide quenching studies were undertaken. Figure 3.5 shows typical Stern-Volmer plots of the acrylamide quenching of monellin in solution at various concentrations of GdHCl. These data were analyzed using equation (2.1). The results are shown in Table 3.5. The quenching of native monellin showed a K_{SV} value of 3.3 M^{-1} and a quenching sphere volume of 0.4 M^{-1}. As the concentration of GdHCl in solution was increased to 2.5 M, the K_{SV} value decreased, indicating that the environment of the Trp residue was altered as the level of denaturant increased. This correlates to the increase in the intensity observed during the intensity based titrations, and confirms that the protein undergoes a slight conformational change upon interaction with GdHCl. Increasing the denaturant concentration to 4.5 M resulted in the main unfolding transition, and caused an increase in the K_{SV} value to 4.2 M^{-1}. In all cases the protein was fully accessible to quencher (i.e. $f_i = 0$) as would be expected for a protein in solution. The K_{SV} value is the combination of the bimolecular quenching constant (k_q) and the unquenched lifetime (τ_0). The mean fluorescence lifetime of native monellin is 2.6 ns,[19b] providing a k_q value of 1.26 x 10^{-9} $M^{-1}s^{-1}$. The fluorescence lifetime drops to 1.8 ns in the presence of 4.5 M GdHCl (measured by J. D. Brennan at University of Windsor), resulting in a k_q value of 2.33x10^{-9} $M^{-1}s^{-1}$, which is almost double the value of the native protein. The k_q is still substantially lower

than that of free tryptophan ($k_q = 5.86 \times 10^{-9}$ $M^{-1}s^{-1}$),[19a] but this is expected owing to the presence of the polypeptide chain which will partially block the accessibility of acrylamide to the Trp in the protein. These results therefore indicate that the Trp does become substantially more exposed upon denaturation with GdHCl.

Table 3.5 Stern-Volmer analysis of acrylamide quenching for native and partially denatured monellin in solution.

[GdHCl] (M)	K_{SV} (M^{-1})	V (M^{-1})	constant	r^2
0	3.3	0.4	1.01	1.00
1.8	2.2	1.0	0.96	0.99
2.5	2.4	0.9	0.97	0.99
4.5	4.2	0.9	0.98	1.00

Table 3.6. Stern-Volmer analysis of acrylamide quenching for native and chemically denatured monellin in wet-aged and dry-aged TEOS slides.

Sample[a]	[GdHCl] (M)	K_{SV} (M^{-1})	V (M^{-1})	f_i	constant	r^2
Monellin (wet-aged monolith)	0	2.3	0.4	0.15	0.96	0.98
	4.5	2.3	0.9	0.12	0.94	0.98
Monellin (dry-aged monolith)	0	2.9	0.6	0.08	0.97	1.00
	4.5	2.5	1.2	0.08	0.97	0.99

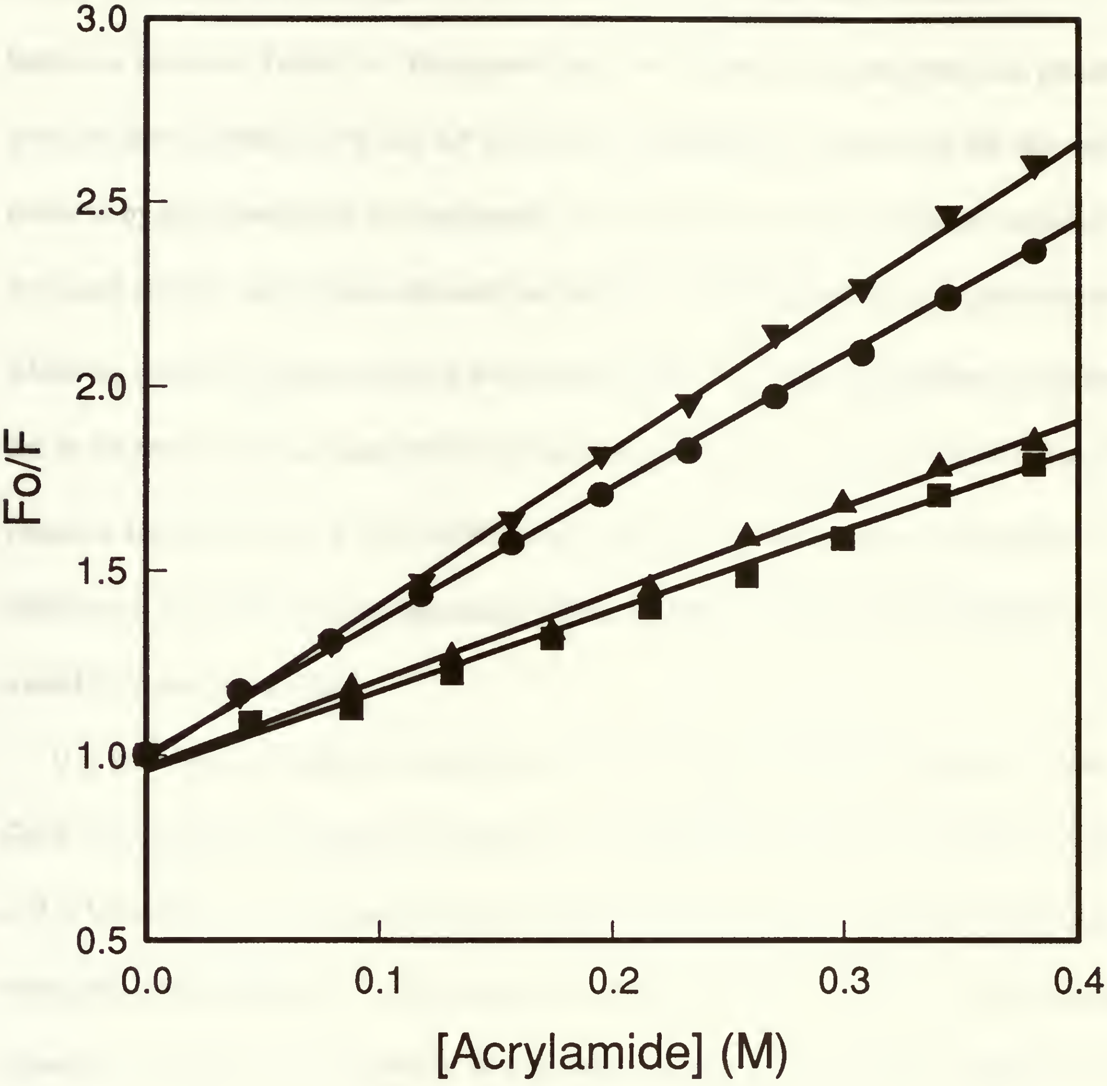

Figure 3.5 Stern-Volmer plots for acrylamide quenching of monellin at 0 M GdHCl (●), 1.8 M GdHCl (■) 2.5 M GdHCl (▲) and 4.5 M GdHCl (▼). The data was plotted according to equation (2.1) and was fit as described in Table 3.5.

Table 3.6 shows the values obtained from Stern-Volmer analysis of monellin in wet-aged and dry-aged slides, with the data fit according to equation 2.1. In all cases, the equation provided an excellent fit to the data, with correlation co-efficients of 0.98 or better, as shown in Table 3.6. The quenching experiments for the encapsulated proteins were performed only at 0 M and 4.5 M GdHCl to provide an overview of the changes incurred by the presence of the denaturant. Acrylamide quenching of native monellin in a wet-aged and dry-aged slide indicated that the K_{SV} value dropped upon encapsulation, while the quenching sphere volume remained relatively constant. In addition, entrapment led to the presence of an inaccessible fraction of protein between 8% and 15%. The K_{SV} values in the presence of 4.5 M GdHCl were similar or less than those in the absence of denaturant, while the V values increased slightly and the f_i values decreased slightly (for monellin in wet-aged slides).

It is interesting to note that monellin in both wet-aged and dry-aged gels at 4.5 M GdHCl had quenching results which were almost identical to those for monellin in solution at 2.5 M GdHCl. These results strongly suggest that the protein did not fully unfold when entrapped, and ended up in a conformation which was similar to that of partially denatured monellin in solution. These results are in agreement with both the smaller change in the emission maximum and the smaller change in anisotropy upon thermal or chemical unfolding of the entrapped protein. This is not surprising given that the average pore size of the dry-aged monoliths was 6.7 nm (chapter 2), which is only slightly larger than the size of the folded protein (3.5 nm). Hence the restriction in conformational motions is most likely due to the steric restrictions imposed by the pore dimensions.

The fractional inaccessibility values obtained from our quenching experiments suggest that only a small amount of protein was completely inaccessible (less than 15%). Interestingly, drying of the slide appears to *decrease* the inaccessible fraction of protein. The reason for this finding is not completely clear to us, however it may be the result of the dry-aged slides having a cross-section which was approximately 10-fold thinner than the wet-aged slides. Our fractional inaccessibility values are significantly lower than those reported by Saavedra and co-workers, who studied the quenching of entrapped BSA.[14] There are several possible explanations for this finding. 1) Monellin is smaller than BSA, and therefore may be more accessible since the protein is not as likely to completely fill the pore within which it resides. 2) Monellin has a single Trp residue, while BSA has two Trp residues. It is well known that inequivalent Trp residues within a single protein can result in non-linear SV plots, and can therefore alter the fits to such plots.[29] 3) The possibility of static quenching of Trp fluorescence was not accounted for in Saavedra's study, which can also lead to difficulties with data fitting. 4) Our sol-gel slides are substantially thinner than those used by Saavedra and co-workers, resulting in a lower fraction of "bulk" protein, and possibly a lower inaccessible fraction. 5) Our studies used the neutral quencher acrylamide while Saavedra and co-workers used the negatively charged quencher iodide. Previous studies have clearly shown that the interaction between entrapped proteins and charged reagents is seriously affected by the charge on the silicate matrix.[14,17c] In addition, BSA is negatively charged at neutral pH, and will therefore repel the quencher and alter the Stern-Volmer quenching constants and the apparent

accessibility.[23] Therefore, it is possible that the entrapped proteins are inaccessible only to negatively charged quenchers, and are significantly more accessible to neutral quenchers.

3.3.4 Long Term Stability

To further investigate protein stability in TEOS slides, the long term stability of monellin was examined. Fluorescence spectra were collected daily over a period of several weeks until there were obvious signs of protein denaturation. Complementary absorbance studies were performed to examine scattering which would indicate protein aggregation and/or adsorption. The studies indicated that monellin in solution remained stable for 9 days prior to aggregation. However, even after 7 days, the FWHM of the fluorescence spectrum had increased and the emission maximum began to shift. Encapsulation of monellin in wet-aged slides caused the protein to retain native spectral characteristics for 40 days, at which time scattering became evident. In dry-aged slides which were aged in air for 4 weeks and then soaked in buffer continuously after aging, there were no changes in the fluorescence spectrum of monellin over a period of 12 weeks from the date of encapsulation. However, during the thirteenth week, there were signs of scattering, even though there were no observable differences in the fluorescence spectra compared to those initially obtained from dry-aged slides (4 weeks old). A red shift of the emission maximum for monellin in dry aged slides was observed only after 14 weeks. These results suggest that there is better than a 10-fold increase in protein stability upon encapsulation into dry-aged slides.

At first it is not apparent why the long-term stability of monellin should be improved in both wet-aged and dry-aged slides, even though free energy of unfolding decreased in both systems (compared to solution) and the T_{un} value was not significantly improved in wet-aged slides. This behavior indicates that the loss of structure over time is most likely determined by aggregation, which is possible in solution but is curtailed in both types of slides. Hence, even though the unfolding temperature was not significantly improved for monellin in wet-aged monoliths, the reduction in protein mobility (especially between pores) resulted in a decrease in protein aggregation, and perhaps also reduced the ability of protease enzymes to enter the monolith and degrade the entrapped protein.

3.3.5 Basis of the Stability Enhancement

The fluorescence results clearly showed that the entrapped protein retained the ability to undergo both thermally and chemically induced conformational changes, although the extent of such conformational changes was restricted as the monoliths aged. Aging also had a beneficial effect on the unfolding temperature of the protein, suggesting that the lower degree of conformational flexibility may be related to increased thermal stability. This suggests that the basis for the enhancement of protein stability may, in part, be the result of a simple steric restriction on the motion of the protein, with the silane "trapping" the protein in an active conformation.[2b,3a] The exact mechanism by which the restricted mobility is related to enhanced stability is not fully understood, although it seems likely that the lower degree of mobility may hinder the movement of the protein into thermodynamically unfavourable conformations.

One possible explanation for the enhanced thermal stability comes from the changes in the ΔS_{un} value upon entrapment. It is likely that the stabilization is aided by highly structured water which surrounds the protein in the pores of the silane. The structured water may be templated through hydrogen bonding interactions with the polyhydroxylated silane. Both fluorescence[5a] and NMR[21a,b] studies have shown that the mobility of entrapped solvents is lower than that of free solvents. Previous results from our group[12] and others[5a] also suggest that the viscosity of the entrapped solvent is higher in dry-aged monoliths than in wet-aged monoliths or solution. This provides evidence that the internal environment of the monoliths is more highly structured and thus less mobile than aqueous solvent.[21] This is also supported by a recent report from Bright and co-workers which shows that the dipolar relaxation time for encapsulated solvents is slower than for free solvents.[4b] The more "structured" solvent within dry-aged monoliths may not be as capable as "free" solvent of adapting to a new protein conformation or of solvating exposed hydrophobic regions of proteins, leading to an overall decrease in ΔS_{un} and the higher T_{un} for the entrapped protein which is reported herein.

3.4 Conclusions

In this section, we demonstrated that monitoring of intrinsic fluorescence can provide an abundance of information about the environment and conformational motions of entrapped proteins which contain a single tryptophan residue. In addition, the thermodynamic treatment of thermal and chemical denaturation curves derived from fluorescence measurements can provide useful information regarding the stability and unfolding behaviour of entrapped proteins. This is the first report of a thermodynamic study of protein stability within sol-gel derived matrices, and has resulted in several interesting findings. Firstly, the changes in fluorescence properties during thermal and chemical denaturation indicate that entrapped proteins have a lower degree of conformational flexibility upon entrapment, and that this restriction in motion may increase as the slides aged. Secondly, denaturation results indicated that entrapment in dry-aged slides resulted in a distribution of microenvironments, each having a different thermodynamic stability. Finally, the results showed that the thermal and long-term stability of the protein improved as the slides dried. Preliminary results suggest that the stabilizing effect observed upon encapsulation was possibly the result of the ability of the silane to restrict the conformational flexibility of the protein, and to promote structural rigidity in the internal water.

Results from chapter 2 and 3 clearly showed that encapsulation of monellin into a TEOS derived sol-gel matrix was able to retain the native structure and stability of the protein. However, for the purpose of the development of a biosensor, it is required that the entrapped proteins not only retain its native structure, but also retain its biological

reactivity. Unfortunately, monellin can not bind with any species, thus the biological reactivity of monellin could not be obtained.

In the following sections, we studied another protein, oncomodulin, which binds with calcium and terbium. Both the stability and the biological reactivity could be examined for this protein. In addition, since the stability and reactivity of oncomodulin both involve the positively charged species Ca^{2+} and Tb^{3+}, further studies regarding the effects of the charged sol-gel matrix on the protein-analyte interaction was also performed. This complementary information provided a better understanding of the basis of the sol-gel encapsulation method.

3.5 References for Chapter 3

1. Braun S.; Rappoport, S.; Zusman, R.; Avnir, D.; Ottolenghi, M. *Mater. Lett.* **1990**, *10*, 1-5.

2. a) Nishida, F.; McKiernan, J.M.; Dunn, B.; Zink, J.I.; Brinker, C.J.; Hurd, A.J. *J. Am. Ceram. Soc.* **1995**, *78*, 1640-1648, b) Ellerby, L.M.; Nishida, C.R.; Nishida, F.; Yamanaka, S.A.; Dunn, B.; Selverstone Valentine, J.; Zink, J.I. *Science* **1992**, *255*, 1113-1115.

3. a) Dave, B.C.; Dunn, B.; Valentine, J.S.; Zink, J.I. *Anal. Chem.* **1994**, *66*, 1120A-1126A, b) Avnir, D.; Braun, S.; Lev, O.; Ottolenghi, M. *Chem. Mater.* **1994**, *6*, 1605-1614, c) Yamanaka, S.A.; Dunn, B.; Valentine, J.S.; Zink, J.I. *J. Am. Chem. Soc.* **1995**, *117*, 9095-96.

4. a) Braun, S.; Rappoport, S.; Zusman, R.; Shteltzer, S.; Drukman, S.; Avnir, D.; Ottolenghi, M. In *Biotechnology: Bridging Research and Applications*; Kamely, D.; Chakrobary, A.; Kornguth, S.E., Eds.; Kluwer Academic Publishers: Amsterdam, 1991, p. 205, b) Heichal-Segai, O.; Rappoport, S.; Braun, S. *Biotechnol.* **1995**, *13*, 798-800, d) Reetz, M.T.; Zonta, A.; Simpelkamp, J. *Agnew. Chem. Int. Ed. Engl.* **1995**, *34*, 301-303.

5. a) Dave, B.C.; Soyez, H.; Miller, J.M.; Dunn, B.; Valentine, J.S.; Zink, J.I. *Chem. Mater.* **1995**, *7*, 1431-34, b) Jordan, J.D.; Dunbar, R.A.; Bright, F.V. *Anal. Chem.* **1995**, *67*, 2436-43.

6. a) Narang, U.; Jordan, J.D.; Bright, F.V.; Prasad, P.N. *J. Phys. Chem.* **1994**, *98*, 8101-8107, b) Narang, U.; Bright, F.V.; Prasad, P.N. *Appl. Spec.* **1993**, *47*, 229-34, c) Matsui, K.; Matsuzuka, T.; Fujita, H. *J. Phys. Chem.* **1989**, *93*, 4991-94.

7. Eftink, M.R. In *Methods of Biochemical Analysis: Vol. 35, Protein Structure Determination*; Suelter, C.H., Ed.; John Wiley and Sons Inc.: New York, 1991; pp 127-206.

8. a) Dahms, T.E.S.; Willis, K.J.; Szabo, A.G. *J. Am. Chem. Soc.* **1995**, *117*, 2321-26, b) Dahms, T.E.S.; Szabo, A.G. *Biophys. J.* **1995**, *69*, 569-76.

9. Demchenko, A.P.; Gryczynski, I.; Gryczynski, Z.; Wiczk, W.; Malak, H.; Fishman M. *Biophys. Chem.* **1993**, *48*, 39-48.

10. Hargrove, M.S.; Krzywda, S.; Wilkinson, A.J.; Dou, Y.; Ikeda-Saito, M.; Olson, J.S. *Biochem.* **1994**, *33*, 11767-11775.

11. Eftink, M.R. *Biophys. J.* **1994**, *66*, 482-501.

12. a) Edmiston, P.L.; Wambolt, C.L.; Smith, M.K.; Saavedra, S.S. *J. Coll. Int. Sci.* **1994**, *163*, 395-406, b) Wambolt, C.L.; Saavedra, S.S. *J. Sol-Gel Sci. Tech.* **1996**, *7*, 53-57.

13. a) Morris, J.; Cagan, R.H. *Biochim. Biophys. Acta* **1972**, *261*, 114-122, b) Van der Wel, H. *FEBS Lett.*, **1972**, *21*, 88-90.

14. Van der Wel, H.; Loeve, K. *FEBS Lett.*, **1973**, *29*, 181-184.

15. a) Ogata, C.; Hatada, M.; Tomlinson, G.; Shin, W-C.; Kim, S-H. *Nature* **1987**, *328*, 739-742, b) Somoza, J.R.; Jiang, F.; Liang, T.; Kang, C-H.; Cho, J.M.; Kim, S-H. *J. Mol. Biol.* **1993**, *234*, 390-404.

16. Brand, J.G.; Cagan, R.H. *Biochim. Biophys. Acta* **1977**, *493*, 178-187.

17. Santoro, M.M.; Bolen, D.W. *Biochemistry*. **1988**, *27*, 8063-8068.

18. a) Eftink, M.R.; Ghiron, C.A. *Biochemistry*. **1976**, *15*, 672-680, b) Eftink, M.R.; Ghiron, C.A. *Biochemistry*. **1977**, *16*, 5546-5551, c) Eftink, M.R.; Ghiron, C.A. *Biochim. Biophys. Acta* **1987**, *916*, 343-349.

19. a) Xu, S.; Ballard, L.; Kim, Y.J.; Jonas, J. *J. Phys. Chem*. **1995**, *99*, 5787-5792, b) Korb, J.-P.; Delville, A.; Xu, S.; Demeulenaere, G.; Costa, P.; Johas, J. *J. Chem. Phys*. **1994**, *101*, 7074-7081, c) Shen, C.; Kostic, N.M. *J. Amer. Chem. Soc*. **1997**, *119*, 1304-1312

20. Lakowicz, J.R.; Weber, G. *Biochemistry*. **1973**, *18*, 4161-4170.

21. Kirby, E.P.; Steiner, R.F. *J. Phys. Chem*. **1970**, *74*, 4480-4490.

22. Lakowicz, J.R. *Principles of Fluorescence Spectroscopy*, Plenum Press: New York, 1983, pp. 129-134.

23. Liu, Y.; Bolen, D.W. *Biochemistry*. **1995**, *34*, 12884-12891.

24. Privolov, P.L. *Annu. Rev. Biophys. Chem*. **1989**, *18*, 47-69.

25. Eftink, M.R.; Ghiron, C.A.; Kautz, R.A.; Fox, R.O. *Biochemistry*. **1991**, *30*, 1193-1199.

26. Privolov, P.L.; Khechinashvili, N.N. *J. Mol. Biol*. **1974**, *86*, 665-684.

27. a) Brinker, C.J.; Scherer, G.W. *Sol-Gel Science*, Academic Press: New York, 1989, b) Hench, L.L.; West, J.K. *Chem. Rev*. **1990**, *90*, 33-72.

28. Pace, C.N.; Laurents, D.V.; Thomson, J.A. *Biochemistry*. **1990**, *29*, 2564-2572.

29. Lehrer, S.S., *Biochemistry*. **1971**, *10*, 3254-3263.

Chapter 4 Effects of Metal Binding Affinity and Metal Loading on the Stability of Rat Oncomodulin Mutants in Solution

4.1. Introduction

Results from chapter 2 and 3 clearly showed that encapsulation of monellin into a TEOS derived sol-gel matrix could be done with retention of the native structure and stability of the protein. However, for the purpose of biosensor development, it is necessary that the entrapped proteins not only retain their native structure, but also retain their biological function. Unfortunately, monellin does not bind with any analytes, thus the biological function can not be examined.

In the following sections, we report studies on another protein, rat oncomodulin, which binds with calcium and terbium ions. Both the stability and the biological function can to be examined for this protein. In addition, since the structure and function of oncomodulin are both affected by the presence of positively charged species Ca^{2+} and Tb^{3+}, further studies regarding the effects of the charged sol-gel matrix on protein-analyte interactions could be done.

Before examining the behavior of rat oncomodulin when encapsulated in sol-gel matrices, a detailed study of the behavior of this protein in solution was required to provide a better understanding of the structure, stability and functionality of this protein. The naturally occurring (wild-type) form of rat oncomodulin does not possess a Trp residue. The site-directed mutagenesis technique made it possible to insert a Trp residue at

different regions of the protein. In the following section, four single Trp OM mutants (each containing a Trp at a different location of the protein) were studied in an effort to probe the structure-stability relationships of the protein.

Structure-stability relationships of proteins have long been of interest since alterations which improve the stability of proteins can have important uses both in commercial and biomedical applications.[1,2] There has been a large amount of work done on the study of protein folding to understand the factors which influence the chemical and thermal stability of proteins. A variety of techniques have been used to examine protein stability, including nuclear magnetic resonance,[3] FTIR,[4] circular dichroism,[5] absorbance spectroscopy[6] and fluorescence spectroscopy[7]. The folding pathways of certain proteins have been extensively characterized only after using a combination of approaches.[8] Fluorescence techniques are most often used in cases where a specific portion of a protein is being investigated. The technique of site-directed mutagenesis makes it possible to place a fluorescent amino acid at a specific site within a protein to provide a probe for investigating the unfolding of a specific region of the protein.

There are many factors that can affect the protein stability. For example, it has been shown that protein stability can be altered through a single point mutation.[9] For metal-ion-binding proteins, loading of metal ions can also affect stability, as has been recently reported for the Ca^{2+} binding protein cod III parvalbumin.[10,11] In this chapter, we are interested in how variations in metal binding affect the stability of the Ca^{2+} binding protein rat oncomodulin (OM). Single Trp mutants have been prepared with differing affinities

for Ca^{2+} and the protein stability has been examined in the presence of different amounts and types of metal ions.

Oncomodulin is a small protein with 108 residues and a molecular weight of 11700 Da, and was originally isolated from rat hepatomas [12] which appear early in the carcinogenic process. [13] Oncomodulin is classified as a parvalbumin-like protein based on its primary structure. The sequences of such proteins possess six stretches of α-helices, lettered A through F. The latter four helices flank two functional metal-ion-binding loops knowing as the CD- and EF- binding loops. [14,15] Typically, the parvalbumin (PV) CD and EF loops are classified as "Ca^{2+}/Mg^{2+}" sites since they both exhibit high affinity for Ca^{2+} ($K_d < 10^{-7}$ M) and substantial affinity for Mg^{2+} ($K_d < 10^{-4}$ M). [16] Even though OM shows a high degree of sequence homology to PV, it displays significantly attenuated affinity for Ca^{2+} and Mg^{2+}. Previous work has suggested that OM possesses a high affinity Ca^{2+}/Mg^{2+} site (EF site, $K_{Ca} \sim 10^{-7}$ M, $K_{Mg} \sim 10^{-4}$ M) and a low affinity Ca^{2+}-specific site (CD site, $K_{Ca} \sim 10^{-6}$M, $K_{Mg} < 10^{-3}$ M). [17]

The naturally occurring form of rat oncomodulin contains no tryptophan and only two tyrosine residues. It has previously been shown that binding of metal ions to different OM mutants can induce specific conformational changes which can be monitored by changes in tyrosine fluorescence. [18,19] It is known that binding of Ca^{2+} causes significant structural changes in the loop region. [20,21,22] Binding of other metal ions such as Mg^{2+} or Tb^{3+} are also able to induce conformational changes. [18,19,21]

Site-specific mutagenesis was used to substitute different residues with tryptophan to provide fluorescent probes at different locations. Such mutants have also indicated

conformational changes of proteins upon metal ion binding. Here, four mutant oncomodulin proteins with single Trp residues were used to probe the stability of the protein; F102W with a Trp replacing a Phe at position 102 of the F-helix, Y57W with a Trp replacing a Tyr within the CD loop, Y65W with a Trp replacing a Tyr at position 65 in the flanking D-helix of the CD loop, and CDOM33 with a modified CD loop prepared by insertion of a 12 amino acid sequence which has significantly higher affinity for Ca^{2+} than the native CD or EF loop, and which has a Trp in position 7 of the binding loop (amino acid position 57) [20]. The mutants Y57W and CDOM33 both have a Trp in the metal binding loop, and that Trp provides a metal ligand via its carbonyl oxygen.

Both the thermal and chemical stability of the single Trp mutants were examined by monitoring the fluorescence signal of the Trp residue. Information on stability was obtained by examining changes in the intensity and wavelength maximum of intrinsic fluorescence during GdHCl induced denaturation or thermally induced denaturation.[7,10,11] These studies provide useful information regarding the effects of the different mutations and of binding of different metals on the unfolding behaviour and stability of the protein.

Terbium was chosen for these studies since it is a trivalent cation and thus has a higher order of ligand binding, up to nonadentate. Therefore, it is expected to bind more tightly to the metal binding loops and exert a greater stabilizing effect to the protein structure than calcium. Another advantage of using Tb^{3+} is that changes in terbium luminescence can be used to generate unfolding curves. Terbium luminescence upon binding to an EF hand loop can be enhanced by energy transfer (ET) from a nearby fluorescent donor, in this case an aromatic amino acid[23,24]. For single Trp proteins, excitation at a wavelength of

295 nm can be used to exclusively excite tryptophan residues and thus rule out energy transfer processes involving Phe and Tyr. Excitation of tryptophan can then exclusively lead to the transfer of energy to a nearby Tb^{3+}, followed by luminescence of Tb^{3+} resulting from transitions between the $^5D_4$ and $^7F_5$ states (545 nm) and the $^5D_4$ and $^7F_6$ states (490 nm). For Y57W and CDOM33 the Trp residue is directly in the loop region, thus signals from both Trp and Tb^{3+} can be used to follow the effects of global unfolding on the loop region. On the other hand, the Trp residue within Y65W and F102W is outside the loop region, and thus signals resulting from Tyr-57 to Tb^{3+} energy transfer (using excitation at 285 nm) can be utilized to determine if the unfolding of the loop region (probed by Tb^{3+} luminescence) occurs at the same time as unfolding of the D- helix or F-helix (probed by Trp fluorescence). These studies are used to determine if the unfolding curves derived from fluorescence measurements accurately reflect the global unfolding of the protein.

The primary goal of this study was to develop an understanding of the effects of metal binding affinity and metal loading on the stability of the calcium-binding protein oncomodulin by examining chemically and thermally induced unfolding of the different oncomodulin mutants. The transition midpoints and free energy values for the two types of unfolding transitions have been calculated and are compared to provide a detailed model for the changes in stability which are observed during binding of metals to oncomodulin.

4.2. Experimental

4.2.1 Chemicals

All protein samples were donated by Dr. A.G. Szabo and were used without further purification. Details of the preparation and purification procedures have been described elsewhere [25]. Piperazine-N,N'-bis2-ethanesulfonic acid (PIPES) , acrylamide (99+%) terbium chloride and sodium azide (99%) were supplied by Aldrich (Milwaukee, WS). Ethylenebis(oxyethylenenitrilo)tetraacetic acid (EGTA) and calcium chloride were supplied by Fisher scientific. The guanidine hydrochloride (GdHCl, Sequanol grade) was from Pierce (Rockford, IL). The Sephadex G-25 fine powder was supplied by Pharmacia Biotech (Uppsala, Sweden). All water was twice distilled and deionized to a specific resistance of at least 18 MΩ.cm using a Milli-Q 5 stage water purification system. All other chemicals were of analytical grade and were used without further purification.

4.2.2 Procedures

4.2.2.1 Sample Preparation

All proteins were dissolved in 10 mM PIPES buffer containing 100mM KCl at pH 6.5. Apo proteins were prepared by addition of a 350-fold excess of EGTA as determined by EGTA titration curves of proteins containing either Ca^{2+} or Tb^{3+}. Metal loaded proteins were prepared by adding a 50-fold excess of Ca^{2+} or a 3-fold excess of Tb^{3+} to the proteins. The concentration of protein was 4μM for apo experiments and 2 μM for other experiments.

4.2.2.2 Absorbance Spectra

UV-Visible absorbance spectra were obtained as described in Chapter 2. The concentrations of the solutions were determined using $\varepsilon_{280} = 6900\ M^{-1}.cm^{-1}$ for Y57W, Y65W and CDOM33, and $\varepsilon_{280} = 8200\ M^{-1}.cm^{-1}$ for F102W. [18-22]

4.2.2.3 Fluorescence Spectra

Fluorescence spectra were collected using instrumentation which is described in chapter 2.[26] Samples were excited at 295 nm and emission was collected from 305 nm to 450 nm for Ca^{2+} free and for Ca^{2+} loaded proteins and from 305 nm to 570 nm for Tb^{3+} loaded proteins. All spectra were collected in 1 nm increments at a rate of 180 $nm.min^{-1}$ and with an integration time of 0.30 seconds. Samples were continuously stirred throughout the experiments and were maintained at a temperature of 20 ± 0.2°C (except where otherwise stated) using a Neslab R110 recirculating water bath. Appropriate blanks were subtracted from each sample and the spectra were corrected for deviations in emission monochromator throughput and PMT response. Spectra were integrated from the emission maximum to the red end of the spectra to avoid scattering contributions at the blue end of the spectra.

4.2.2.4 EGTA Titration

A volume of 1700 μl of a solution containing 4 μM protein in the presence of a 3-fold excess Tb^{3+} or 50-fold excess of Ca^{2+} was placed into a quartz cuvette. A total of eighteen aliquots of 50 mM EGTA was added (2 μl x 10 + 4 μl x 8) with constant stirring to reach a ratio of EGTA versus protein of 350 to 1. A fluorescence spectrum was taken

at each point for both a sample and a blank containing the same amount of EGTA to follow the removal of the metal ions from the different proteins.

4.2.2.5 Terbium Titration

A 1.0 M terbium chloride stock solution was made in 0.1 N HCl and kept in the freezer. A 100 μM working solution was prepared weekly in 10 mM PIPES buffer at pH 6.5 by serial dilution of the stock. The exact concentration of the Tb^{3+} solution was determined by a dipicolinic acid (DPA) titration [27] described below. A volume of 2 mL of protein with a concentration of 2 μM was titrated with 30 aliquots of the 100 μM Tb^{3+} solution (4μl per aliquot) to reach a 3:1 molar ratio of terbium to protein.

4.2.2.6 DPA Titration

A 3 mM DPA solution was prepared in 100 mM PIPES buffer at pH 6.5. A higher buffer capacity was required to maintain the pH at a constant value since DPA forms an acidic solution upon dissolving. The exact concentration of DPA was determined by weighing an appropriate mass of DPA, and dissolving this to exactly 1000 ml of buffer. This solution was further diluted for the determination of different terbium solutions. The increase of the terbium luminescence peaks at 490 nm or 545 nm was monitored during titration. The DPA solution was always titrated with the terbium solution to keep an excess of DPA so that tris $Tb(DPA)_3^{3-}$ was the only complex formed during titration. If the titration was reversed, mono, bis and Tris complexes would all formed, thus, a linear titration curve wouldn't be obtained. For the determination of the exact concentration of the 100 μM working solution, a volume of 1500 μl of 150 μM DPA solution was titrated

with the terbium solution (about 60 µl x 15 aliquots) until the titration curve reached a plateau when the ratio of DPA versus terbium reached 3:1. The concentration of terbium was calculated from the titration curve.

4.2.2.7 Thermal Denaturation Studies

Careful removal of oxygen before each experiment was required to prevent protein aggregation. Removal of oxygen was performed as described in Chapter 2. Aggregation of protein was observed to decrease the thermal stability as well as decrease the percent recovery after taking the temperature back to the room temperature. For this reason, all thermal denaturation experiments were done with nitrogen purging and the percent recovery was greater than 85% for all the proteins studied.

A volume of 1.0 mL of the protein solution was placed into a quartz fluorimeter cuvette. The cuvette was sealed to avoid concentration changes which could be caused by evaporation of buffer solution at high temperatures. The temperature was raised in *ca.* 5°C increments starting at 20°C and going to 95°C, then lowered to 20°C to check reversibility. A fluorescence spectrum was collected from the sample and from an appropriate "no protein" blank at each temperature. The temperature of the solution in a second cuvette which was also present in the 4 sample turret was measured directly using a thermistor probe (Hanna Instruments model 9043A) to account for loss of heat through the tygon tubing connecting the sample holder and the water bath. The samples were allowed to equilibrate for at least five minutes at each temperature before readings were taken. Spectra were integrated from the emission maximum to the red end of the spectra. The integrated intensity was normalized to the intensity at the starting temperature

(usually 20°C) and was plotted against temperature to generate the unfolding curve. The unfolding curves were corrected for contributions from thermally induced quenching using standard methods.[7] This resulted in non-sloping initial and final portions to the curve,[28] as expected for a thermally induced unfolding of a protein. The unfolding enthalpy change (ΔH^0_{un}) and entropy change (ΔS^0_{un}) was calculated by fitting the unfolding curve to equation 1.14.[7] The free energy change for unfolding (ΔG_{un}) was determined by using equation 1.16, with a reference temperature (T_r) of 20°C and a $\Delta C_{p,un}$ value of zero.

4.2.2.8 Chemical Denaturation Studies

A volume of 1.75 mL of the protein solution was added to a quartz cuvette. A total of twenty aliquots of 8.0 M GdHCl in buffer were added (5 x 50µl + 15 x 100µl) with constant stirring and a minimum of 5 minutes was allowed for equilibration. A fluorescence spectrum was collected at each point for both the sample and a blank containing an identical concentration of GdHCl. Unfolding transitions were fitted using equation 1.13.[29] The reversibility of unfolding was determined by measuring the spectra after dialyzing denatured protein against fresh buffer and running the denatured protein through a Sephadex G-25 column.

4.2.2.9 Acrylamide Quenching Studies

2.0 mL of a 2 µM protein solution was titrated by adding a total of twenty-two 10 µL aliquots of 8.0 M acrylamide in buffer. A fluorescence spectrum was collected from the sample and an appropriate blank after each addition. Spectra were corrected for sample dilution and were integrated as described earlier. The data were analyzed using

equation 1.7. Mean lifetime values for denatured proteins were obtained by the time-correlated single photon counting method using instrumentation and fitting procedures which are described in detail elsewhere[30]. The decays were assumed to be a sum of discrete exponential decay components, and all decays were fit to a sum of three decay components.

4.3. Results and Discussions

4.3.1 Fluorescence Properties of Native Oncomodulin Mutants

The fluorescence properties of the native proteins in the presence and absence of Ca^{2+} and Tb^{3+} are shown in Table 1 along with the changes in the spectral properties and quantum yield values resulting from chemical denaturation. Initial studies focussed on apo proteins which were prepared by addition of the chelating agent EGTA. To test the effectiveness of this method, each protein was loaded with a 3-fold excess of Tb^{3+} (which binds more strongly to OM than does Ca^{2+}) and the emission of the Tb^{3+} peak at 545 nm was monitored as EGTA was added. In all cases, the Tb^{3+} emission peak was completely eliminated upon addition of a 350-fold excess of EGTA, indicated that the proteins were apo under these conditions. The similarity of our spectral data for the apo proteins (shown in Table 4.1) to that of Szabo and co-workers [18-22] (who used trichloroacetic acid precipitation for decalcification of proteins) indicates that the use of EGTA for preparation of apo proteins is an acceptable method. Thus, all studies of apo proteins reported herein were done with a 350-fold excess of EGTA present.

The fluorescence characteristics of the holo proteins were substantially different than those of the apo proteins. Binding of Ca^{2+} generally caused only small blue-shifts in wavelength (1-2 nm) as was observed by Hutnik *et al.*.[19,21] However, the changes in intensity upon binding of Ca^{2+} were significant, as shown by the fluorescence quantum yields reported in Table 1. For F102W, binding of Ca^{2+} caused the emission intensity to increase by *ca.* 30% with no significant changes in the shape or position of the spectrum. These finding are consistent with those of Hutnik *et al.*.[21] The emission maximum and full-width-at-half-maximum (FWHM) values for the holo-F102W mutant suggested that the Trp was in a hydrophobic region which was shielded from solvent. This is consistent with the position of the F-helix from x-ray diffraction data.[31] Acrylamide quenching results, shown in Table 2, also support this suggestion. K_{SV} values were measured and were used to obtain bimolecular quenching constants using fluorescence lifetime data which was reported elsewhere[18-22]. The fluorescence decays of most mutants showed two or three components and thus intensity-weighted mean lifetimes were calculated (using the equation provided in the footnotes in Table 2) to obtain the k_q values. The acrylamide quenching results showed that the environment of the Trp residue in F102W became significantly less exposed upon addition of Ca^{2+}, with the k_q value decreasing by 35%.

In the case of Y65W there was only very small increase in intensity (~5%) and no shift in the emission maximum upon binding of Ca^{2+}. This small intensity change indicated that the environment around Trp at position 65 did not change significantly upon addition of calcium. This is supported by the small change (< 10%) in the k_q value on going from the apo to the holo form of the protein.

Inspection of the quantum yield and k_q values for apo Y57W and CDOM33 indicated that the Trp residue was likely in a somewhat different environment for each protein, with the Trp residue of Y57W being more solvent exposed than that of CDOM33, even though the quantum yield of Y57W was higher than that of CDOM33. Addition of Ca^{2+} caused the local environment of the Trp residue to change dramatically for both proteins, with an enhancement in the quantum yield of Trp within CDOM33, but a significant quenching of intensity for Y57W. Overall, the intensity of CDOM33 increased by 40% while the intensity of Y57W decreased by 40% upon binding of Ca^{2+}.

The k_q values also showed that the environment of Trp in Y57W and CDOM33 was significantly different upon binding of Ca^{2+}. However, the k_q value of Y57W unexpectedly decreased from 3.58 to 2.55 $M^{-1}.ns^{-1}$ while the k_q value for CDOM33 increased from 2.77 to 3.05 $M^{-1}.ns^{-1}$ upon binding of Ca^{2+}. These results clearly show that the Trp at position 57 in Y57W became less exposed on addition of calcium, while that in CDOM33 became more exposed, indicating significantly different structural responses to the addition of calcium. Interestingly, the changes in exposure to solvent are opposite to those expected from the changes in quantum yield. Generally, greater exposure of a Trp residue to solvent results in an increase in collisional quenching, producing a decrease in the quantum yield. The apparent inconsistency between the k_q and quantum yield values can be resolved by recognizing that the addition of Ca^{2+} will dramatically alter the electrostatic environment in the region of Trp-57. It has previously been reported that the relative change in fluorescence lifetime for Y57W upon binding of Ca^{2+} does not correspond to the relative change in quantum yield, even though there is no evidence for static quenching of

the Trp at position 57. The assertion has been made that the binding of Ca^{2+} can result in substantial changes in the radiative lifetime (τ_R) of the Trp residue (note: $\tau_R = \tau_S/\Phi$ where the singlet state lifetime (τ_S) is given by $\tau_S = \Sigma\alpha_i\tau_i$) .[19, 32] Our calculations show that the binding of Ca^{2+} to Y57W resulted in an increase in the radiative lifetime from 18.3 to 23.4 ns (using the data in ref. 19), while binding of Ca^{2+} to CDOM33 produced a decrease of k_R from 26.5 ns to 16.9 ns. This strongly suggests that the conformational changes in the loop region upon binding of Ca^{2+} are substantially different for the two mutants.

Binding of terbium to oncomodulin mutants caused substantial quenching of Trp fluorescence and a large increase in terbium luminescence for both CDOM33 and Y57W when compared to the holo-forms. This is consistent with the short Trp-to-Tb^{3+} donor-acceptor distance for CDOM33 and Y57W (*ca.* 4.5 and 8.0 Angstroms from the CD and EF loops, respectively [19]). On the other hand, there were only small changes in the emission intensity of the Trp residue in F102W and Y65W, suggesting that energy transfer to Tb^{3+} was not efficient for these proteins. From the crystal structure of wild-type OM, the gamma-carbon of F-helix Phe 102 is 10.8 Angstroms away from the nearest calcium in the EF loop,[31] while the gamma-carbon of the D-helix Tyr-65 is 11.4 Angstroms away from the CD loop calcium. Hence, the Trp residue within these proteins is not within the required distance for efficient energy transfer by the electron exchange mechanism.[23,24]

Table 4.1 Changes in fluorescence properties for apo and Ca^{2+}-loaded oncomodulin mutants during chemical denaturation.

Protein	$\Phi_{(native)}$	$\Phi_{(denatured)}$	Change of λ_{max} (nm)	Change of FWHM (nm)	Change of intensity (Tb^{3+} peak)
Y57W					
Ca^{2+}-free	0.133	0.095	341-337-345[a]	55 - 58	
Ca^{2+}-loaded	0.078	0.101	339-345	54 - 58	
Tb^{3+}-loaded	0.027	0.106	339-345	54 - 58	decreased 92%
Y65W					
Ca^{2+}-free	0.143	0.105	343-346	55 - 57	
Ca^{2+}-loaded	0.157	0.126	343-345	56 - 57	
Tb^{3+}-loaded	0.156	0.113	343-345	56 - 57	decreased 50%
F102W					
Ca^{2+}-free	0.190	0.087	317-345	47 - 64	
Ca^{2+}-loaded	0.240	0.070	315-345	39 - 64	
Tb^{3+}-loaded	0.212	0.082	315-345	39 - 64	decreased 92%
CDOM33					
Ca^{2+}-free	0.101	0.109	340-345	55 - 57	
Ca^{2+}-loaded	0.152	0.097	339-345	55 - 58	
Tb^{3+}-loaded	0.023	0.058	339-345	55 - 58	decreased 95%

a) In this case, the wavelength first blue-shifted, then red-shifted.

4.3.2 Chemical Denaturation of Apo Proteins

Initial studies concentrated on the stability of apo proteins which contained no metal ions bound in the loops. The unfolding curves of apo proteins are shown in Figure 4.1.

Several aspects of these curves merit special attention. First, the intensity of both F102W and Y65W decreased immediately upon addition of denaturant, resulting in the absence of a pre-unfolding baseline. In both cases, both the intensity and wavelength data indicated that the unfolding process was completed at a relatively low GdHCl concentration. Second, the unfolding profiles of Y57W and CDOM33 showed opposite intensity trends on unfolding. The intensity of Y57W decreased by about 30% with an initial blue shift of 4-5 nm in the emission maximum followed by a red-shift to the characteristic emission maximum of 345 nm which is indicative of a fully exposed Trp residue. The intensity of CDOM33, on the other hand, increased by approximately 20% followed by a decrease of 10% during the addition of GdHCl. The transition between 1.0 and 1.5 M of GdHCl showed a red-shift in the emission maximum which corresponded to the initial increase of intensity. Finally, the final quantum yield values for the Y57W and CDOM33 suggested similar environments for the exposed Trp residue in the two proteins.

The reversibility of the chemically induced unfolding was tested for all oncomodulin mutants by dialyzing the denatured protein against fresh buffer and then running denatured proteins through a Sephadex G-25 column. The spectra reversed fully and the refolded proteins showed similar binding behavior to the native protein. This indicated that thermodynamic analysis of the unfolding curves generated by chemical denaturation could be done.

The unfolding free energies and transition midpoints for each apo protein were obtained by fitting the integrated intensity data. In the case of the Y57W mutant, the initial rise in intensity upon the first addition of denaturant made it impossible to fit the

baseline region if the initial point was included. For this reason, the fitting was done starting at the second point in the titration. This has the effect of shifting the entire unfolding curve upward, and affects that values of s_N and F_{0N} in equation 1.13. However, this fitting procedure has no affect on the values of m_G, ΔG_{un}, or $C_{1/2}$ since these values depend on slopes, and thus are not affected by shifting the curve in the y-direction. In fitting the unfolding curves, it was assumed that the unfolding transitions followed a two-state model. Our unfolding curves clearly indicated two-state unfolding processes for the various proteins, indicating that this assumption was valid. We also assumed that the Trp fluorescence reported on changes in the global structure of the protein. The validity of the assumption is described further in Section 4.3.4.

The fitting results for all apo proteins are shown in Table 4.2. The ΔG_{un} and $C_{1/2}$ values of Y57W and CDOM33 were quite similar suggesting that there was not a significant difference in the chemical stability of the protein when the modified CD loop was present but had no metal ions bound. The free energy and transition midpoint values for F102W were significantly lower than for the proteins with the Trp present in the loop region. This may indicate that the presence of the Trp residue at position 102 slightly destabilized the apo protein. Y65W had the lowest free energy and transition midpoint among these mutants (about 1.0 kcal.mol^{-1} and 0.37 M lower than F102W). Position 65 is interesting in that it is a kink point in the D-helix. The kink in this helix seems necessary to allow the D-helix to wrap tightly around the hydrophobic core of the protein. It appears that the apo protein is significantly affected by the insertion of a Trp at position 65, resulting in the low local free energy of unfolding when the Trp is at position 65.

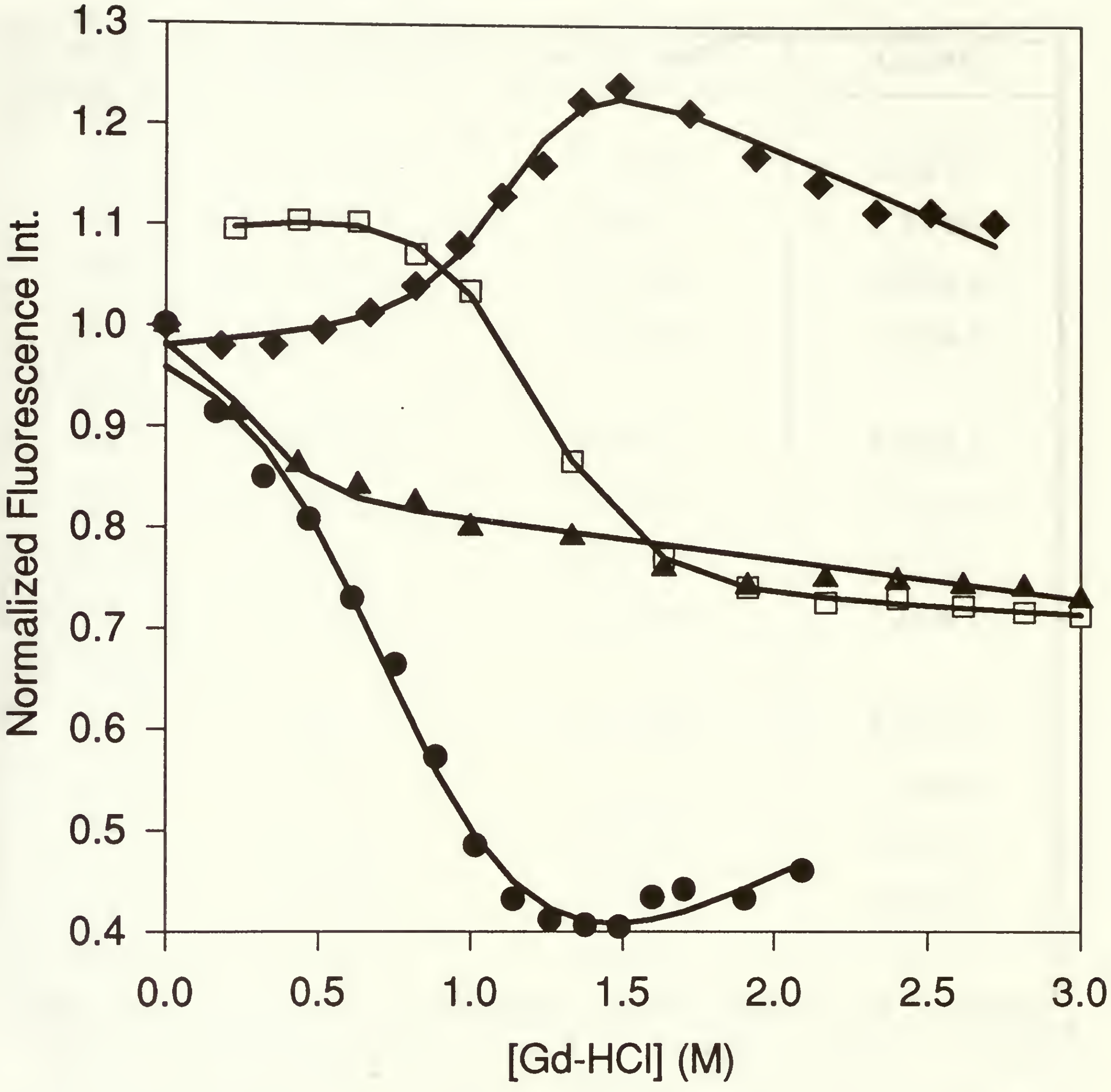

Figure 4.1 Fluorescence intensity changes as a function of GdHCl concentration for calcium free F102W (●), Y57W(□), Y65W (▲) and CDOM33(◆). The symbols are the experimentally derived data points. The solid lines are the lines-of-best-fit as determined by fitting to equation 1.13.

Table 4.2. Free energy changes for chemical unfolding of oncomodulin obtained by fitting of unfolding curves to equation (1.13).

Proteins	**ΔG_{un} (kJ.mol^{-1})**	**m_G (kJ.L.mol^{-2})**	**$C_{1/2}$ (M)**
Ca^{2+}-free[a]			
Y57W	16.3 ± 1.3	13.4 ± 0.8	1.2 ± 0.1
Y65W	2.5 ± 0.4	7.9 ± 1.7	0. 3 ± 0.1
F102W	7.9 ± 0.4	9.2 ± 0.8	0.8 ± 0.1
CDOM33	12.5 ± 1.3	11.3 ± 1.3	1.2 ± 0.1
Ca^{2+}-loaded[b]			
Y57W[d]	28.0 ± 2.1	13.8 ± 1.3	2.0 ± 0.1
Y65W	27.6 ± 2.1	14.2 ± 1.3	1.9 ± 0.1
F102W	21.7 ± 2.1	12.1 ±1.3	1.8 ± 0.1
CDOM33	28.8 ± 1.7	13.0 ± 0.8	2.2 ± 0.1
Tb^{3+}-loaded[c]			
Y57W[e]	32.6 ± 2.1	11.7 ± 0.8	2.8 ± 0.1
Y65W	28.0 ± 2.9	9.6 ± 1.3	2.9 ±0.1
F102W	33.4 ± 3.3	13.0 ± 1.3	2.6 ± 0.2
F102W[c]	46.4 ± 6.3	17.6 ± 2.1	2.6 ± 0.3
CDOM33[c]	35.5 ± 3.8	8.8 ± 0.8	4.0 ± 0.1

a) Fitting parameters for apo proteins were as follows: **F102W:** $F_N = 1.00$, $F_U = 0.137$, $m_N = 0.00$, $m_U = 0.157$; **Y65W:** $F_N = 1.00$, $F_U = 0.848$, $m_N = 0.00$, $m_U = -0.039$; **Y57W:** $F_N = 1.091$, $F_U = 0.768$, $m_N = 0.037$, $m_U = 0.108$; **CDOM33:** $F_N = 0.980$, $F_U = 1.444$, $m_N = 0.030$, $m_U = 0.133$.

b) Fitting parameters for Ca^{2+}-loaded proteins were as follows: **F102W:** $F_N = 1.010$, $F_U = 0.260$, $m_N = 0.121$, $m_U = 0.023$; **Y65W:** $F_N = 0.982$, $F_U = 0.745$, $m_N = 0.016$, $m_U = -0.016$; **Y57W:** $F_N = 339$, $F_U = 345$, $m_N = 0.00$, $m_U = 0.00$; **CDOM33:** $F_N = 1.042$, $F_U = 0.772$, $m_N = 0.00$, $m_U = -0.013$.

c) Fitting parameters for Tb^{3+}-loaded proteins were as follows: **F102W (Trp):** $F_N = 1.009$, $F_U = 0.357$, $m_N = -0.112$, $m_U = -0.002$; **F102W (Tb^{3+}):** $F_N = 0.994$, $F_U = 0.273$, $m_N = -0.172$, $m_U = -0.008$; **Y65W:** $F_N = 0.995$, $F_U = 0.316$, $m_N = 0.021$, $m_U = 0.056$; **Y57W:** $F_N = 0.996$, $F_U = 0.377$, $m_N = 0.016$, $m_U = -0.021$; **CDOM33:** $F_N = 1.031$, $F_U = 0.261$, $m_N = 0.032$, $m_U = -0.006$.

d) The thermodynamic parameters were obtained by fitting emission maxima data.

e) The thermodynamic parameters were obtained by fitting Tb^{3+} luminescence data.

4.3.3 Chemical Denaturation of Holo (Ca^{2+} loaded) Proteins

As described earlier, the presence of Ca^{2+} in the binding loops of the OM mutants caused significant spectroscopic changes for each protein, indicative of conformational changes upon metal binding. Denaturation of each of the holo proteins caused a typical red-shift in the emission maximum (λ_{max}) and a change in fluorescence intensity. The results are summarized in Table 1a. The F102W OM showed the greatest change in both intensity (75% decrease) and λ_{max} (30 nm increase). The FWHM of this protein also increased by 25 nm upon unfolding. The unfolding profile of F102W showed a wide transition range when the intensity was monitored. The intensity started to decrease immediately upon addition of denaturant; however, the λ_{max} value didn't begin to shift until 1.8 M GdHCl was present. The unfolding of the protein was complete after addition of 2.2 M GdHCl according to both intensity and wavelength measurements. The broadness of the transition range obtained from measurements of intensity suggested that the interaction of GdHCl with the protein may have caused the protein structure to be loosened and the quantum yield to decrease before the main unfolding process, indicated by the changes in the emission maximum, had begun.

This explanation is also supported by acrylamide quenching experiments at different GdHCl concentrations, given in Table 4.3a. The active quenching sphere V (from equation 1.7) increased by 0.8 M^{-1} when the concentration of GdHCl increased from 0 to 1.6 M, but the values of the Stern-Volmer constant (K_{SV}) stayed relatively constant (4.0 - 5.0 M^{-1}). There was a large increase in both the V and K_{SV} values when the concentration of GdHCl exceeded 1.9 M, at which point the main unfolding process began. The

completely unfolded protein had a *V* value of 2.4 M^{-1} and a K_{SV} value of 9.25 M^{-1} at 2.55 M GdHCl, indicative of a fully exposed Trp residue[34].

The unfolding curves for the various mutants are shown in Figure 4.2. The unfolding curve of Y65W showed an intensity and wavelength profile which matched closely. Both the intensity and the wavelength values showed a narrow transition range (1.6 - 2.5M GdHCl). The intensity of Y65W increased slightly followed by a decrease of 20% with respect to the initial intensity. There was only a 4 nm red-shift of the λ_{max} and only a 1 nm increase in the FWHM, indicating that the conformation of the protein in the region of Trp-65 was not altered significantly during unfolding. This was also supported by acrylamide quenching data, given in Table 4.3b, which showed that both *V* and K_{SV} values stayed relatively the same for native and denatured proteins. This result is consistent with Trp-65 being an exposed residue in the folded and unfolded states.

Table 4.3a K_{SV} values from acrylamide quenching of holo F102W OM.

[Gd-HCl]	V (M^{-1})	K_{sv} (M^{-1})	Constant	R^2
0	0.2	3.98	1.028	0.995
0.32	0.5	4.20	1.005	0.999
0.64	0.6	4.73	0.973	0.991
1.0	0.6	4.33	0.960	0.990
1.3	0.85	4.90	0.992	0.995
1.6	1.0	5.00	0.979	0.991
1.9	2.2	7.82	1.005	0.996
2.55	2.4	9.25	1.060	0.980

Table 4.3b. Stern-Volmer quenching constants and bimolecular quenching rate constants from acrylamide quenching of oncomodulin mutants.

Protein	V (M^{-1})	K_{sv} (M^{-1})	$\langle\tau\rangle$ (ns)[a]	k_q ($M^{-1}.ns^{-1}$)
Y57W				
apo	0.8[b]	8.69 ± 0.08	2.43 ± 0.01[c]	3.58 ± 0.03
holo	0.8	4.66 ± 0.04	1.83 ± 0.02[c]	2.55 ± 0.02
denatured	1.0	8.13 ± 0.06	2.96 ± 0.01[f]	2.75 ± 0.03
Y65W				
apo	1.2	7.03 ± 0.06	2.29 ± 0.02[c]	3.07 ± 0.03
holo	0.9	6.39 ± 0.04	2.33 ± 0.01[c]	2.74 ± 0.03
denatured	1.5	7.48 ± 0.06	3.41 ± 0.01[g]	2.19 ± 0.02
F102W				
apo	1.0	5.00 ± 0.04	3.12 ± 0.02[d]	1.60 ± 0.02
holo	0.2	3.98 ± 0.03	3.80 ± 0.02[d]	1.05 ± 0.01
denatured	2.4	9.25 ± 0.08	2.93 ± 0.02[h]	3.16 ± 0.03
CDOM33				
apo	1.0	7.33 ± 0.07	2.65 ± 0.02[e]	2.77 ± 0.03
holo	0.8	7.83 ± 0.07	2.53 ± 0.02[e]	3.09 ± 0.03
denatured	1.1	7.23 ± 0.07	2.89 ± 0.02[i]	2.50 ± 0.02

a) Intensity-weighted mean lifetime values were calculated using $\langle\tau\rangle = \Sigma(\alpha_i\tau_i^2)/\Sigma(\alpha_i\tau_i)$ b) All *V* values have errors of ± 0.1 M^{-1}, c) from reference [19], d) from reference [21], e) from reference [20], f) $\alpha_1 = 0.24$, $\alpha_2 = 0.49$, $\alpha_3 = 0.27$, $\tau_1 = 4.132$ ns, $\tau_2 = 1.893$ ns $\tau_3 = 0.283$ ns, SVR = 1.98, $\chi^2 = 1.048$, g) $\alpha_1 = 0.30$, $\alpha_2 = 0.44$, $\alpha_3 = 0.26$, $\tau_1 = 4.507$ ns, $\tau_2 = 1.968$ ns $\tau_3 = 0.308$ ns, SVR = 1.91, $\chi^2 = 0.997$, h) $\alpha_1 = 0.22$, $\alpha_2 = 0.35$, $\alpha_3 = 0.43$, $\tau_1 = 3.801$ ns, $\tau_2 = 1.303$ ns $\tau_3 = 0.147$ ns, SVR = 1.88, $\chi^2 = 1.023$, i) $\alpha_1 = 0.27$, $\alpha_2 = 0.47$, $\alpha_3 = 0.26$, $\tau_1 = 4.316$ ns, $\tau_2 = 1.961$ ns $\tau_3 = 0.264$ ns, SVR = 2.01, $\chi^2 = 1.000$.

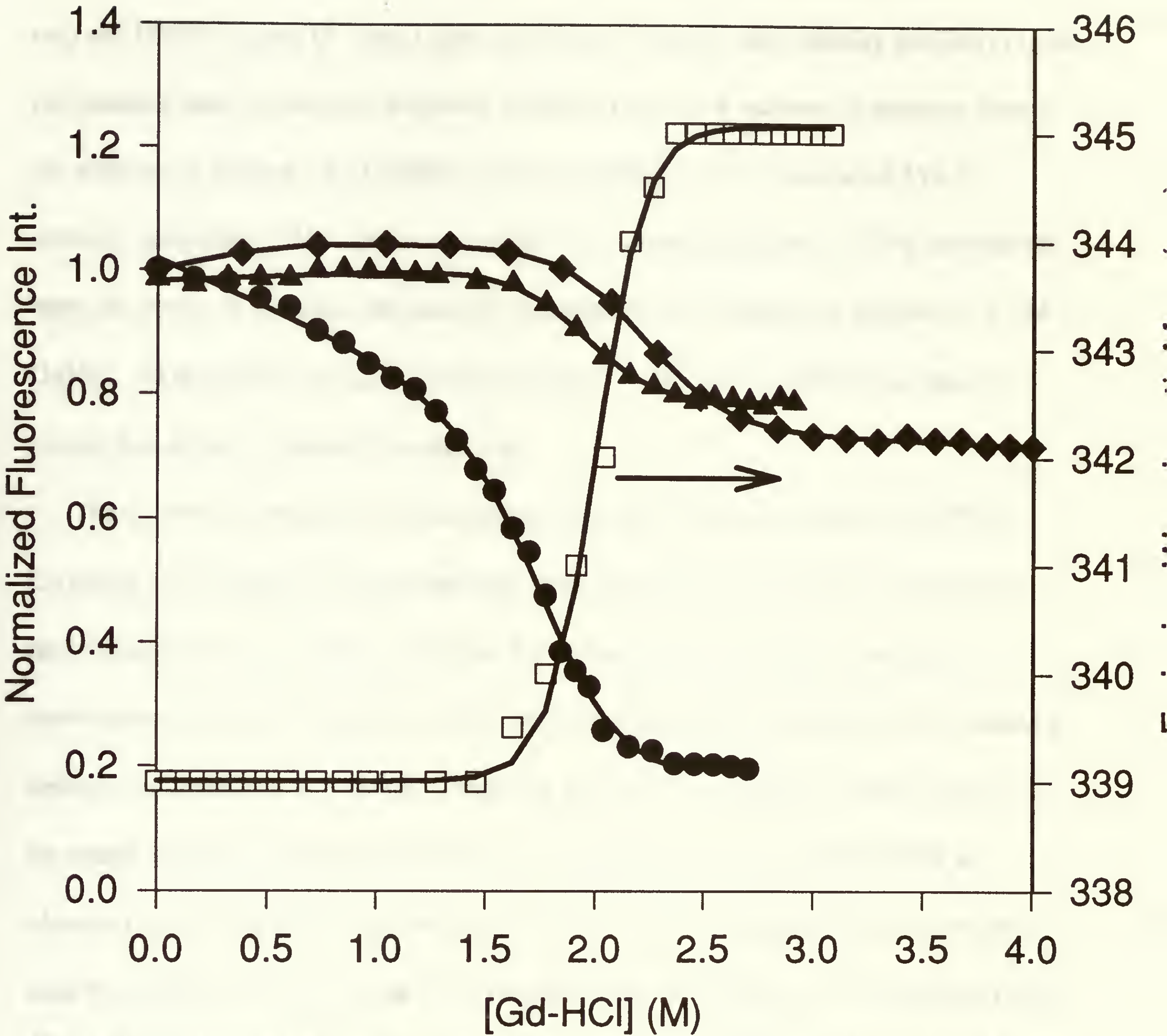

Figure 4.2 Fluorescence intensity changes as a function of GdHCl concentration for calcium Loaded F102W (●), Y57W(□), Y65W (▲) and CDOM33(◆). The symbols are the experimentally derived data points. The solid lines are the lines-of-best-fit as determined by fitting to equation 1.7

CDOM33 and Y57W OM showed similar changes in the emission maximum (6 nm) and FWHM values (3 - 4nm) upon unfolding. However, the intensity profiles of these two proteins were remarkably different. CDOM33 had a 5% increase in intensity during the addition of the first 1.5 M GdHCl. This was followed by a decrease of 35% in intensity until about 3 M GdHCl was present. The unfolding curve of Y57W showed the opposite trend. In this case, the intensity increased by 30% during the addition of 2.1 M GdHCl. At this point, the λ_{max} had already shifted to 345nm which indicated that the protein had already denatured substantially.

The observed increase in the fluorescence intensity upon denaturation of Y57W is intriguing. The addition of denaturant may have caused a process which is similar to the decalcification process which caused the Trp residue of Y57W OM to end up in an environment with higher quantum yield. The unfolding process, which generally causes a decrease in intensity was probably competing with the decalcification process, resulting in an overall increase in intensity of 30% for the unfolding process instead of 70% as observed for the decalcification process. The origin of the changes in intensity probably arise from different charge interactions between the point charge (i.e., the metal ion) and the dipoles of the Trp residue, thus causing changes in both the radiative and non-radiative rate constants.

Further information was obtained by acrylamide quenching studies of these two proteins, as shown in Table 4.3b. These studies indicated that for the native state, the Trp residues of Y57W and CDOM33 were in significantly different environments. The K_{SV}

values of native Y57W and CDOM33 were 4.66 M^{-1} and 7.83 M^{-1}, respectively. For the apo and denatured states, the K_{SV} values for the two mutants were very similar. Calculation of k_q also showed that the environment of Trp in Y57W and CDOM33 was significantly different. The k_q value of Y57W increased from 2.55 ns^{-1} to 3.35 ns^{-1} while k_q for CDOM33 decreased from 3.05 ns^{-1} to 2.77 ns^{-1} for the holo and apo forms, respectively. These results clearly show that the changes in the CD loop caused major changes in the conformation of the Trp residue, causing unexpected changes in fluorescence intensity upon denaturation.

The most obvious difference between the holo and apo proteins is that the stability of each protein increased substantially upon binding of Ca^{2+}, indicating that the metal ions preferentially bind to the folded form of the protein. However, not all proteins were stabilized to the same degree. For example, the stabilization, or $\Delta(\Delta G_{un})$ value, on going from the apo to the holo form of Y57W (11.7 $kJ.mol^{-1}$) , F102W (13.8 kJ.mol-1) or CDOM33 (16.3 $kJ.mol^{-1}$) was substantially lower than that for Y65W (25.1 $kJ.mol^{-1}$). Hence, we observe that Ca^{2+} binding can overcome the destabilizing effects of inserting a Trp into position 65 of the D-helix. The F102W mutant was stabilized to a similar degree when compared to Y57W or CDOM33, but still had the lowest unfolding free energy and transition midpoint. Thus even for the Ca^{2+}-loaded form, the insertion of the Trp into the F-helix still results in partial destabilization of the protein.

CDOM33 was observed to have the highest free energy and transition midpoint (2.2 M). Since the whole CD loop was modified for CDOM33 to provide higher binding affinity[20], the higher free energy and higher transition midpoint were not unexpected.

This result proved that increases in the binding affinity can stabilize the native structure of the holo-protein. Altering of binding affinity can be achieved by either replacing the loop with residues which can provide a higher binding affinity or by loading the protein with other metal ions which have higher binding affinity.

4.3.4 Chemical Denaturation of Tb^{3+}-loaded Proteins

To further explore the effects of metal ions on protein stability, unfolding experiments were done for proteins containing a 3:1 molar ratio of Tb^{3+}:protein. It is important to note that the concentration of Tb^{3+} used in this part of the study was significantly less than that used for the study of Ca^{2+}-loaded proteins (50:1 Ca^{2+}:protein). In general, the stability of a ligand binding protein will depend on the concentration of ligand,[10-11] and hence the thermodynamic parameters determined in this work will depend on metal ion concentration. However, the purpose of this study was not to examine protein stability as a function of metal ion concentration, but rather as a function of binding affinity. The choice of metal ion concentration was determined by the level at which maximum stability was obtained. For Ca^{2+}, maximum stability occurred at a concentration of metal ion which was 50-fold higher that the protein concentration. For Tb^{3+}, the addition of a 50-fold excess of the metal ion resulted in aggregation of the protein, and thus could not be used. Instead, the level for maximum stability (in this case a 3:1 Tb^{3+}:protein ratio) was used.

The terbium luminescence peaks at 545 nm and 490 nm resulting from ET from nearby Trp residues can be used to provide additional signals which can be utilized to monitor the unfolding process. According to the ranking of calcium binding proteins by terbium sensitivity obtained by Hogue *et al.*,[28] when excited at 285 nm, the terbium signal ratio of

This result proves that increases in Tb binding affinity [illegible] the entire structure of the three-domain. Affinity of binding [illegible] can be enhanced by [illegible] the loop with residues which can provide a [illegible] binding affinity [illegible] or other metal ions which have higher binding affinity.

6.1.4 Chemical Denaturation of Tb^{3+}-Loaded Proteins

To further explain the effects of metal ions on protein stability, [illegible] were done for the proteins [illegible] in the presence of Tb^{3+}/protein. It is important to note that the concentration of Tb^{3+} used in this part of the study was significantly less than that used for the study of Ca^{2+}-loaded proteins (100 Ca^{2+}/protein). In general, the ligand binding protein will depend on the concentration of ligand,[illegible] and hence the thermodynamic parameters determined in this work will depend on metal ion concentration. However, the purpose of this study was to examine protein stability as a function of metal ion concentration, not rather as a function of binding affinity. The choice of metal ion concentration was determined by the levels at which [illegible] was observed. For Ca^{2+}, [illegible] and [illegible] 30 fold higher than the protein concentration. For Tb^{3+}, the addition of [illegible] excess of the metal ion resulted in [illegible] of the protein and thus [illegible] limited the level for [illegible] to 1:1 Tb^{3+}/protein [illegible]

The [illegible] luminescence [illegible] was [illegible] Trp [illegible] can be used to [illegible] unfolding process. According to the [illegible] by [illegible]

CDOM33:Y57W:Y65W:F102W is 30:6:4:1. At an excitation wavelength of 295 nm, the sensitivity of the Tb^{3+} luminescence enhancement for Y65W and F102W is further decreased since energy transfer contributed from Tyr 57 is removed. However even at 295 nm excitation it is still possible to utilize the Tb^{3+} peaks as a secondary signal to monitor the unfolding process of proteins. In the case of Y57W and CDOM33 the Trp residue is located within the binding loop, resulting in very efficient energy transfer from Trp to Tb^{3+}. Therefore, for these proteins the terbium peak was used as a primary signal while the Trp peak was used as a secondary signal. The use of Tb^{3+} or Trp luminescence is noted in the Figure captions.

The unfolding curves of the Tb^{3+} loaded proteins is shown in Figure 4.3. It was noticed that in some cases the curves originally appeared to show 2 unfolding steps. However, it was determined that the initial decrease in intensity was the result of dissolution of aggregates which had formed during storage of Tb^{3+} loaded proteins. Titrations on freshly prepared samples always showed a single transition, indicative of a 2-step unfolding process. The free energy and transition midpoint values are shown in Table 4.2. It was necessary to use Tb^{3+} luminescence data to fit the unfolding transitions of Y57W and CDOM33 since the intensity of the Trp residue was affected by both changes in energy transfer to Tb^{3+} and exposure of Trp to solvent upon protein unfolding, resulting in non-linear baseline regions. The unfolding of Y65W was fit using changes in Trp intensity upon unfolding, while both the Trp signal originating from position 102 (excitation at 295 nm) and the Tb^{3+} signal resulting from energy transfer from Try-57 (excitation at 285 nm) were measured during chemical denaturation of the F102W mutant.

CBD(M3) [illegible] [illegible] excitation wavelengths of 295 nm, the sensitivity of the Tb³⁺ luminescence measurement for Y97W and CBD(M3) is further increased [illegible] [illegible] (Trp 37) [illegible]. [illegible] at 295 nm excitation it is not possible to obtain the Tb³⁺ signal in [illegible] monitor the unfolding process of proteins. In the case of Y97W and CBD(M3) the Trp residue is located within the binding loop resulting in very efficient energy transfer from Trp to Tb³⁺. Therefore, the [illegible] peak was used as a probe [illegible] while the Trp peak was used [illegible] signal. The use of Tb³⁺ or Trp [illegible] as noted in the Figure legends.

The unfolding curves of the Tb³⁺ loaded proteins is shown in Figure 4.1. It was assumed that [illegible] two-state unfolding curve. However, it was discovered that [illegible] dissociation of [illegible] of Tb³⁺ loaded proteins. Therefore we [illegible] step unfolding process. The [illegible] and transition midpoints [illegible] are shown in Table 4.2. It was necessary to use Tb³⁺ [illegible] of the unfolding transitions of Y97W and CBD(M3) since the [illegible] the Trp residue was [illegible] in energy transfer to Tb³⁺ [illegible] of Trp [illegible] unfolding [illegible] in non-linear [illegible]. The unfolding of Y97W [illegible] intensity upon unfolding, while the Trp signal [illegible] excitation at 295 nm and the Tb³⁺ signal [illegible] excitation at 285 nm [illegible]

This last experiment was done to examine the key question of whether Trp fluorescence reported on local or global unfolding of the protein.

Upon binding of Tb^{3+}, the stability of Y57W increased by 17%, showing that the changes in the conformation of the loop upon binding of Tb^{3+} were significant. Terbium-loaded CDOM33 showed an enhancement in free energy (23%) which was slightly larger than that observed for Y57W, and a substantial enhancement of $C_{1/2}$ (from 2.2 M to 4.1 M) compared to Y57W. This behaviour was not unexpected since the binding affinity of the modified CD loop is about ten times higher than the original CD loop [20]. For Y65W the free energy did not change upon binding of Tb^{3+}. However, the transition midpoint increased by 43% compared to Ca^{2+}-loaded protein.

For F102W both the Trp and terbium signal decreased steadily by about 25-30% before unfolding started at about 2.0 M GdHCl, and then decreased sharply by about 40% during the unfolding process until unfolding finished at about 3.0 M GdHCl. The data in Table 3 indicate that the free energy and denaturant index both increased slightly when Tb^{3+} luminescence was monitored instead of Trp fluorescence. However, the $C_{1/2}$ value was identical in both cases. These results suggested that both the F-helix and the loop regions unfolded at the same time, as reported earlier. Remarkably, the free energy of the unfolding process of F102W in the presence of Tb^{3+} was 54% greater than was obtained in the presence of Ca^{2+}. Furthermore, the $C_{1/2}$ value increased by *ca.* 44%, which was in reasonable agreement with the changes in $C_{1/2}$ for Y57W.

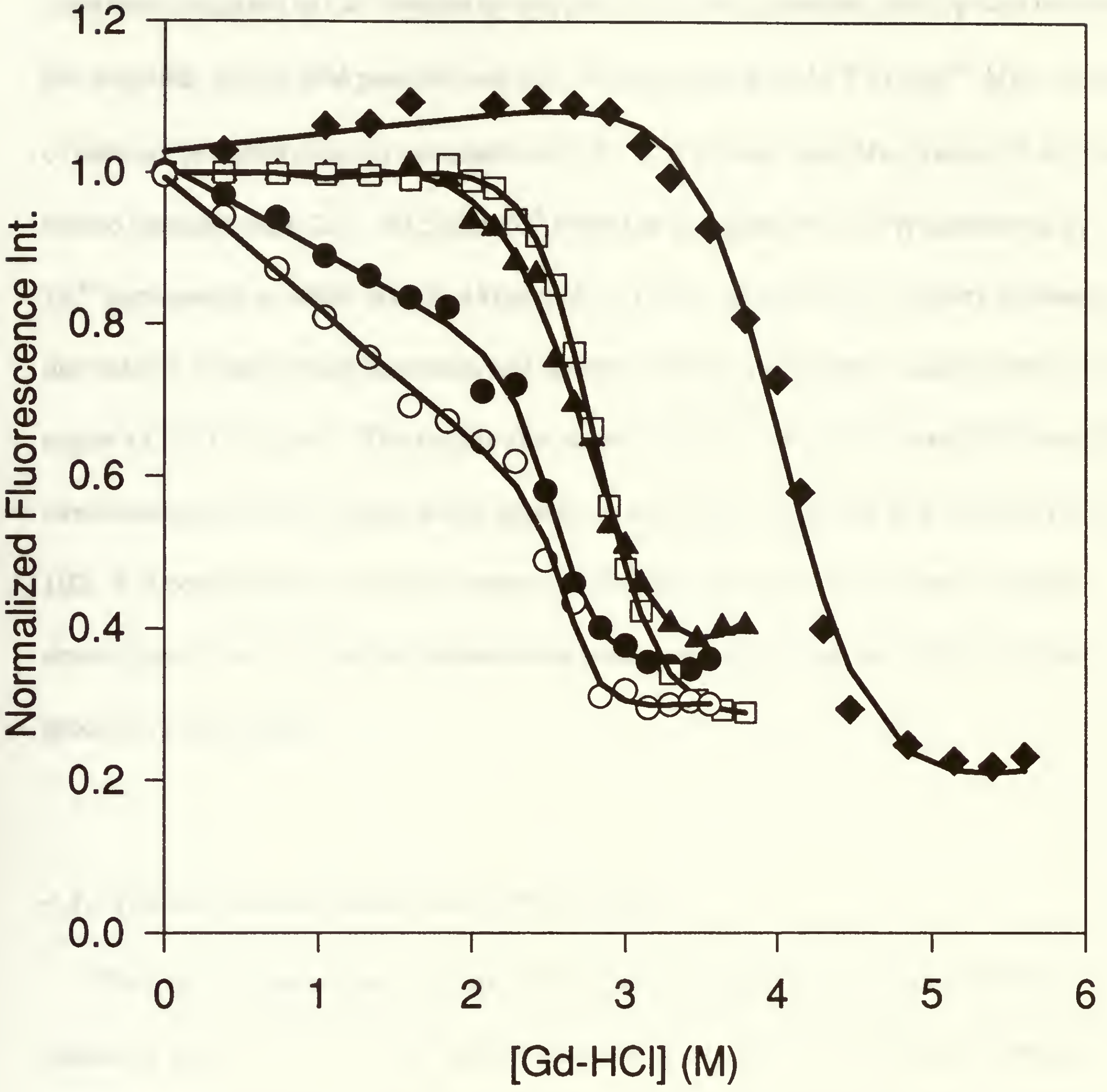

Figure 4.3 Changes of fluorescence intensity during chemical denaturation of terbium loaded F102W excited at 295 (Trp emission) (●), F102W excited at 285 (Tb^{3+} emission) (○), Y65W (▲), Y57W(□) and CDOM33(◆).The symbols are the experimentally derived data points. The solid lines are the lines-of-best-fit as determined by fitting to equation 1.13.

It is noteworthy that the $C_{1/2}$ and free energy values of the terbium-loaded proteins all increased compared to Ca^{2+}-loaded or apo proteins no matter where the Trp was located. For example, all apo OM proteins had ΔG_{un} values lower than 16.7 kJ.mol^{-1}. ΔG_{un} values of calcium bounded proteins increased to 22.2 - 30.9 kJ.mol^{-1} and ΔG_{un} values of terbium-loaded proteins were 28.0 - 35.5 kJ.mol^{-1} (with the exception of F102W monitored by Tb^{3+} luminescence, which was 46.4 kcal.mol^{-1}). Hence, as the binding affinity increases, the stability of the protein increases, and reaches what appears to be a limiting value in the region of 35-37 kJ.mol^{-1}. The results also show that the more tightly bound Tb^{3+} ion fully overcomes the destabilization which appears to occur upon insertion of a Trp into position 102. It is possible that the higher valence of Tb^{3+} may increase the number of oxygen donor groups from the protein bound to the metal, thus increasing the stability of the protein-metal complex.

4.3.5 Thermal Denaturation of Ca^{2+} -free Proteins

The spectral characteristics of apo OM proteins during thermal denaturation are shown in Table 4.4. As was the case for chemical denaturation, all spectra showed a substantial red-shift and an increase of FWHM during unfolding. The thermal unfolding curves for apo proteins are shown in Figure 4.4. In all cases, the unfolding process started at a relatively low temperature, and finished unfolding within a relatively narrow temperature range. Thermally induced unfolding profiles were analyzed by fitting the unfolding curve to equations 1.14 and 1.15, and the results are given in Table 4.5. Calculation of the ΔG_{un} value required that the temperature dependence of ΔH_{un} and ΔS_{un}

be accounted for by including a term for the differential heat capacity of the folded and unfolded protein ($\Delta C_{p,un}$). The value we used was 5559 J.(deg.mol)$^{-1}$ for the apo form, and 4598 J.(deg.mol)$^{-1}$ for the Ca^{2+}- and Tb^{3+}-loaded forms.[16]

The results showed that the thermal stability of the apo proteins were quite low. For single-Trp OM mutants the transition midpoint (T_{un}) values were very close (within 5°C of each other). The free energy values showed that, when compared to Y57W, the apo-form of Y65W was less stable whereas the apo-CDOM33 mutant was more stable. This trend was in agreement with that found during chemical denaturation of the apo mutants. Interestingly, the F102W mutant appeared to have the highest free energy among these proteins even though the T_{un} value was the lowest of the four proteins studied. This correlates to the increased values of both the enthalpy and entropy terms. Given that the apo form of the F102W mutant showed very poor stability towards chemical denaturation, it is possible that the increased free energy is the result of incomplete removal of the Ca^{2+} from the protein. It is also possible that GdHCl is better able to denature proteins compared to thermal denaturation methods, possibly due to electrostatic interactions between the positively charged denaturant and the protein, which has a net charge of -15 at neutral pH.[33]

CDOM33 appeared to have the highest transition midpoint (over 15°C higher than the other mutants) and slightly lower free energy than F102W (about 3.8 kJ.mol^{-1} lower). These results may reflect slight differences in the stability imparted by the novel CD loop structure as compared to the native CD loop of the other proteins.

Table 4.4 Changes in fluorescence properties of apo and Ca^{2+}-loaded oncomodulin mutants during thermal denaturation

Proteins	**Change in Intensity (Trp)**[a]	**Change in FWHM (nm)**	**Change in λ_{max} (nm)**	**Change in intensity (Tb^{3+})**
Y57W				
Ca^{2+}-free	47% decrease	55 - 60 - 57[b]	339 - 345 - 339[c]	
Ca^{2+}-loaded	17% decrease	53 - 59 - 55	339 - 345 - 339	
Tb^{3+}-loaded	20% increase	53 - 60 - 54	339 - 345 - 339	75% decrease
Y65W				
Ca^{2+}-free	33% decrease	55 - 57 - 55	343 - 345 - 343	
Ca^{2+}-loaded	36% decrease	55 - 57 - 55	343 - 345 - 343	
Tb^{3+}-loaded	20% decrease	55 - 57 - 56	343 - 345 - 343	77% decrease
F102W				
Ca^{2+}-free	40% decrease	47 - 64 - 51	316 - 345 - 316	
Ca^{2+}-loaded	72% decrease	39 - 64 - 40	315 - 345 - 315	
Tb^{3+}-loaded	80% decrease	39 - 63 - 41	315 - 345 - 316	80% decrease
CDOM33				
Ca^{2+}-free	47% decrease	54 - 58 - 56	339 - 345 - 339	
Ca^{2+}-loaded	61% decrease	53 - 59 - 53	339 - 343 - 339	
Tb^{3+}-loaded	58% decrease	53 - 59 - 54	339 - 343 - 340	40% decrease

a) Data were corrected by the thermal quenching curve of Lys-Trp-Lys, b) Data represented FWHM of native protein, denatured protein and recovered protein, c) Data represent λ_{max} values of native, denatured and recovered protein, respectively.

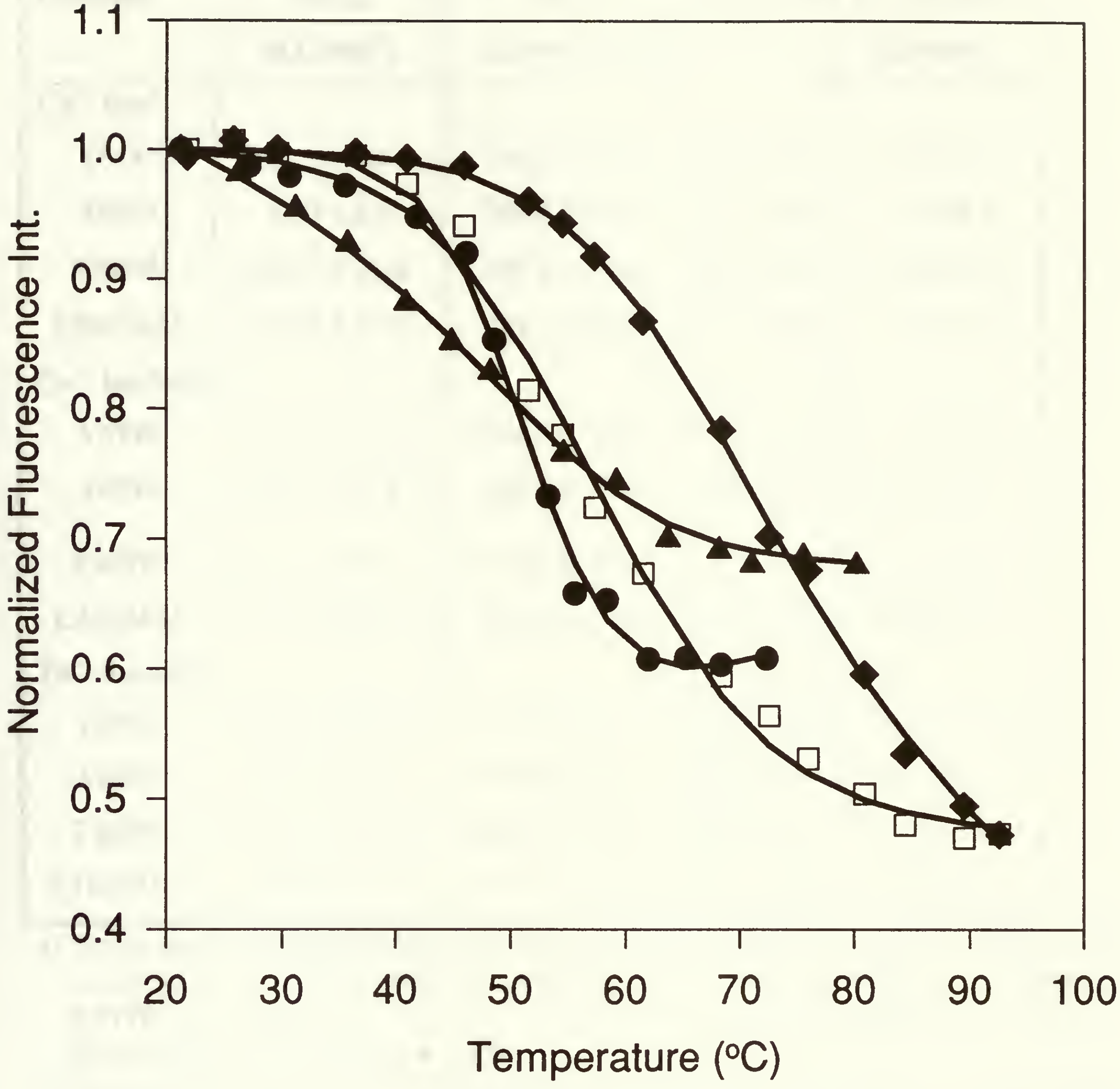

Figure 4.4 Changes of fluorescence intensity as a function of temperature for calcium-free oncomodulin mutants F102W (●), Y57W(□), Y65W (▲) and CDOM33(◆). The symbols are the experimentally derived data points. The solid lines are the lines-of-best-fit as determined by fitting to equation (1.14).

Table 4.5 Enthalpy changes for thermal unfolding of oncomodulin mutants.

Proteins	**ΔH^0_{un} (kJ./mol^{-1})**	**ΔS^0_{un} (J.mol^{-1}.K^{-1})**	**T_m (°C)**	**ΔG_{un} (20°C)^e (kJ.mol^{-1})**
Ca^{2+} free[a]				
Y57W	112.9 ± 18.4	355.6 ± 24.9	55.9 ± 0.5	10.0 ± 1.3
Y65W	81.0 ± 8.4	248.6 ± 20.1	52.8 ± 0.4	5.9 ± 0.8
F102W	225.7 ± 25.9	697.2 ± 74.0	50.9 ± 0.4	19.2 ± 1.9
CDOM33	120.4 ± 11.3	351.1 ± 33.1	70.1 ± 0.5	12.5 ± 1.3
Ca^{2+} loaded[b]				
Y57W	118.7 ± 13.0	346.3 ± 36.5	70.0 ± 0.5	12.5 ± 1.6
Y65W	99.9 ± 10.4	301.7 ± 23.3	58.0 ± 0.4	8.4 ± 1.1
F102W	375.1 ± 38.2	1082 ± 79.0	73.8 ± 0.3	52.2 ± 5.3
CDOM33	321.7 ± 32.7	913.6 ± 44.5	79.1 ± 0.3	46.8 ± 5.0
Tb^{3+} loaded[c]				
Y57W[d]	282.8 ± 31.5	797.3 ± 70.6	81.7 ± 0.4	41.4 ± 4.3
Y65W	258.0 ± 27.8	771.0 ± 81.3	61.6 ± 0.4	28.4 ± 3.0
F102W	305.0 ± 34.8	868.5 ± 152.1	86.4 ± 0.4	41.5 ± 4.5
CDOM33[d]	380.8 ± 40.1	1057 ± 107.9	87.7 ± 0.4	62.3 ± 7.1

a) Fitting parameters for apo proteins were as follows: **F102W:** $F_{ON} = 1.011$, $F_{OU} = 0.721$, $s_N = -0.012$, $s_U = -0.007$; **Y65W:** $F_{ON} = 0.998$, $F_{OU} = 0.669$, $s_N = -0.004$, $s_U = -0.006$; **Y57W:** $F_{ON} = 0.997$, $F_{OU} = 0.821$, $s_N = -0.010$, $s_U = -0.008$; **CDOM33:** $F_{ON} = 1.001$, $F_{OU} = 0.724$, $s_N = -0.009$, $s_U = -0.006$.

b) Fitting parameters for Ca^{2+}-loaded proteins were as follows: **F102W:** $F_{ON} = 1.005$, $F_{OU} = 0.301$, $s_N = 0.009$, $s_U = 0.002$; **Y65W:** $F_{ON} = 0.999$, $F_{OU} = 0.470$, $s_N = -0.008$, $s_U = -0.004$; **Y57W:** $F_{ON} = 1.001$, $F_{OU} = 0.922$, $s_N = -0.013$, $s_U = -0.007$; **CDOM33:** $F_{ON} = 1.034$, $F_{OU} = 0.484$, $s_N = -0.009$, $s_U = -0.003$.

c) Fitting parameters for Tb^{3+}-loaded proteins were as follows: **F102W:** $F_{ON} = 1.030$, $F_{OU} = 0.160$, $s_N = -0.009$, $s_U = 0.000$; **Y65W:** $F_{ON} = 1.009$, $F_{OU} = 0.076$, $s_N = -0.014$, $s_U = 0.002$; **Y57W:** $F_{ON} = 1.002$, $F_{OU} = 0.086$, $s_N = 0.040$, $s_U = 0.000$; **CDOM33:** $F_{ON} = 1.012$, $F_{OU} = 0.280$, $s_N = -0.008$, $s_U = -0.000$.

d) The thermodynamic parameters were obtained by fitting Tb^{3+} luminescence data.

e) Free energy values were calculated using equation 3 with $\Delta C_{p,un} = 5559$ (J.mol^{-1}.K^{-1}) for the apo form and 4598 (J.mol^{-1}.K^{-1}) for the Ca^{2+}- and Tb^{3+}-loaded forms[16], with a reference temperature of 293K.

4.3.6 Thermal Denaturation of Ca^{2+} -loaded Proteins

The spectral characteristics of holo OM mutants during thermal denaturation are shown in Table 4.4 and the unfolding curves are shown in Figure 4.5. The results of the thermodynamic analysis of the unfolding curves is given in Table 4.5. In all cases, denaturation caused a decrease of fluorescence intensity, a red shift in λ_{max} and an increase in the FWHM. The unfolding curves were significantly different than those obtained from chemical denaturation, mainly owing to the additional contribution from thermally induced quenching of fluorescence. The holo form of the proteins had T_{un} values which were higher than the values obtained for the apo form, consistent with binding of the metal ions to the folded state of the protein. Interestingly, the thermal denaturation profiles of the holo-oncomodulin mutants showed a different trend compared to the chemical denaturation profiles. Binding of Ca^{2+} caused the unfolding temperature of Y57W to increase by 14°C while the free energy of unfolding increased by 1.2 $kcal.mol^{-1}$. The Y65W protein showed smaller Ca^{2+}-dependent increases in local unfolding temperature and free energy, in agreement with the results from chemical denaturation.

F102W showed a significant increase in both the unfolding midpoint (73.8°C) and the free energy of thermal unfolding upon binding of Ca^{2+}, suggesting that the binding of Ca^{2+} is fundamentally important in stabilizing the F-helix against the hydrophobic core. Perhaps most important is the significant increase in both the local enthalpy and entropy of unfolding as probed by Trp-102 on going from the apo to the holo forms. Neither Y57W nor Y65W show such large increases. This is consistent with destabilization of the apo form of the protein when Trp is located at position 102, in agreement with the chemical

denaturation results. Once again, the F102W protein showed lower stability for chemical denaturation as compared to thermal denaturation, supporting the suggestion that electrostatic interactions between GdHCl and the protein may have affected the unfolding behaviour.

In the case of the CDOM33 there was also a large increase in thermal stability upon binding of Ca^{2+}. Both the enthalpy and entropy of the unfolding transition increased dramatically, resulting in an increase in both the unfolding transition temperature and the free energy of unfolding. These results agreed with the results from the chemical stability studies which showed that altering the binding affinity of the loop improved the stability of calcium binding proteins. The large increase in enthalpy and entropy for CDOM33 compared to Y57W is most likely due to the differences in the mode of binding to metal ions in the two loops. For Y57W, there is a bridging water in the binding loop at Asp-59 which participates in the binding process. For CDOM33, the Glu-59 residue participates directly in co-ordinating to the bound metal ion without the bridging water. The entropy and enthalpy of the nearby Trp residue would be expected to change dramatically upon binding of metal ions. The direct co-ordination without the need for bridging water molecules may also explain the much higher overall stability of CDOM33 during both chemical and thermal denaturation.

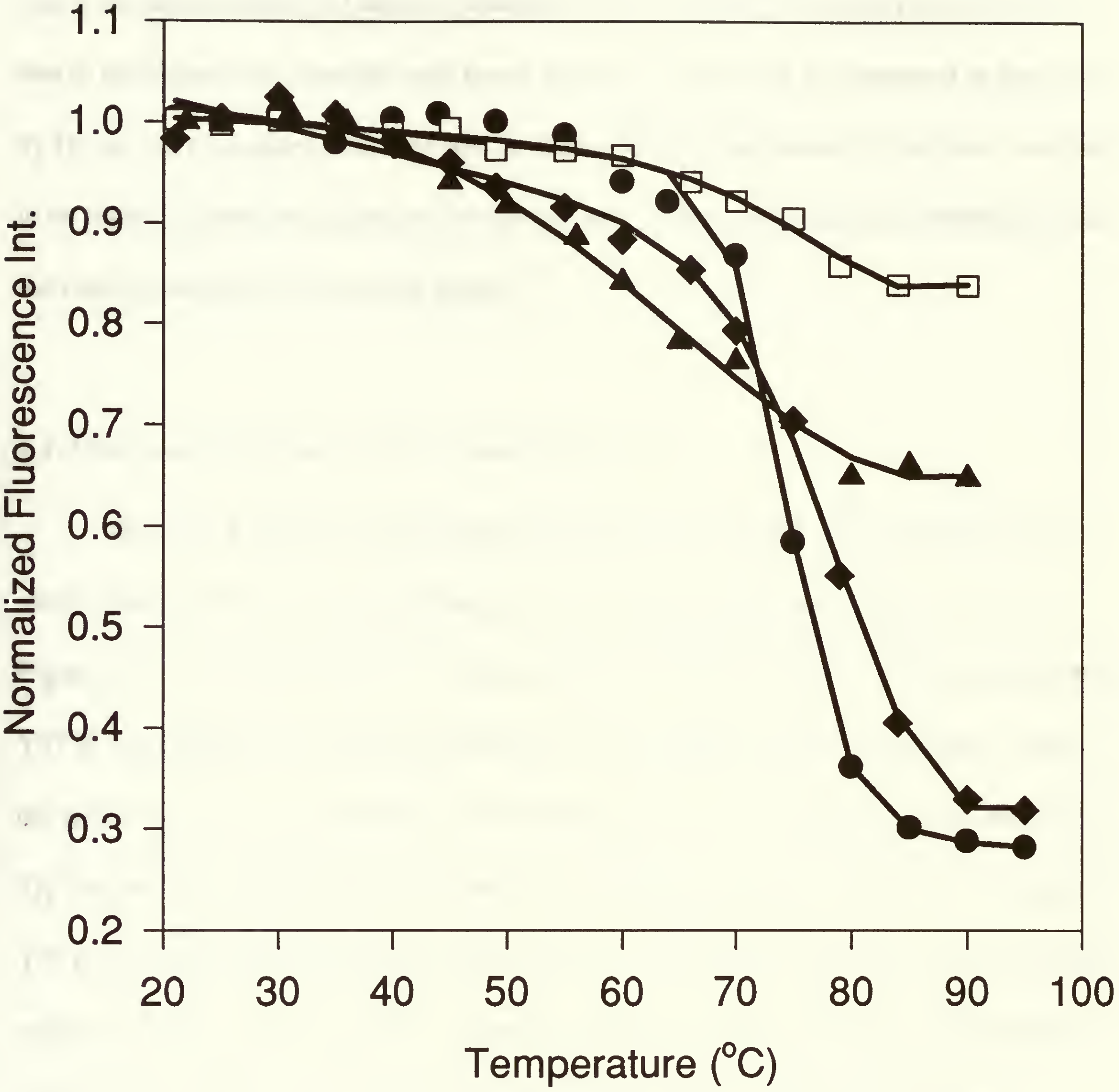

Figure 4.5. Changes of fluorescence intensity during thermal denaturation of calcium loaded F102W (●), Y57W(☐), Y65W (▲) and CDOM33(◆). The symbols are the experimentally derived data points. The solid lines are the lines-of-best-fit as determined by fitting to equation 1.14.

The free energy and unfolding temperature values obtained for Ca^{2+}-loaded OM mutants were in all cases lower than the values obtained by Henzl and co-workers[16]for native rat oncomodulin and various mutants with Ca^{2+} bound. This discrepancy is likely due to the lower ionic strength used in our work (100 mM KCl) as compared to the work by Henzl and coworkers (150 mM NaCl). The stability of oncomodulin has been reported to be highly dependent on the level of salt present, owing to electrostatic contributions to the conformational stability of the protein.[34]

4.3.7 Thermal Denaturation of Tb^{3+}-loaded Proteins

Binding of terbium instead of calcium also improved the thermal stability of each protein studied. The thermal unfolding curves of terbium loaded proteins are shown in Figure 4.6, while the thermodynamic data is given in Table 4.5. The unfolding curves for Y57W and CDOM33 mutants were obtained from changes in Tb^{3+} luminescence, while the unfolding curves for Y65W and F102W were obtained from changes in the intensity of Trp fluorescence. Interestingly, the transition midpoints and free energy of unfolding for Y57W increased significantly compared to the case where Ca^{2+} was bound. This is further supported by the large increases in the enthalpy and entropy of unfolding on going from Ca^{2+} to Tb^{3+}. The enthalpy, entropy and free energy of the Y65W also increased substantially upon binding of Tb^{3+}, suggesting that there was a major conformational change in the protein upon binding of the more highly charged lanthanide ion, in agreement with the chemical denaturation results. Interestingly, the free energy of terbium-loaded F102W appeared to be lower than calcium-loaded protein even though the

T_{un} value was improved. However, the standard deviation in the enthalpy and entropy values was quite large since the unfolding curve showed no post-unfolding region owing to the upper temperature limit of our instrument (95°C), which was past the point where unfolding was completed. Hence, it is possible that there was not a significant difference in stability upon binding of Tb^{3+}. For CDOM33, the binding of Tb^{3+} increased all thermodynamic values. This is consistent with the higher co-ordination number for Tb^{3+} as compared to Ca^{2+}, and is in agreement with the chemical denaturation studies.

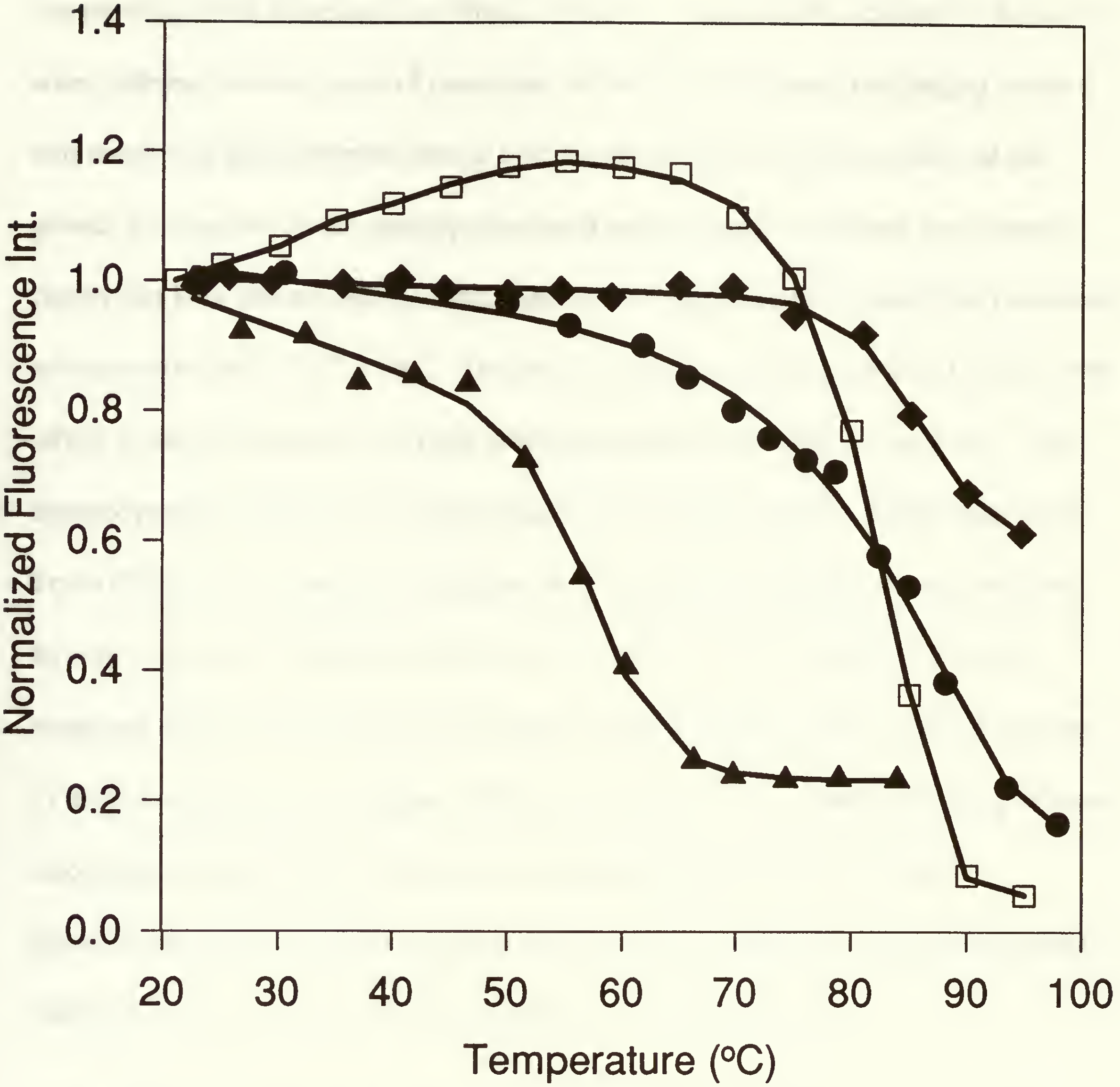

Figure 4.6. Fluorescence intensity changes during thermal denaturation of terbium loaded F102W (●), Y57W(□), Y65W (▲) and CDOM33(◆). The symbols are the experimentally derived data points. The solid lines are the lines-of-Sbest-fit as determined by fitting to equation 1.14.

4.4. Conclusion

This study has shown that single Trp mutants of the Ca^{2+}-binding protein oncomodulin can provide useful information on effects of point mutations on the stability of the protein when different levels or types of metal ions are bound. In all cases, the binding of metal ions resulted in large improvements in both the chemical and thermal stability of the protein. Comparison of the stability of proteins upon binding of different ions showed clearly that both thermal and chemical stability were improved upon binding of metal ions with the order apo < Ca^{2+} < Tb^{3+}. The thermodynamic parameters obtained in this work reflect global denaturation of protein structure reported from different locations. The thermodynamic values provided information on the degree to which the presence of the Trp at different locations either stabilized or destabilized the folding of the protein, and how the presence of different metal ions influenced this effect. Overall, the results suggested that increasing the number of metal ligating oxygens in the binding site, either by using a metal ion with a higher coordinate number (i.e. Tb^{3+}) thereby drawing in more carboxylate ligands, or by providing more ligating groups, as in the CDOM33 replacement, produces notable improvements in protein stability. This strongly suggests that the metal ion must be removed before protein unfolding occurs.

4.5 References for Chapter 4

1. Kidd, R.D.; Yennawar, H.P.; Sears, P., Wong. C.; Farber, G.K. *J. Am. Chem. Soc.* **1996**, 118, 1645.
2. Farver, O.; Skov, L.K., Young, S.; Bonander, N.; Karlsson, B.G.; Vanngard, T.; Pecht, I. *J. Am. Chem. Soc.*, **1997**, 119, 5453.
3. Blancuzzi, Y.; Padilla, A.; Parallo, J.; Cave, A. *Biochemistry*, **1993**, 32, 1302.
4. Bauer, H.H.; Müller, M. ; Goette, J.; Merkle; H.P.; Fringeli, U.P. *Biochemistry*, **1994**, 33, 1227.
5. Roskoski, R.; Gahn, L.G. *Biochemistry*, **1995**, 34, 252.
6. Beasty, A.M.; Hurle, M. J.; Manz, T.; Stackhouse, T.; Mathews, C.R. *Protein Structure, Folding and Design* Oxender, D. L., Ed,, Alan R. Liss Inc, New York , **1986** p.259.
7. Eftink, M. R. *Biophy. J.*, **1994**, 66, 482.
8. Sanz , J.M.; Fersht, A.R. *FEBS Lett.* **1994**, 344, 216.
9. Sampson, N.S.; Kass, I. J. *J. Am. Chem. Soc.*, **1997**, 119, 855.
10. Sudhakar, K.; Philips, C. M.; Owen, C.S.; Vanderkooi, J.M. *Biochemistry*, **1995**, 34, 1355.
11. M. Laberge, W.W. Wright, K. Sudhakar, P.A. Liebman and J.M. Vanderkooi, *Biochemistry*, **1997**, 36, 5363.
12. MacManus, J.P. *Cancer Res.* **1979**, 39, 3000.
13. Bernaert, D.; Brewer, L. M.; MacManus, J. P.; Galand, P. *Int. J. Cancer.* **1989**, 43, 719.

14.MacManus, J.P.; Brewer, L. M.; Yaguchi, M. *Eur. J. Biochem.* **1983**, 136, 9.

15. Barker, W.C.; Ketcham , L. K.; Dayhoff, M. D. *Atlas of Protein Sequences and Structure* Dayhoff, M. D. Ed,, **1978**, p.273.

16. Henzl, M.T.; Hapak, R. C.; Goodpasture, E. A. *Biochemistry*, **1996**, 35, 5856.

17. Cox, J.A.; Milos, M.; MacManus, J. P. *J. Biol. Chem.*, **1990**, 265, 6633.

18. MacManus, J.P.; Szabo, A. G.; Williams, R. E. *Biochem. J.*, **1984**, 220, 261.

19. Hutnik, C.M.L.; MacManus, J.P.; Banville, D.; Szabo, A.G. *Biochemistry*, **1991**, 30, 7652.

20. Clark, I.D.; Bruckman, A.J.; Hogue, C.W.V.; MacManus, J.P.; Szabo, A.G. *J. Fluorescence*, **1994**, 4, 235.

21. Hutnik, C.M.L.; MacManus, J.P.; Banville, D.; Szabo, A.G. *J. Biol. Chem.*, **1990**, 265, 11456.

22. Hutnik, C.M.L.; MacManus, J.P.; Szabo, A.G. *Biochemistry*, **1990**, 29, 7318.

23. Docktor, M.E. *Calcium and cell function* Cheng, W.Y., Ed,, Academic Press, New York, **1983**, Vol. IV, p.175.

24. Horrocks, W.D. *Advances in Inorganic Biochemistry Erichorn*, G. L., & Marizilli, L. G., Eds,, Elsevier Science Publishers B. V., Amsterdam , 4, **1982**, p.201.

25. MacManus, J.P.; Hutnik, C.M.L.; Sykes, B.D.; Szabo, A.G.; Williams, T.C.; Banville, D. *J. Biol. Chem.*, 1988, **264**, 3470.

26. Zheng, L.; Reid, W.R.; Brennan, J. D. *Anal. Chem.* **1997**, 69, 3940.

27. Barela, T.D.; Sherry, A.D. *Anal. Biochem.*, **1976**, 71, 351.

28. Kirby, E.P.; Steiner, R.F. *J. Phys. Chem.*, **1970**, 74, 4480.

29. Santoro, M.M.; Bolen, D.W. *Biochemistry*, **1988**, 27, 8063.

30. a) Hutnik, C.M.L.; Szabo, A.G. *Biochemistry*, **1989**, 28, 3923, b) Willis, K.J.; Szabo, A.G., *Biochemistry*, **1989**, 28, 4902.

31. Ahmed, F.R.; Przybylska, M.; Rose, D.R.; Birnbaum, G.I.; Pippy, M.E.; MacManus, J.P., *J. Mol. Biol*., **1990**, 216, 127.

32. She, M.; Dong, W.-J.; Umeda P.K.; Cheung, H.C., *Biophys. J*., **1997**, 73, 1042.

33. Gillen, M.F.; Banville, D.; Rutledge, R.G.; Narang, S.; Seligy, V.L.; Whitfield J.F.; MacManus, J.P., *J. Biol. Chem*. **1987**, 262, 5308.

34. Filimonow, V.V.; Pfeil, W.; Tsalkova, T.N.; Privalov, P.L., *Biophys. Chem*. **1978**, 8, 117.

Chapter 5 Controlling of the Thermal Stability and Terbium Binding Ability of Rat Oncomodulin Entrapped in a Sol-Gel Matrix

5.1 Introduction

The biological applications of sol-gel derived materials have been extensively studied during the last few years. The encapsulation of a variety of proteins, enzymes and other biological molecules have been reported,[1,2] and these studies have clearly established that biological molecules entrapped in inorganic matrices retain their characteristic chemical and biochemical functionality such as ligand binding, oxidation/reduction, fermentation and enzymatic activity. However, in most cases, the encapsulated biological molecules retained only a fraction of their activities in solution. This indicated that there were at least 2 possible problems: 1) There might be a distribution of environments inside the porous sol-gel matrices which results in inaccessibility of a portion of the biological molecules to the analytes; 2) The sol-gel process might affect the protein structure, especially for some “soft” proteins,[3] resulting in partial denaturation of the proteins and a loss of biological activity.

In the previous chapters (Chapters 2 and 3), we demonstrated that monellin could be successfully encapsulated into a TEOS derived sol-gel matrix and that the thermal stability and long term stability of this protein was improved. However, a distribution of environments was also observed upon encapsulation. The successful encapsulation of monellin was mainly due to the following reasons. First, monellin is a small protein. Therefore, the pore size reduction during the aging process was likely not sufficient to

cause a severe alteration of the protein structure. Second, monellin is stable over a wide pH range in aqueous solution, which indicated that monellin should be able to withstand the weak acidic condition of the sol. Third, monellin is stable at high alcohol levels, thus high ethanol levels during gelation is not a problem. Fourth, the stability of monellin is not dependent on the extent of ligand binding. Thus, the effects of changing the ligand concentration via interaction with the charged silicate matrix was avoided. However, when a metal-ion-binding protein is encapsulated in a sol-gel derived glass, the effects of the silica network on the ability of ligand to bind to protein must be considered.

Ellerby *et al.*[4] have reported that metalloproteins such as copper-zinc superoxide dismutase (CuZnSOD), horse heart cytochrome c, and horse heart myoglobin can be encapsulated inside TMOS derived sol-gel monolith and that these proteins retained their spectroscopic properties and reactivity. Removal and addition of metal ions within CuZnSOD could be repeated reversibly without altering the spectroscopic properties of the protein. However, there was no quantitative measurement done to determine whether full reactivity or just partial reactivity was retained when metal ions were removed and replaced. It can be argued that if the entrapped protein only retained partial reactivity, a change of color upon reacting with CN^- could still be observed. A potential problem with this work was that it was done using monolithic blocks, thus no results concerning the kinetics of the interaction of entrapped proteins with the analytes were reported.

As discussed in Chapter 2, alkoxysilane derived matrices are negatively charged at physiological pH, causing the kinetics of reactions with entrapped proteins to be complex when charged analytes are involved. In addition, the distribution of the pore sizes can

result in differences in protein accessibility and also will result in a distribution of environments for the entrapped protein. These factors will affect the signal produced by protein-analyte interactions and will also affect important parameters such reproducibility, detection limit, response time and the linear range of the calibration curve, and thus play a critical role in sensors which utilize entrapped proteins. Currently, there is still a lack of understanding regarding how the sol-gel matrices affect the function of entrapped proteins as well as how sol-gel matrices affect the reaction kinetics of protein-analyte interactions.

As introduced in chapter 4, the oncomodulin protein processes two calcium binding loops[5,6] in its structure and the stability of this protein is dependent on the loading of metal ions such Ca^{2+}, Mg^{2+} or Tb^{3+}.[7,8,9] Upon binding of Tb^{3+}, two major terbium luminescence peaks at 490 nm and 545 nm are generated due to Dexter energy transfer from a nearby Trp residue. The intensity of terbium luminescence peaks will increase steadily upon binding of terbium and reach a plateau when the ratio of terbium versus protein reaches 2:1. At this point, the ratio of Trp versus Tb^{3+} peak intensities can be used to quantitate the degree of binding in a ratiometric manner which does not depend on protein concentration. Thus, problems such as the distribution of the protein concentration caused by photobleaching, instrumental instabilities, protein denaturation or changes in the thickness of the slide can be avoided.

Based on the study of oncomodulin in solution presented in chapter 4, two mutants were chosen for encapsulation into sol-gel matrices; CDOM33 and Y57W. These two proteins were chosen since they both contain a single Trp residue at position 57 of the CD loop. Thus, upon binding of terbium, they both can provide large terbium luminescence

peaks which can be easily monitored due to the short distance between the Trp residue and bound Tb^{3+}. Terbium ions which are within the silicate matrix but not bound to protein should show no signal owing to the very short distance for Dexter energy transfer.[10] Thus, a signal from unbound terbium can be ruled out. CDOM33 appears to be the most suitable mutant for the following reasons: 1) It is a very stable protein (in the holo form) since the modified CD loop provides very high binding affinity; 2) It provides the highest terbium luminescence enhancement upon binding of terbium among the OM mutants; 3) There is a significant change in intensity and spectral characteristics of the Trp residue upon denaturation which can be easily monitored to examine the entrapped protein structure. The Y57W mutant can also generate a significant signal upon binding of terbium, however, previous work, as described in Chapter 4, has shown that there is only a small change in the intensity and spectral characteristics upon denaturation which is difficult to measure accurately. For this reason, Y57W was used mainly to compare the Tb^{3+} binding ability to that of CDOM33.

In this section, the effects of sol-gel matrices on the binding capacity of CDOM33 and Y57W OM were examined. These proteins are similar in size and structure, but differ in stability. In addition, the kinetics of metal ion loading of entrapped proteins with the positively charged species Tb^{3+} was examined with different levels of Ca^{2+} concentration in the matrix and surrounding buffer solution. The effects of metal ion loading on the stability of entrapped proteins was also examined. The results are compared to those of Edminston *et. al* who reported on the encapsulation of a "hard" protein (BSA) and a "soft" protein (myoglobin) in TMOS derived sol-gel matrices.[3]

5.2 Experimental Procedures

5.2.1 Preparation of Protein Doped Sol-Gel Slides

All experiments were done using chemicals and equipment as described in chapter 2 and 4.

Proteins were dissolved in 10 mM PIPES buffer with 100 mM KCl at pH 7.2. The preparation of the hydrolyzed sol was described in Chapter 2. A volume of 300 µl of the prehydrolyzed TEOS solution was rapidly mixed with an equal volume of cold PIPES buffer (10 mM, pH 7.2, with 100 mM KCl, 10 µM protein, 0 to 100-fold excess of calcium or 3-fold excess of terbium) and immediately placed into a disposable acrylate cuvette (1 cm pathlength) which was then sealed with Parafilm and placed on its side until gelation occurred (normally about 5-10 minutes). The slides were kept sealed at 4 °C overnight and then dry-aged under the same conditions as described earlier for a period of 25 days. At this point, the gels were stored in sealed cuvettes to prevent further drying. The washing step was omitted since leaching of the OM proteins from wet-aged slide was observed. The slides were carefully rehydrated before each experiment as described in Chapter 2.

5.2.2 Measurement of Fluorescence Excitation Spectra

Fluorescence excitation spectra of the samples were collected at emission of 350 nm. Spectra were collected from excitation 250 nm to 320 nm in 1 nm increments at a rate of

0.95 nm.sec^{-1} and with an integration time of 1 second. All the spectra were corrected for deviations in excitation monochromator throughput and PMT response and were normalized at 250 nm.

5.2.3 Response Time and Kinetics Studies

The rehydrated slides were placed in a quartz cuvette at the optimal position as described in chapter 2. The fluorescence intensity at 545 nm was recorded at 5 second intervals using a 4.99 second integration time with excitation at 295 nm immediately after 2 ml of a 1 mM terbium solution was added. The change in intensity was recorded until the signal reached a plateau. The response curves were analyzed using non-linear curve fitting algorithms available in the Microcal Origin software package (Ver. 4.0, Microcal Software Inc., Northampton, MA).

5.2.4 Thermal Denaturation Studies

All thermal denaturation experiments were done and data were analyzed as previously described in Chapter 3 and 4. In order to compare the results with previous solution work, the thermal denaturation of sol-gel encapsulated proteins were done on encapsulated CDOM33 with no extra calcium added, a 50-fold excess of calcium in the matrix but no excess calcium in the buffer, and 50-fold excess of calcium in both the matrix and the buffer.

5.2.5 Reversibility and Regenerability Studies

The Tb^{3+} loaded sol-gel slide was rinsed with 10 mM PIPES buffer several times to remove excess terbium. A volume of 250 ml of 40% (M/V) trichloroacetic acid (TCA) was added to the slide in 2 ml of PIPES buffer with continuous stirring for ~5 minutes. The slide was then rinsed with distilled water several times to remove the remaining TCA and Tb^{3+}, then washed with 10 mM PIPES buffer containing 15 mM Ca^{2+}. The regenerated slide was kept in the calcium containing buffer before addition of terbium.

5.3 Results and Discussion

5.3.1 Spectroscopic Properties of Entrapped Proteins

5.3.1.1 No Extra Calcium Added

Initially, holo CDOM33 and Y57W OM were encapsulated in the TEOS derived matrices without adding extra calcium. The fluorescence emission spectra of these two proteins are shown in Figure 5.1a. A very small red-shift of the emission maximum (1-2 nm) was observed for both proteins. Additionally, there was a 2 nm increase in the FWHM for both of these proteins. This evidence suggested that the negatively charged sol-gel matrix may have removed the calcium ions from the proteins by ion exchange and thus generated the apo protein. Previous work (Chapter 4) indicated that apo CDOM33 and Y57W both showed a small red-shift in the emission maximum and were very unstable compared to holo proteins. The apo proteins were not tightly folded and therefore may have been able to adsorb on the surface of the glass matrix during aging, causing the increase of the FWHM.

The excitation spectra also showed that entrapped proteins showed characteristics similar to the apo mutants (Figure 5.2). Holo proteins show a flat shoulder at 292 nm on their excitation spectra while apo proteins do not. The excitation spectra of the entrapped proteins did not possess a distinct 292 nm shoulder, suggesting that the entrapped proteins were likely made apo as a result of encapsulation. These results were also supported by other studies on the Ca^{2+}-binding protein Cod III parvalbumin (K. Flora and J. D. Brennan, unpublished results) which is much more sensitive to Ca^{2+} than oncomodulin in terms of intensity and wavelength shift. Preliminary studies on this protein have shown that the emission maximum of this protein shifted from 315 nm to 330 nm upon encapsulation and that this shift could be reversed by adding Ca^{2+}. Clearly, the sol-gel matrix had a very large effect on the free concentration of calcium and hence on the structure of the metal-ion-binding proteins.

5.3.1.2 Extra Calcium Added in Gelation Buffer

The two proteins were encapsulated into sol-gel matrices using a gelation buffer which contained a 50-fold excess of calcium, and were examined after aging for 25 days. The emission spectra of these two proteins are shown in Figure 5.1b. Interestingly, for CDOM33, the addition of Ca^{2+} resulted in the entrapped protein having an identical emission spectrum to that obtained in solution (both λ_{max} and FWHM were the same), suggesting that the entrapped protein maintained its folded structure and that no adsorption occurred. The excess Ca^{2+} likely interacted with the negatively charged siloxide groups of the glass, preventing the glass matrices from removing the Ca^{2+} from the

protein. Even with excess calcium added, the excitation spectrum of CDOM33 was still in between of that of apo for and holo form. It is likely that CDOM33 was trapped in a combination of apo and holo form.

Addition of a 50-fold excess of Ca^{2+} during the preparation of sol-gels containing Y57W showed slightly different results from CDOM33. In this case, the λ_{max} of the entrapped Y57W was still slightly red-shifted (1-2 nm) while the FWHM of the protein was wider than in solution but narrower than in the case where the protein was entrapped without adding extra Ca^{2+}. This suggested that addition of Ca^{2+} only partially maintained the structure of Y57W. The excitation spectrum of Y57W showed that, even with the excess of calcium, the entrapped Y57W was in a form which was more like an apo protein than a holo protein (spectra are shown in Figure 5.2). The EF loops of these two proteins are the same, but the binding affinity of the engineered CD loop of CDOM33 is approximately 10-fold higher[7] than for the CD loop in Y57W, therefore it is not unexpected that addition of excess of calcium was not able to fully restore the folded structure of Y57W inside the sol-gel matrices.

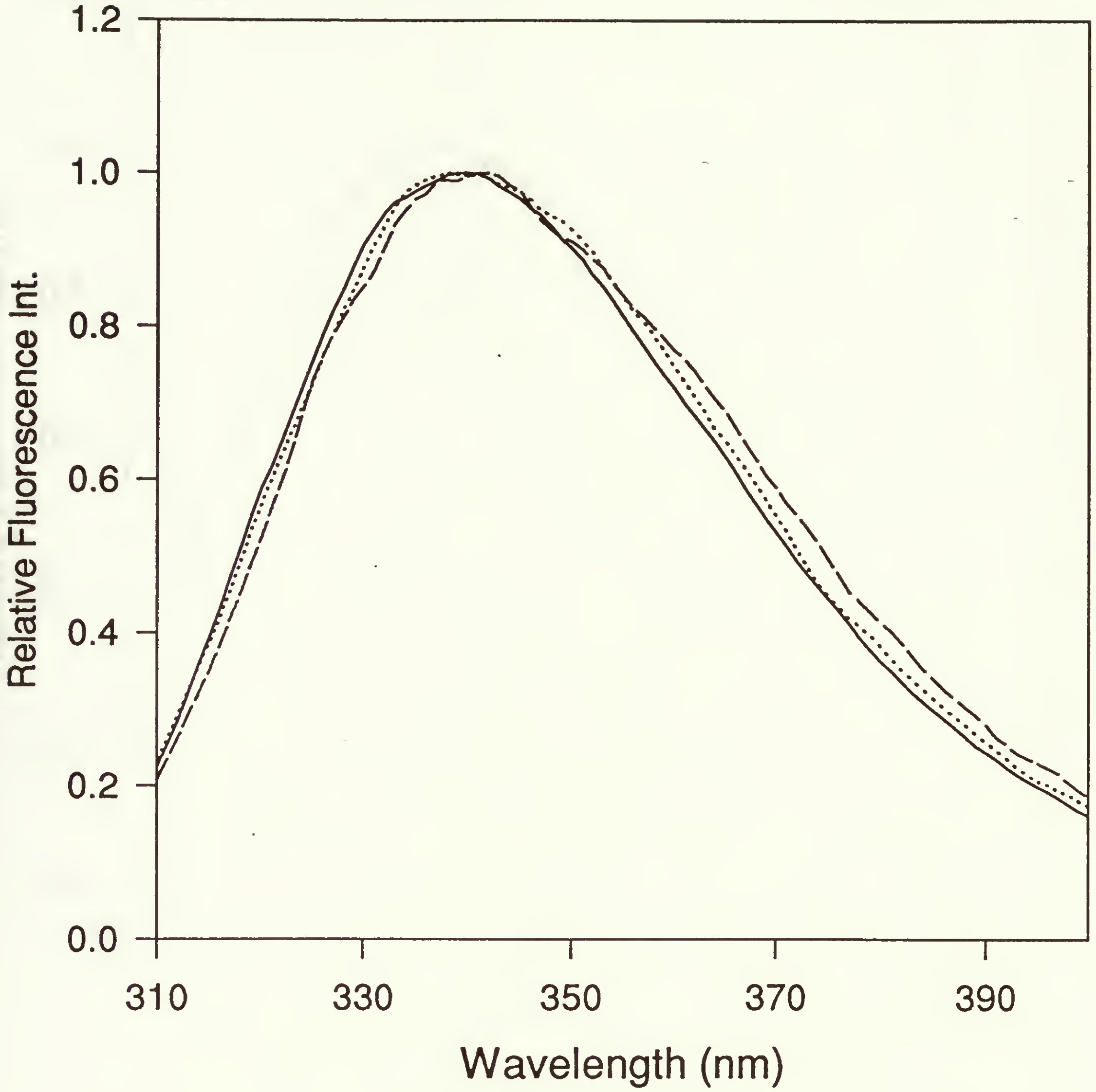

Figure 5.1a. Fluorescence emission spectra of CDOM33. (—) holo in solution, (----) encapsulated with no extra Ca^{2+} added, (···) encapsulated with 50-fold excess of Ca^{2+}

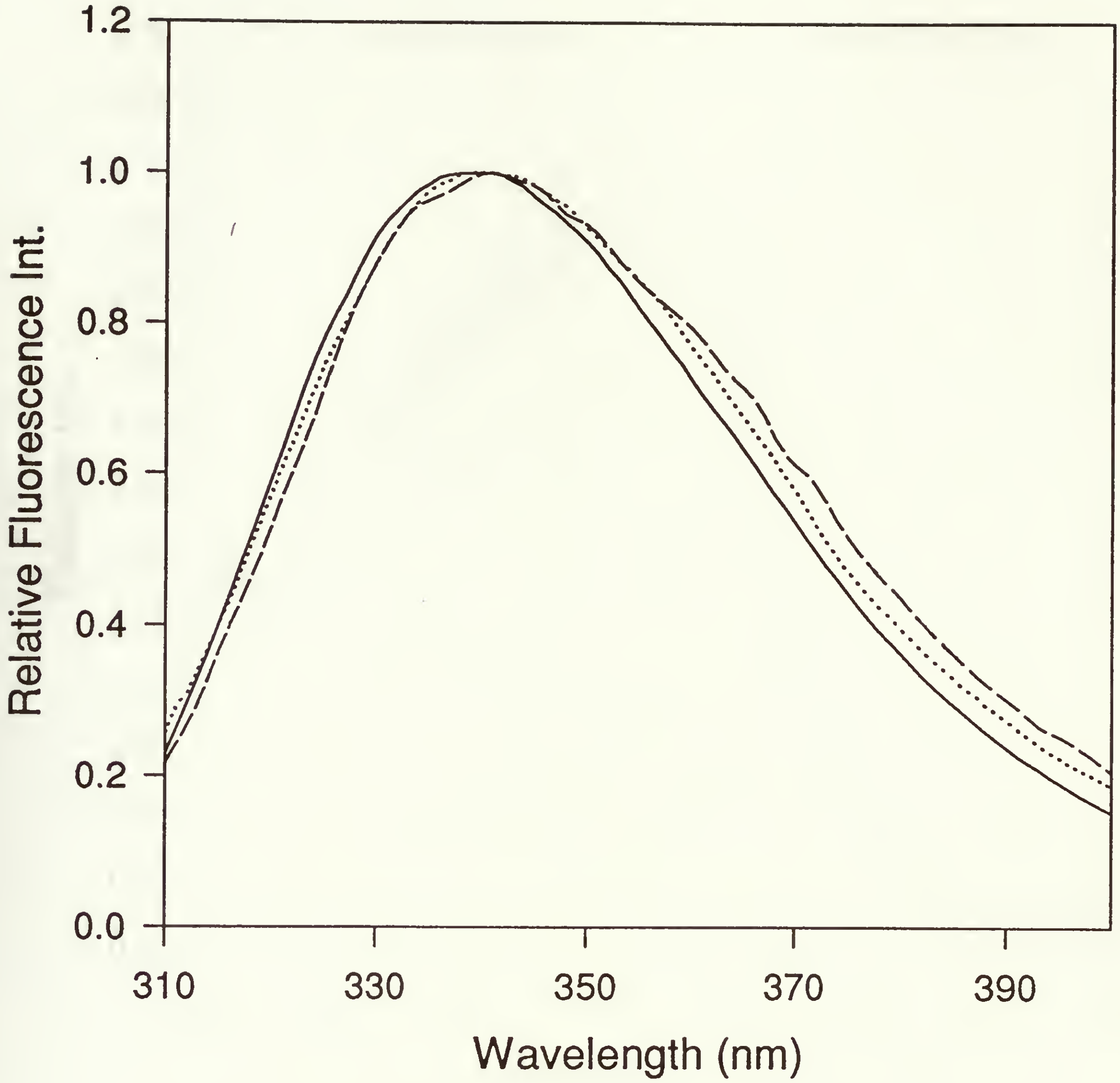

Figure 5.1b. Fluorescence emission spectra of Y57W. (—) holo in solution, (----) encapsulated with no extra Ca^{2+} added, (···) encapsulated with 50-fold excess of Ca^{2+}.

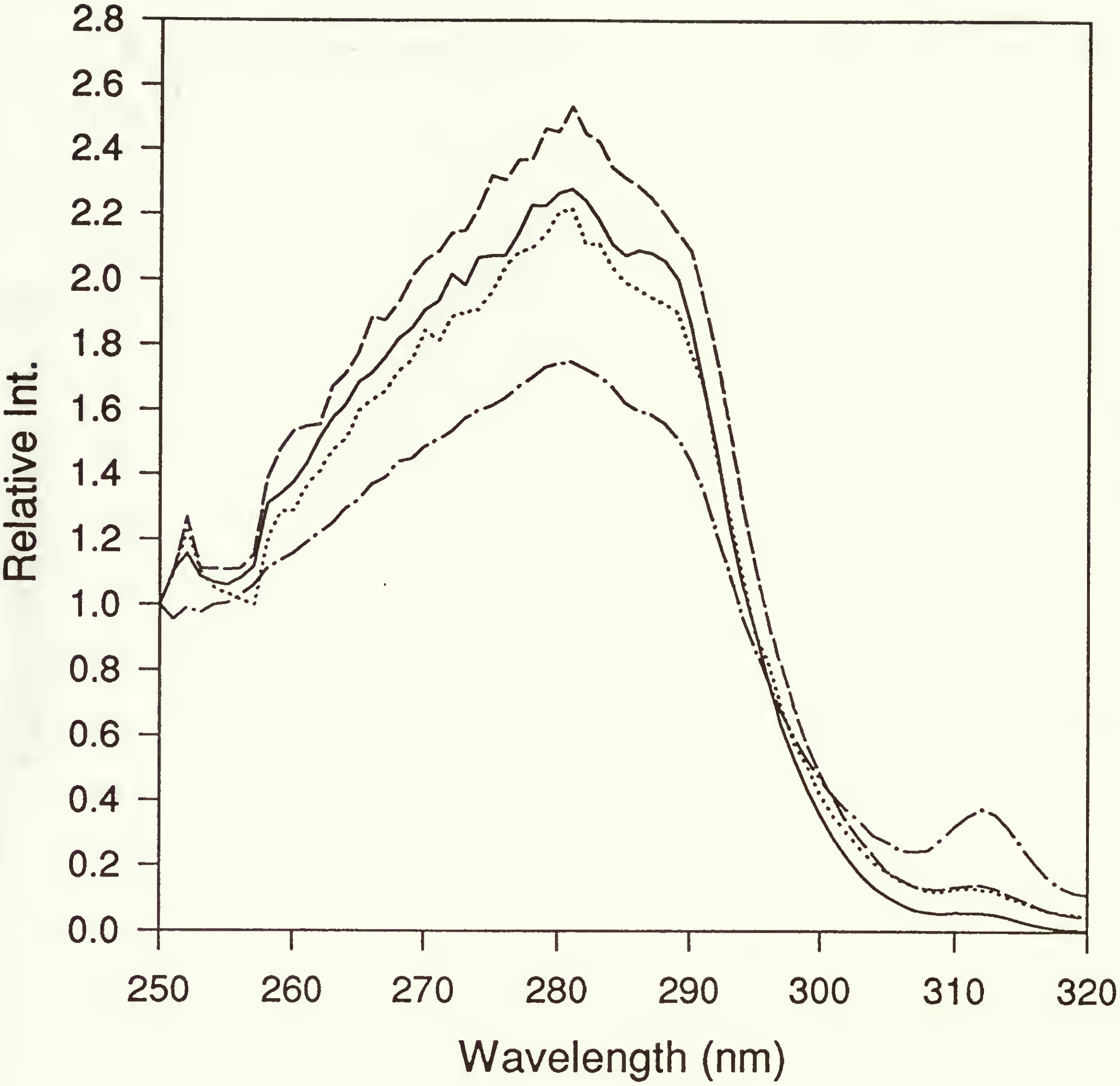

Figure 5.2a. Fluorescence excitation spectra of CDOM33. (—) holo in solution, (----) apo in solution, (···)encapsulated with 50-fold excess of Ca^{2+}, (– · –) encapsulated with no extra Ca^{2+} added.

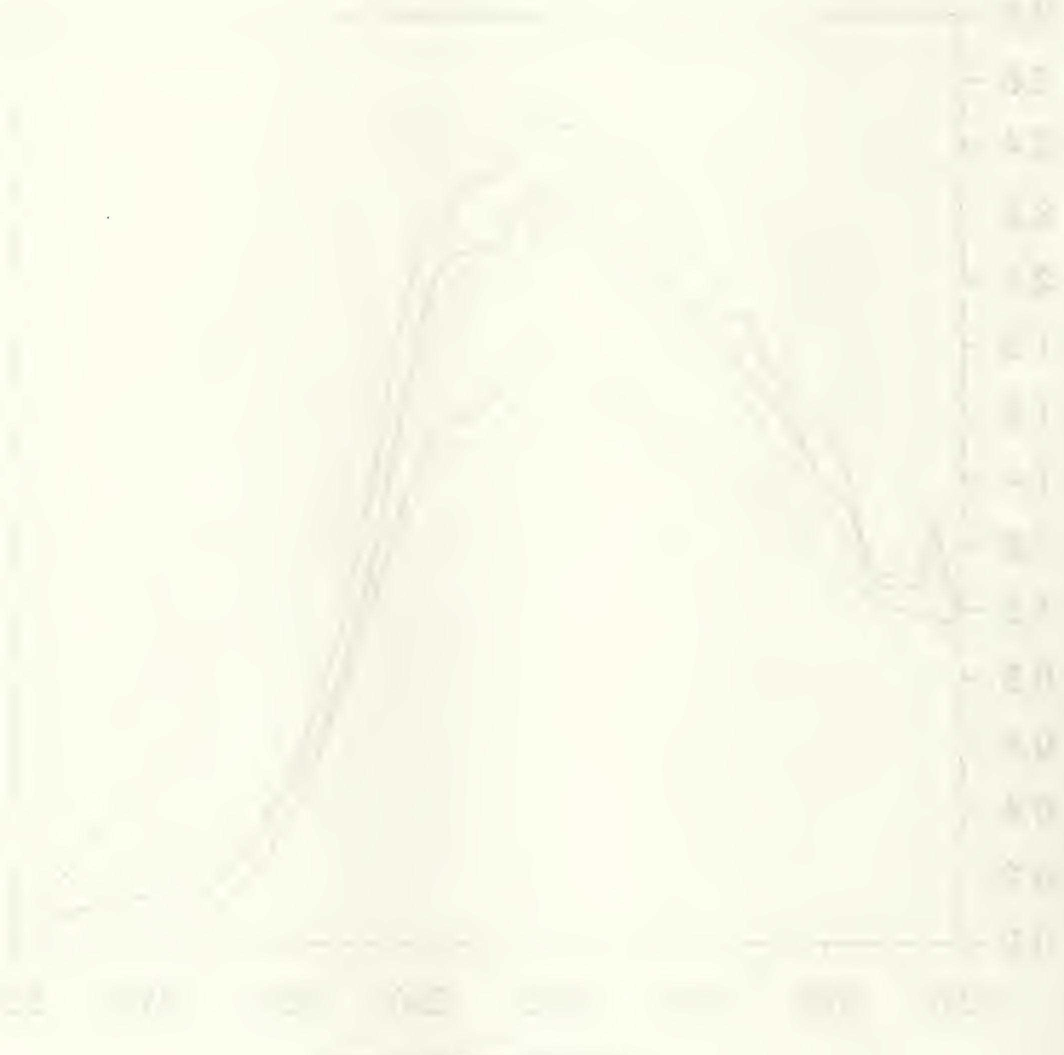

[illegible]

[illegible]

[illegible]

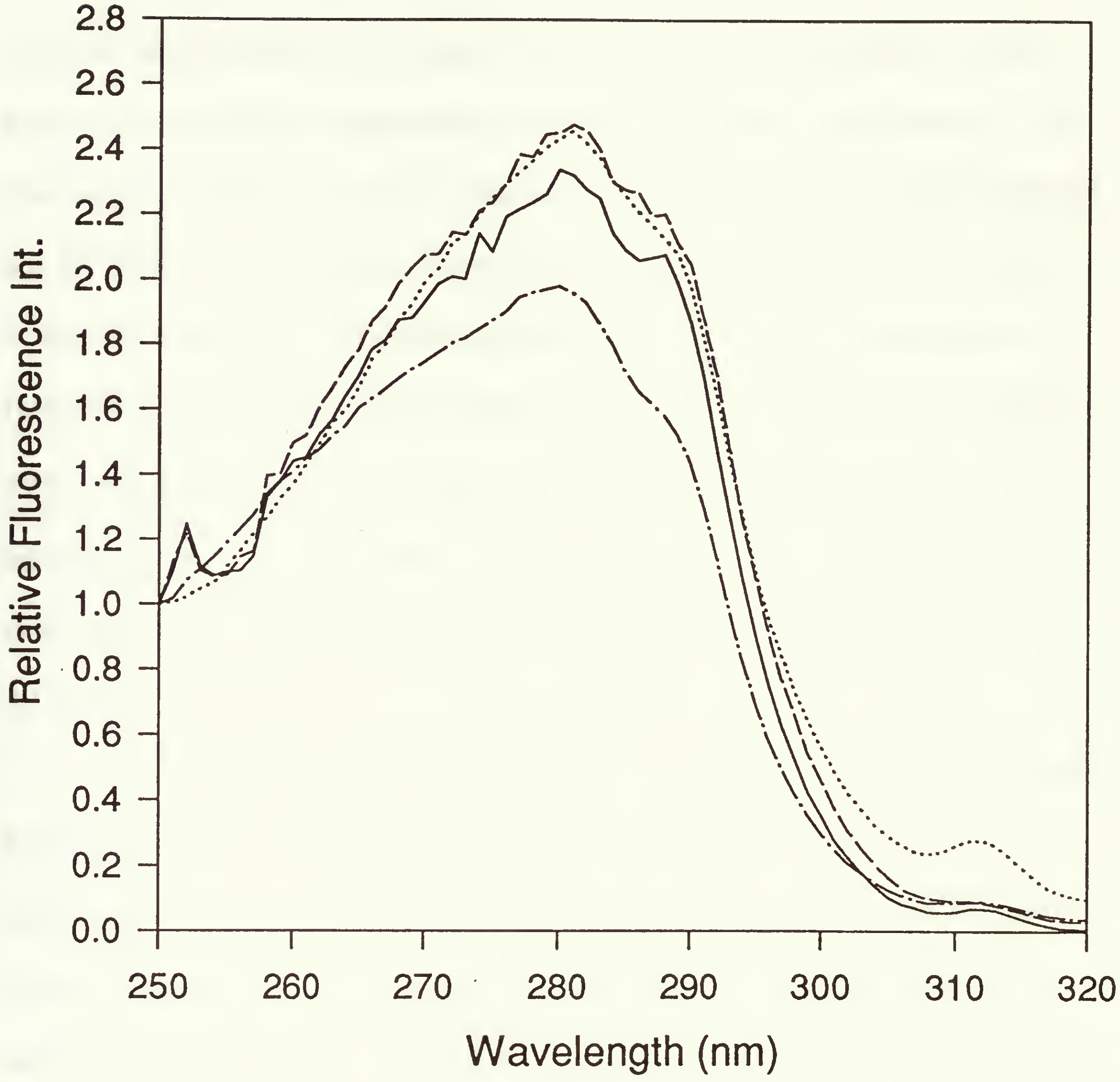

Figure 5.2b. Fluorescence excitation spectra of Y57W. (—) holo in solution, (----) apo in solution, (···)encapsulated with 50-fold excess of Ca^{2+}, (– · –) encapsulated with no extra Ca^{2+} added

5.3.2 Response Time and Kinetic Studies of Entrapped Proteins

The ability of analytes to enter the glass and interact with the entrapped proteins is essential when developing sol-gel based biosensors. Previous work has shown that the kinetics of interaction of charged species with entrapped proteins was complicated.[11,12] In this study, the response curves for the interaction of Tb^{3+} with sol-gel entrapped CDOM33 and Y57W were monitored with different loadings of Ca^{2+}. The response curve for the interaction of terbium with CDOM33 is shown in Figure 5.3. Data were analyzed by fitting the response curve to the exponential equations provided by the Microcal Origin software package, and the mean response times $\langle t \rangle$ (time required to reach $1/e$ of the total signal change) were calculated. The time to reach the 100% signal level were also determined and are defined as the maximum response times ($t_{\max}$) for the system. (Table 5.1 and 5.2)

In most cases, the response curves could be fit to a single first order time constant. In some cases, especially for CDOM33 with low level of calcium in the matrix, the response curve had to be fit into a sum of two first order time constants. This finding correlated with the studies of the interaction of the neutral quencher acrylamide with entrapped monellin[12] (Chapter 2) and adds support to the suggestion that the analytes are able to interact with the silane matrix via the negatively charged siloxide groups.

The kinetic studies showed several interesting results. The mean response time showed that the interaction of Tb^{3+} and entrapped proteins in the absence of extra Ca^{2+} was extremely slow. This would be expected since the terbium ions likely interact with the glass matrix first via ion exchange, slowing their passage through the silicate matrix and

thus interfering with the binding to entrapped proteins. Since the entrapped proteins in the absence of excess calcium were observed to be only partially functional, the reaction kinetics should be even more complicated since there are multiple parameters affecting the protein-analyte interaction. However, in most case, the reresponse curves were able to be fit to single first order constants. This suggested that the possibility of Tb^{3+} ions to enter the glass matrix was the main issue that affected the kinetics of terbium-protein interaction, and that this is an important issue when the sol-gel format is used for protein encapsulation.

Addition of calcium to the gelation buffer before encapsulation resulted in both a substantial reduction of the response time for both CDOM33 and Y57W and simpler kinetics. The mean response time dropped from over 200 sec to around 50 and 70 sec when the calcium level increased from 0 to over 30-fold. This is an exciting finding since it demonstrates that the response time and kinetic order can be tuned by adjusting the calcium level before encapsulation. The basis for the reduced response time is likely that it is much easier for the terbium ions to enter the glass matrices when the glass is loaded with calcium ions, mainly due to the elimination of the delay time required for the interaction of Tb^{3+} with the glass matrices since the siloxide groups had already bound Ca^{2+}.

Table 5.1. Kinetics study of the interaction of Tb^{3+} with entrapped CDOM33

$[Ca^{2+}]$ /[Pro]	t_1 (sec)	A_1	t_2 (sec)	A_2	$< t >$	t_{max} (sec)	χ^2
0	73.0	0.54	362.2	0.46	207.0	1020	1.43E-05
5	132.2	0.63	303.8	0.37	195.5	920	4.08E-05
10	56.3	0.64	342.0	0.36	160.4	800	2.78E-05
20	183.9	1			183.9	700	1.45E-06
30	93.9	1			93.9	380	1.86E-06
40	50.0	0.82	180.9	0.18	74.1	580	1.06E-06
50	86.0	1		0.39	86.0	320	7.31E-06
60	48.3	0.58	166.8	0.42	98.3	530	1.14E-05
80	116.9	1			116.9	670	2.42E-06
100	112.9	1			112.9	560	2.80E-06

Table 5.2. Kinetics study of the interaction of Tb^{3+} with entrapped Y57W.

$[Ca^{2+}]$/ [pro]	t_1(sec)	t_{max} (sec)	χ^2
0	356.5	1275	6.17E-05
5	121.8	490	6.49E-05
10	96.3	410	1.08E-04
20	55.6	295	2.49E-04
30	51.5	190	3.64E-04
40	71.0	260	1.04E-04
50	65.2	285	5.72E-05
60	102.4	520	9.76E-05
80	93.3	355	4.99E-05
100	80.4	305	2.21E-04

Table 5.3. Percent of Tb^{3+} signal obtained from encapsulated CDOM33 and Y57W.

$[Ca^{2+}]$/[protein]	0	5	10	20	30	40	50	60	80	100
CDOM33	27%	32%	45%	55%	65%	98%	99%	100%	88%	95%
Y57W	10%	27%	34%	37%	40%	39%	45%	32%	35%	42%

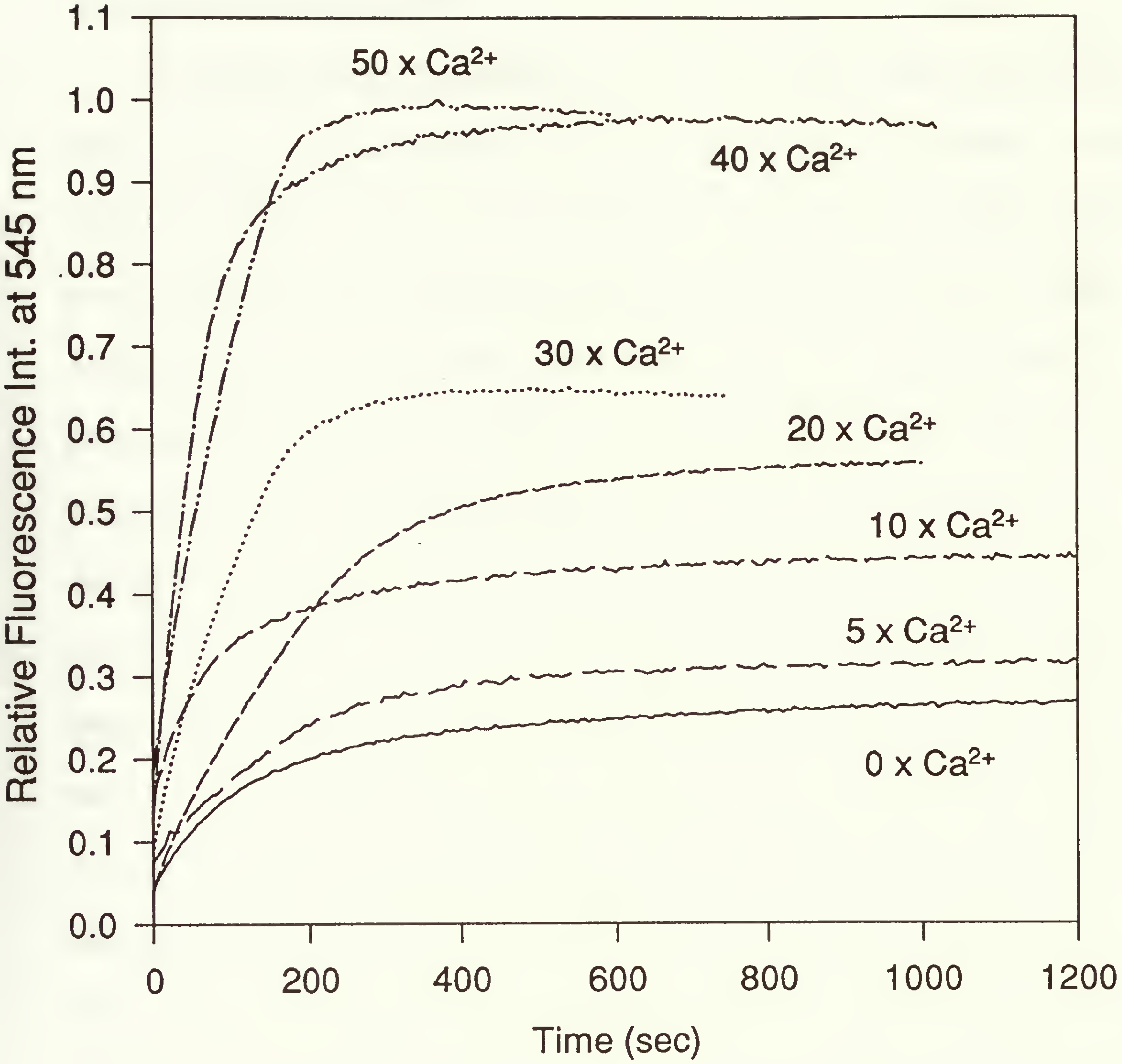

Figure 5.3 Response curves for interaction of terbium with entrapped CDOM33 with different levels of calcium in the sol-gel matrices.

5.3.3 Comparison of the Terbium Binding Ability of CDOM33 and Y57W OM

5.3.3.1 No Extra Calcium Added

The binding ability of the entrapped proteins was studied to further investigate the effect of the glass matrix on the structure and reactivity of the proteins. Initially, entrapped CDOM33 was tested by adding 2 ml of a 100 µM Tb^{3+} solution. However, there was only a very small terbium peak at 545 nm (0.35% of the full signal) observed after 1.5 hours. Assuming that the gels shrunk 80% by weight after aging for 25 days, the entrapped proteins should have been concentrated to a local concentration of about 25 µM in a volume of less than 0.1 cm^3 before testing. Assuming that the sol-gel matrix acts as a dialysis tubing, the analyte can diffuse in freely. The concentration of terbium inside the matrix should be the same as in the surrounding solution. Thus, the local concentration of terbium inside the matrix should be four times that of the entrapped proteins. However, terbium ions will posibily interact and associate with the negtively charged silicate matrix first, causing the matrix to be filled with positively charged species. Thus, it will be more difficult for the free terbium ions in the surrounding solution to overcome the electrostatistic force to enter the matrix. Thus, the true concentration of the Tb^{3+} solution inside the pores can be much lower than it was intended to be and the amount of terbium bound was insignificant. When a more concentrated Tb^{3+} solution (1mM) was used, a higher terbium signal was observed in a shorter period. However, even with the addition of the 1mM terbium solution, there was only 27% of the maximum terbium signal observed for CDOM33 and only 10% for Y57W. The aged gels were also soaked in a 3 mM calcium solution before addition of terbium. Even under these conditions, there was

only 40% of terbium signal obtained. These findings confirmed that a fraction of the protein had a structure which was likely altered upon encapsulation in a way which was not fully recoverable. Thus, the entrapped proteins were only partially functional. Overall, a higher terbium signal was observed for CDOM33 compared to Y57W, indicating that the sol-gel matrix affected Y57W more than CDOM33, likely due to the lower binding affinity and lower stability of Y57W in comparison to CDOM33.

5.3.3.2 Extra Calcium Added

Since the sol-gel matrix was able to remove Ca^{2+} from the protein upon encapsulation, it was obvious that addition of extra calcium before encapsulation was required. In the following experiments, CDOM33 and Y57W were entrapped with 5, 10, 20, 30, 40, 50, 60, 80 and 100-fold excess of Ca^{2+} in the gelation buffer. The terbium binding capacity of these entrapped proteins was tested by addition of 2 ml of a 1 mM terbium solution. As expected, there was an increase in the terbium binding ability as the concentration of calcium increased, as shown in Table 5.3 and Figure 5.4. CDOM33 was able to retain full reactivity when a 40-fold excess of calcium was added before encapsulation. Full reactivity of the entrapped protein was also observed for sol-gels with a 50 and 60-fold excess of calcium. When the calcium level was over 60-fold with respect to the protein, the binding capability of CDOM33 decreased slightly. The decrease in binding capability was quite possibly due to aggregation of the protein at high calcium levels before encapsulation[13]. Y57W also showed an increase in terbium binding ability when the calcium loading increased. However, the highest terbium signal was observed to be only about 45% of that obtained in solution when a 30 to 50-fold excess of calcium was

present. As was the case for CDOM33, the terbium binding ability of Y57W decreased slightly when the calcium level was over 50-fold.

The ability to control both the kinetics and the binding capacity of an entrapped protein by tuning the reaction conditions before encapsulation is an extremely important finding. Clearly, the sol-gel process affected the structure of the Ca^{2+} binding protein oncomodulin greatly. The negatively charged sol-gel matrices were able to remove the calcium from the binding loops, leaving the apo protein with a loosened structure and resulting in a loss of the biological activity due to irreversible processes such as adsorption onto the glass matrices or aggregation during aging. Loading of excess calcium before encapsulation was able to provide enough divalent metal ions to bind with the negatively charged sites on the glass matrix with sufficient free Ca^{2+} remaining to keep the protein in a fully folded form and maintain its biological reactivity. However, it is important to note that not all proteins were able to withstand the sol-gel process even though this modification was made. For example, Y57W OM was observed to be only partially active using the same encapsulation conditions as for CDOM33. The reason why Y57W only retained part of its activity may involve the lower thermodynamic stability of Y57W compared to CDOM33, as discussed in the previous chapter. This result correlates well with the suggestion by Edminston *et al.* that the sol-gel entrapment process is more disruptive to the structure of "soft" proteins (i.e., thermodynamically unstable proteins) than "hard" proteins (i.e., thermodynamically stable proteins).[3]

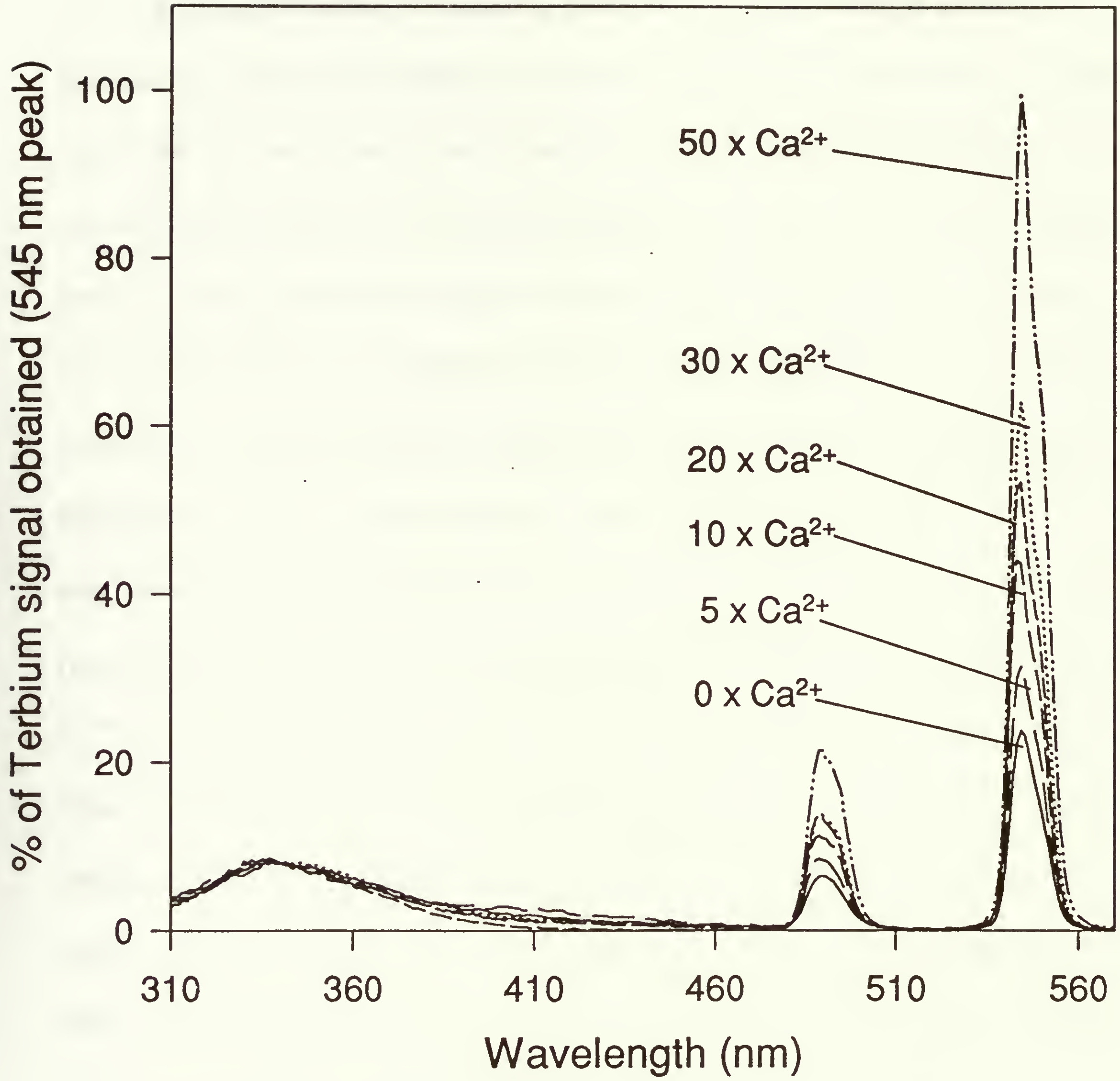

Figure 5.4. Spectra of terbium loaded CDOM33 encapsulated in the sol-gel matrices with different levels of calcium in the matrices.

5.3.4 Reversibility for Loading of Tb^{3+} with encapsulated CDOM33

A common method for removing bound metal ions from OM in solution is precipitation of the protein using trichloroacetic acid(TCA). It was discovered that the bound terbium can also be removed from the entrapped CDOM33 by addition of a TCA solution. Upon addition of TCA to the entrapped protein, the terbium peak at 545 nm completely disappeared within 5 min. This was likely due to protonation of negative charges in the binding loops which removed the bound ions. The TCA and free Tb^{3+} were removed by rinsing the slide with distilled water (pH~5) several times. About 5% of the initial terbium signal reappeared after the rinsing step, likely owing to residual Tb^{3+} which was bound to the silicate matrix and thus was not completely removed. The slide was then rinsed with 10 mM PIPES buffer with 25mM Ca^{2+} several times to exchange the residual Tb^{3+} out of the matrix and adjust the pH to physiological values. The intensity of Trp signal was fully recovered after the second rinsing step with no additional Tb^{3+} signal present. Addition of a 2 ml 1 mM terbium solution to the regenerated slide resulted in the recovery of 83% of terbium signal. This indicated that the addition and removal of the Tb^{3+} from the entrapped CDOM33 could be done with a reasonable degree of binding activity being retained. The regenerability of entrapped CDOM33 can likely be improved by optimizing the regeneration conditions and also by using a thin film format or a flowthrough system for rinsing.

5.3.5 Thermal Stability Studies for Encapsulated CDOM33 and Y57W

To further explore the assertion that the binding capacity was correlated to protein stability in solution, we examined protein stability when encapsulated. This is also important in the development of biosensors with encapsulated proteins since maximum stability of entrapped proteins is required.

The rehydrated gels containing CDOM33 were mounted in a quartz cuvette at the optimal position and 3 ml of N_2 purged PIPES buffer was added to the cuvette before starting the experiment. The thermal denaturation experiments were performed using the following samples: encapsulated CDOM33 with no extra Ca^{2+} in either the gel or the buffer, with a 50-fold excess of calcium in the gel but no extra Ca^{2+} in the buffer, and with a 50-fold excess of calcium in both the matrix and the buffer. The unfolding curves are shown in Figure 5.5a. Thermodynamic parameters were calculated by the method described in the theory section in Chapter 1 and the results were compared with the solution work presented in the previous chapter. The results are shown in Table 5.4.

It is obvious that encapsulation of CDOM33 without extra calcium resulted in a destabilization of the protein when compared to solution. Both the T_{un} value and the free energy ΔG_{un}^{0} decreased substantially compared to the values obtained in solution. The enthalpy and entropy values also dropped, indicating that either the protein did not fully unfold, or was already partially unfolded upon encapsulation. Thermal denaturation of CDOM33 with a 50-fold excess of calcium in the gel but no calcium in the buffer resulted

in an improvement in T_{un}, ΔG^0_{un} , ΔH^0_{un} and ΔS^0_{un} compared to the case where no Ca^{2+} was present. Thus, the addition of Ca^{2+} in the gelation buffer improved the protein stability. However, there was still a decrease in ΔS^0_{un}, ΔG^0_{un} , ΔH^0_{un} and T_{un} compared to the values in solution. This is likely due to leaching of Ca^{2+} from the glass matrix to the buffer causing a decrease in the actual calcium concentration present for the entrapped proteins. Previous work has shown that the stability of several Ca^{2+}-binding proteins including OM, is dependent on the amount of Ca^{2+} loading.[14,15]

When a 50-fold excess of Ca^{2+} was also present in the buffer surrounding the entrapped proteins, the ΔS^0_{un}, ΔG^0_{un} and ΔH^0_{un} values all increased compared to the values obtained in solution. In addition, the T_{un} values were observed to be the same as in a solution with same the level of Ca^{2+}. This result suggested that the entrapped protein was able to maintain a similar stability or even had improved stability compared to the protein in solution when encapsulated with excess Ca^{2+}. The increase in the ΔS^0_{un} value suggested that the protein was able to fully unfold in the sol-gel matrix. This is supported by the emission maximum values which showed that the λ_{max} values for the entrapped protein was able to red shift to 345 nm upon denaturation, indicating that the protein was fully unfolded. Again, Ca^{2+} played an essential role in both the reactivity and the stability of the encapsulated OM proteins.

Thermal denaturation of entrapped Y57W was also done with a 50-fold excess of calcium in both the matrix and buffer solution. The unfolding curve is shown in Figure 5.5b. Fitting of the curve to equation 1.14 was unsuccessful because of the narrow transition range of the unfolding curve and the two-step unfolding profile. However,

comparison of the unfolding curve with that of the protein in solution clearly showed that the entrapped Y57W underwent a two-step unfolding with the first step having a lower T_{un} and the second step having a higher T_{un} value than was obtained for the protein in solution. This result may explain why Y57W only retained a fraction of it binding capacity. It is obvious that even with excess calcium present, a portion of the encapsulated Y57W still could not survive the sol-gel encapsulation process.

Table 5.4. Comparison of the thermodynamic parameters for thermally induced denaturation of entrapped CDOM33.

Sample matrix	ΔH^0_{un} (kJ.mol^{-1})	ΔS^0_{un} (J.K^{-1}.mol^{-1})	T_{un} (°C)	ΔG^0_{un} (kJ.mol^{-1})	χ^2
solution 50x Ca^{2+}	321.7 ± 32.7	913.6 ± 44.5	79.1 ± 0.3	54.0 ± 5.0	0.0067
sol gel no Ca^{2+} added	225.3 ± 21.2	668.0 ± 50.3	64.1 ± 0.3	29.5 ± 2.4	0.0064
sol-gel 50 x Ca^{2+} in the matrix	239.1 ± 20.1	690.9 ± 42.6	69.1 ± 0.3	34.3 ± 2.9	0.0089
sol-gel 50 x Ca^{2+} in the matrix and buffer	383.7 ± 23.4	1090.6 ± 79.2	78.8 ± 0.2	64.4 ± 3.2	0.0045

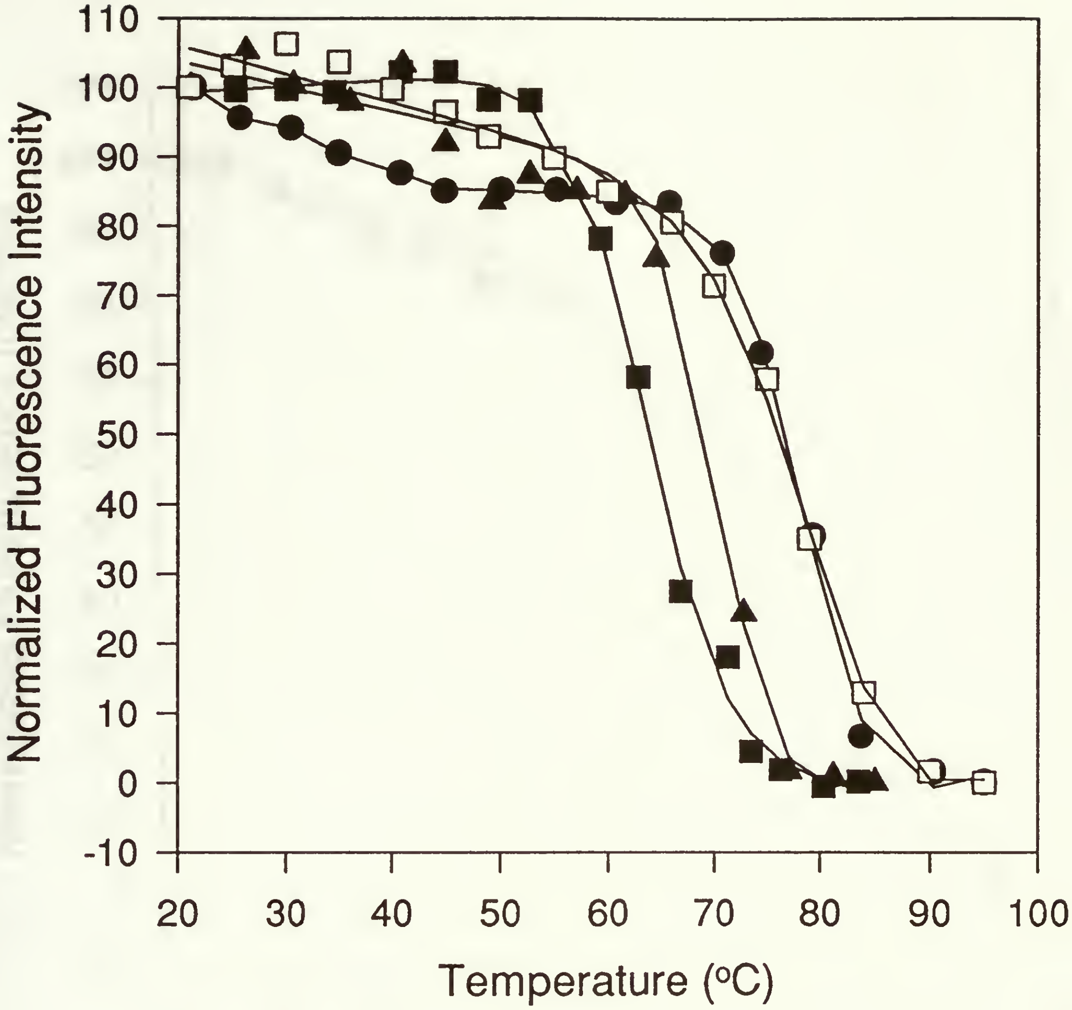

Figure 5.5a Changes in fluorescence intensity for CDOM33 as a function of temperature in solution (□), in the sol-gel matrix with no extra Ca^{2+}(■), in the sol-gel matrix with 50-fold extra Ca^{2+} only in the matrix (▲), in the sol-gel matrix with 50-fold excess Ca^{2+} in both the matrix and buffer(●). The symbols are the experimentally derived data points. The solid lines are the lines-of-best-fit as determined by fitting to equation 1.14. The data was normalized by setting the initial intensity to a value of 100 and the final intensity to a value of 0 to provide an overlap of each unfolding curve.

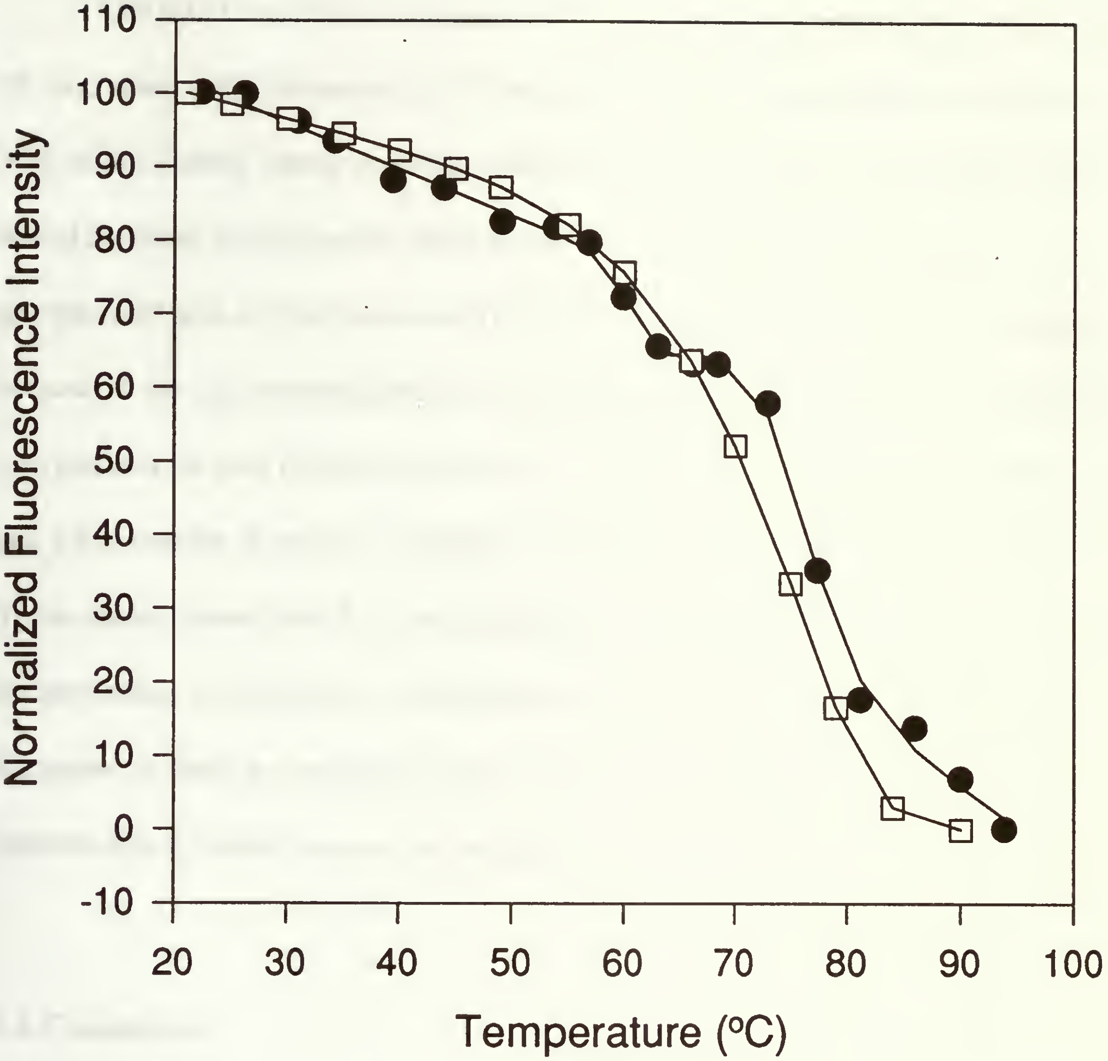

Figure 5.5b Changes in fluorescence intensity for Y57W as a function of temperature in solution (□) and n the sol-gel matrix with 50-fold excess Ca^{2+} in both the matrix and buffer(●).The data was normalized by setting the initial intensity to a value of 100 and the final intensity to a value of 0 to provide an overlap of each unfolding curve.

5.3.6 Long Term Stability of CDOM33

CDOM33 was able to maintain over 90% of its binding ability for a period of over 50 days when a 50-fold excess of Ca^{2+} was added in the gelation buffer. However, only 30% of the binding ability remained after three and a half months when the gels were stored in sealed cuvettes under 100% humidity conditions. CDOM33 was also encapsulated with a 3-fold excess of Tb^{3+}. The full terbium signal remained after aging because of the high binding affinity of the protein for terbium. The full terbium signal was also retained for over 60 days, but there was only 40% of the initial signal left after three and a half months of storage. CDOM33 was very stable when stored in aqueous solution. These studies showed that full binding capacity can be maintained over 2 months. Clearly, further studies on the effects of the storage conditions on the long term stability of the entrapped proteins are required to improve the long term stability of the entrapped proteins and to further improve the encapsulation protocols.

5.4 Conclusions

In this section, two oncomodulin mutant proteins were encapsulated into TEOS derived sol-gel matrices. The effects of the sol-gel matrices on the structure, reactivity, stability and reversibility were studied. CDOM33 was able to maintain full binding capability, and had improved stability compared to the protein in solution when encapsulation was done with an excess of calcium added in the gelation buffer. However, Y57W only maintained a fraction of the binding capability under the same encapsulation conditions. This work showed that the sol-gel matrix was able to alter the protein

structure in a deleterious way. This effect could be avoided in some cases by modifying the encapsulation protocol. However, the glass matrix was still able to affect “soft” proteins more than “hard” proteins. This indicated that special precautions need to be taken when immobilizing different proteins. Additionally, further studies need to be done regarding the reaction kinetics and long term storage conditions in terms of sensor development.

5.5 References for Chapter 5

1. Avnir, D.; Braun, S.; Lev, O.; Ottolenghi, M. *Chem. Mater.* **1994**, 6, 1605.

2 . Dave, B. C.; Dunn, B.; Valentine, J. S.; Zink, J. I. *Anal. Chem.* **1994**, 66, 1120A.

3. Edmiston, P.L.; Wambolt, C.L.; Smith, M.K.; Saavedra, S.S. *J. Coll. Int. Sci.* **1994**, 163, 395.

4. Ellerby, L. M.; Nishida, C. R.; Nishida, F.; Yamanaka, S. A.; Dunn, B.; Valentine, J.S.; Zink, J.I. *Science* **1992**, 255, 1113.

5. MacManus, J.P.; Brewer, L. M.; Yaguchi, M. *Eur. J. Biochem.* **1983**, 136, 9.

6. Barker, W.C.; Ketcham; L. K.; Dayhoff. M. D. *Atlas of Protein Sequences and Structure* (Dayhoff, M. D. ed), **1978**, p273.

7. Clark, I.D.; Bruckman, ; Hogue, C.W.V.; MacManus, J.P.; Szabo, A.G. *J. Fluorescence*, **1994**, 4, 235.

8. Hutnik, C.M.L.; MacManus, J.P.; Banville, D.; Szabo, A.G. *J. Biol. Chem.*, **1990**, 5, 456.

9. Hutnik, C.M.L.; MacManus, J.P.; Szabo, A.G. *Biochemistry*, **1990**, 29, 7318.

10. Dexter, D. L.J. *Chem. Phys.* **1953**, 21, 836.

11. Shen, C.; Kostic, N.M. *J. Amer. Chem. Soc.* **1997**, 119, 1304.

12. Zheng, L.; Reid, W. R.; Brennan, J. D. *Anal. Chem.* **1997**, 69, 3940.

13. Ahmed, F. R.; Przybylska, m.; Rose, D. R.; Birnbaum, G. I.; Pippy, M. E., MacManus, J. P. *J. Mol. Bio.*, **1990**, 261, 127

14. Sudhakar, K.; Philips, C. M.; Owen, C.S.; Vanderkooi, J.M. *Biochemistry*, **1995**, 34, 1355.

15. M. Laberge, W.W. Wright, K. Sudhakar, P.A. Liebman and J.M. Vanderkooi, *Biochemistry*, **1997**, 36, 5363

Chapter 6 Conclusions and Future Prospects

6.1 Conclusions

Research on biosensors has been done for over three decades. However, there are only two mass marketed commercially available biosensing devices based on protein recognition which are the early pregnancy test (Ciba Self Medications) and the glucose oxidase based blood glucose biosensor (LifeScan Canada). Both the analytical method in aqueous conditions and the instrumentation required for the sensor development are already very well developed, the main reason for the lack of commercial biosensors is that the immobilization method for interfacing the biological molecules onto the physical transducer connected with the instrument almost always leads to an irreversible loss of activity and poor long term stability.

The application of the low temperature sol-gel immobilization method has opened a new pathway for the biosensor development. Numerous reports have shown that biological molecules can be entrapped into the sol-gel derived matrix and maintained their biological reactivity and stability.

This thesis described an initial investigation on the effect of the sol-gel matrix on the protein structure and stability, in an effort to understand the basis of why the inorganic sol-gel process is able to successfully immobilize biological molecules. The small proteins monellin and oncomodulin were encapsulated into the TEOS derived sol-gel matrices and the thermodynamic stability of the entrapped proteins was compared versus proteins in aqueous solution. Results suggested that the proteins can maintain or possibly improve their stability by using proper sol-

gel immobilization protocols. The stabilization of the entrapped proteins might be due to a steric restriction on the motion of the protein, the highly structured water within the sol-gel matrix keeping the protein in an active conformation, leading to an overall decrease in ΔS_{un} and the higher T_{un} for the entrapped proteins. Full reactivity of proteins can also be retained if proper protocols are used. However, the sol-gel process can also damage the protein structure to some degree, leaving the protein only partially active. This appears to happen mainly to some "soft" proteins which are thermodynamically unstable. However, the stability of the entrapped proteins can be controlled by altering the encapsulation protocol in some cases.

Reaction kinetics of the protein-analyte interaction were also studied in this thesis. We demonstrated that the negatively charged sol-gel matrix will tremendously affect the interaction of entrapped proteins with the analyte, especially when charged species are involved. These findings are very important for future sol-gel based sensor development since such factors will affect the signal generated from the protein-analyte interaction and further affect the calibration curve, linear range and detection limit of the sensor.

In conclusion, the proposed low temperature sol-gel process is a new and efficient immobilization format for the sensor development. However, for different proteins, the working protocols need to be modified to efficiently immobilize the proteins. Many factors such pore size, charge effects, aging and storage conditions must be taken into account for designing sensors.

6.2 Suggestions for Future Work

6.2.1 Modification of the sol-gel matrix

Studies have shown that the sol-gel matrix will affect the protein structure and activity. However, there is still a lack of understanding about how the sol-gel process affects proteins. There are many factors which should be considered for designing sensors using the sol-gel format.

Controlling of the pore sizes is the first issue which should be considered. Methods for altering pore sizes which are amenable to protein encapsulation need to be determined so that the glass can be engineered for specific proteins. Further research should be carried out to study the effects of the storage time of the sol, aging conditions, addition of additives such as polyethyleneglycol and polyvinylalcohol as well as organic silane modification on the tuning of the pore sizes.

The storage conditions of the aged gels is another issue which should be considered. The aging of the gel can last for several months and the internal environments of the gel will keep changing during the aging process. For the purpose of designing sensors, it is necessary to stop the aging at a certain point to prevent cracking of the gel and damage of the entrapped proteins caused by over-aging of the gel. The aged gels are usually rehydrated and kept under a higher humidity condition or are kept directly in buffer. These storage methods may result in decreasing of the biological reactivity of the entrapped proteins over time. Investigations on the effects of storage conditions on the protein stability and reactivity must be carried on to improve the long term stability for the purpose of commercializing biosensors.

Studies of encapsulation of the proteins on the sol-gel derived thin films must also be performed. Thin films provide short response times and require less protein to perform real time analyses. Thus, thin films are always the ideal format for the sensor development. Some of the problems associated with sol-gel slides such as distribution of environments and long aging periods might be eliminated by using thin film format. However, new problems such as requirement of co-solvent (i.e. ethanol or methanol) in addition to remaining problems such as charge effects and long term storage problems still need to be studied.

6.2.2 Encapsulation Proteins with Different Size and Further Stability Studies

In this thesis, we only studied two relatively small proteins. In future research work, the sol-gel encapsulation method should be applied on proteins or enzymes with different sizes to further investigate the factors affecting the stability and activity of the entrapped biological molecules. Regarding the stability study of the entrapped proteins, GdHCl as a chemical denaturant is not recommended because of the charge effect which may alter both the response time and the amount of denaturant which can possibly enter the matrix and interact with the entrapped proteins. Urea as a neutral denaturant should be used to carry out the chemical denaturation studies. Thus, studies of chemically induced stability combined with the thermally induced stability studies will provide abundant information to understand the basis of protein stabilization by the sol-gel process in terms of the thermodynamics.

3160